Structural Control Systems in High-speed Railway Bridges

DISSERTATION

Zur Erlangung des akademischen Grades eines
Doktor-Ingenieur
an der Fakultät Bauingenieurwesen
der Bauhaus-Universität Weimar

vorgelegt von
M. Eng. Mai Luu
aus Vietnam
Weimar, August 2014

Mentor:

Prof. Dr.-Ing. habil. Carsten Könke, Bauhaus Universität Weimar

Gutachter:

Univ.Prof. Dipl.-Ing. Dr.techn. Christian Bucher, Vienna University of Technology, Austria

Univ.-Prof. Dr. Dipl.-Ing. Guido Morgenthal, Bauhaus Universität Weimar

Disputation am 18. Dezember 2014

Abstract

Structural vibration control of high-speed railway bridges using tuned mass dampers, semi-active tuned mass dampers, fluid viscous dampers and magnetorheological dampers to reduce resonant structural vibrations is studied. In this work, the addressed main issues include modeling of the dynamic interaction of the structures, optimization of the parameters of the dampers and comparison of their efficiency.

A new approach to optimize multiple tuned mass damper systems on an uncertain model is proposed based on the H_∞ optimization criteria and the *DK-iteration* procedure with norm-bounded uncertainties in frequency domain. The parameters of tuned mass dampers are optimized directly and simultaneously on different modes contributing significantly to the multi-resonant peaks to explore the different possible combinations of parameters. The effectiveness of the present method is also evaluated through comparison with a previous method.

In the case of semi-active tuned mass dampers, an optimization algorithm is derived to control the magnetorheological damper in these semi-active damping systems. The use of the proposed algorithm can generate various combinations of control gains and state variables. This can lead to the improvement of the ability of MR dampers to track the desired control forces. An uncertain model to reduce detuning effects is also considered in this work.

Next, for fluid viscous dampers, in order to tune the optimal parameters of fluid viscous dampers to the vicinity of the exact values, analytical formulae which can include structural damping are developed based on the perturbation method. The proposed formulae can also be considered as an improvement of the previous analytical formulae, especially for bridge beams with large structural damping.

Finally, a new combination of magnetorheological dampers and a double-beam system to improve the performance of the primary structure vibration is proposed. An algorithm to control magnetorheological dampers in this system is developed by using standard linear matrix inequality techniques. Weight functions as a loop shaping procedure are also introduced

in the feedback controllers to improve the tracking ability of magnetorheological damping forces. To this end, the effectiveness of magnetorheological dampers controlled by the proposed scheme, along with the effects of the uncertain and time-delay parameters on the models, are evaluated through numerical simulations. Additionally, a comparison of the dampers based on their performance is also considered in this work.

Nomenclature

Symbol	Description
a	Acceleration
a_k	Distance from the kth wheel-axle set to the first wheel-axle set
A	MR model parameter to be identified
c_0	Viscous damping constant of MR damper
c_{0a}, c_{0b}	MR model parameter to be identified
c_B, c_b	Viscous damping coefficients of the main and auxiliary beams
C_D	Equivalent damping coefficient of FVDs
c_s	TMD damping coefficient
d	Rated distance between the two bogies of a coach
d_j	Distance from the left end of the beams to the jth MR damper
D	Full length of each coach
EI_B, EI_b	Bending stiffness of the main and auxiliary beams
F_0	Gravity force of the wheel-axle set
$F_1(t), F_d(t)$	Real time-varying parameters with Lebesgue measurable elements
F_{cB}	Damper force of MR damper
F_{cBi}, F_{cBi}	Modal damper forces of the main and auxiliary beams
$F_{MR}(x,t)$	Total force generated by the MR dampers
$F_v(x,t)$	Vertical force of the train acting on the main beam
F_{FVD}	Fluid viscous damper force
F_T	Total vertical force of TMDs
$H_B(\omega)$	Acceleration transfer function
$H_{aB}(\omega)$	Displacement transfer function
$h_B(\omega)$	Main beam height
$h_b(\omega)$	Auxiliary beam height
I	Beam cross-sectional area moment along the central line of beam
$J_{\gamma i}$	H_∞ performance index
k_0	Stiffness coefficient of MR damper
k_s	TMD stiffness
m_b	Distributed mass of auxiliary beams
m_B	Distributed mass of main beams
m_s	TMD mass
L	Length of each span
$\overline{m}_B, \overline{m}_b$	Mass per unit length of the main and auxiliary beams
n	MR model parameter to be identified
N	Total number of intermediate coaches
N_B, N_b	Number of modes to be considered for the main and auxiliary beams
N_D	Total number of MR dampers

N_s	Total number of sensors
N_v	Total number of train axles
N_T	Total number of TMDs
p_k	Coefficient of stiffness variation
p_c	Coefficient of damping variation
p_m	Coefficient of mass variation
q_B, q_b	Generalized coordinates of the main and auxiliary beams
t	Continuous time variable
t_k	Time when the kth wheel-axle reaches the bridge
$V_i(x,t)$	Lyapunov function
u	Input voltage
u_i	Modal control force
$u_{\max}$	Largest modal control force
v	Speed of the train
x	Coordinate of beam
x	Damper displacement (only used in section 3)
x_0	Initial displacement of MR damper
z	Evolutionary variable
Z_B, Z_b	Vertical displacements of the main and auxiliary beams
$\mathbf{A}_{0i}, \mathbf{B}_{0i}, \mathbf{C}_{0i}$	Modal state-space matrices
$\mathbf{A}_{ci}, \mathbf{B}_{ci}, \mathbf{C}_{ci}, \mathbf{D}_{ci}$	State matrices of LPF
$\mathbf{A}_i, \mathbf{B}_{di}, \mathbf{B}_{wi}$	State matrices of the system considering LPF
$\mathbf{C}_i, \mathbf{H}_{di}, \mathbf{D}_{wi}$	State matrices of the controlled output considering LPF
$\mathbf{D}_B, \mathbf{D}_b$	Modal matrices corresponding to the sensors positions $x_1, x_2 ...$
$\mathbf{D}_i$	Block-diagonal scaling matrix
$\mathbf{E}_{1i}, \mathbf{D}_i, \mathbf{E}_{2r}$	Modal state matrices of controlled output
$\mathbf{f}_c$	Control force vector in physical space
$\mathbf{G}_i$	Control gain
$\mathbf{J}_1, \mathbf{J}_2, \mathbf{J}_3$	Submatrices in LMIs
$\mathbf{K}_i$	Control gain considering LPF
$\mathbf{L}_B, \mathbf{L}_b$	Modal matrices of the main and auxiliary beam
$\mathbf{L}_1, \mathbf{L}_d, \mathbf{E}_1$	Real constant matrices representing the structure of uncertainties
$\mathbf{M}_c, \mathbf{G}_c, \mathbf{U}_c, \mathbf{N}_c$	Submatrices in LMIs
$\mathbf{q}_B, \mathbf{q}_b$	Generalized coordinate vectors of the main and auxiliary beams
$\mathbf{R}_1, \mathbf{R}_2, \mathbf{R}_3, \mathbf{R}_4$	Linear matrix inequalities
$\mathbf{T}_i(s)$	Modal transfer function
$\mathbf{U}_w, \mathbf{J}_w, \mathbf{U}_{c2}$	Submatrices in LMIs
$\mathbf{v}_i$	Modal state vector
$\mathbf{x}_{ci}$	State variable vector of LPF
$\mathbf{x}_i$	State variable of the system considering LPF

$\mathbf{X}$, $\mathbf{P}_1$, $\mathbf{P}_2$, $\mathbf{P}_3$, $\mathbf{Q}$	Symmetric positive definite submatrices in LMIs
$\mathbf{z}_{0i}$	Controlled output
$\mathbf{z}_i$	Controlled output vector of the system considering LPF
$\mathbf{Z}_{Bs}, \mathbf{Z}_{bs}$	Structural response vectors corresponding to sensors positions x_1, x_2...
α	Scaling factor
α_a	MR model parameter to be identified
α_b	MR model parameter to be identified
β	MR model parameters to be identified
γ	MR model parameters to be identified
γ_i	Upper bound of H_∞ control performance
δ_k	Coefficient of stiffness uncertainty
δ_c	Coefficient of damping uncertainty
δ_m	Coefficient of mass uncertainty
$\Delta A_i, \Delta B_{di}$	Matrix representing time-varying parameter uncertainties
$\Delta\omega$	Detuning frequency width ratio
ε_i	Scalar in LMIs
μ_j	Modal mass ratio of the main and auxiliary beam
μ_s	TMD mass ratio
ζ_B, ζ_b	Modal structural damping of the main and auxiliary beams
ζ_s	TMD damping ratio
η_j	Frequency ratio between the auxiliary and main beam
η_s	TMD frequency ratio
ρ_0	Factor to control the largest control force in LMIs
$\overline{\sigma}$	the maximum eigenvalue
$\underline{\sigma}$	the minimum eigenvalue
τ	Time-delay of the system
$\overline{\tau}$	Largest time-delay of the system
ϕ_B, ϕ_b	Mode shapes of the main and auxiliary beams
Φ_B, Φ_b	Mode shape vectors of the main and auxiliary beams
ω_B, ω_b	Natural frequencies of the main and auxiliary beams
ω_c	Cut-off frequency
Ω	Excitation frequency ratio
ξ_D	Supplemental damping ratio of FVD
$\mathscr{F}$	Linear fraction transformation
$\mathscr{D}$	Set of scale matrices $\mathbf{D}_i$
$\mathscr{L}$	Laplace transform

Contents

List of Figures

List of Tables

Chapter 1

Introduction

1.1 Motivation

The results of experimental investigations of railway bridges[13,14] have shown the significant dynamic responses exceeding that anticipated on certain railway bridges. The theoretical research has clarified that this phenomenon is caused by resonance due to repeated actions of train axle loads at high speed[15,16]. The resonance vibration of railway bridges might result in the deterioration of passenger comfort, reduction of traffic safety such as possibility of derailment of vehicles and the destabilization of ballast causing higher maintenance costs. To overcome these, the traditional approach to resonance vibration mitigation is to design structures with sufficient strength capacity. Alternatively, the use of structural control systems such as passive, active and semi-active control devices might be a very promising solution to attenuate undesirable vibration, especially for existing structures.

One of the commonly structural protecting devices is tuned mass damper (TMD). Its simplest form might consist of a mass that is attached to a vibrating primary structure with spring and damping elements in order to attenuate any undesirable vibration. Due to the damper, energy dissipation occurs whenever the mass of the TMD oscillates with no-vanishing displacement or velocity relative to the primary system. This is achieved by transferring as much energy as possible from the primary system to the TMD by a careful tuning of the natural frequency and damping ratio of the TMD.

However, it is well-known that a TMD is only effective when properly tuned to a specific frequency. Thus, it is very sensitive to changes of frequencies of the primary structure which are often varied with time. To overcome this problem, semi-active tuned mass dampers (STMD), in which a controllable device may be added or used to replace the damping element in tuned mass damper systems, are developed. They can

offer an adjustable damping force in a large range with very low power consumption, highly reliable operation and robustness.

Another passive damping device successfully implemented in real structures to improve their dynamic performance is fluid viscous dampers (FVD). In recent years, it has been developed to reduce excessive vibrations of high-speed railway bridges in combination with a double-beam system. Previous research showed that FVDs can control structure vibrations effectively in a wide frequency range.

Alternatively, FVDs in double-beam systems can be replaced by magnetorheological (MR) dampers to become a semi-active control system. This new combination can reduce damper forces transmitted to superstructures and the amplitudes of structural resonant responses more than the case of FVDs.

Although structural vibration control has been an extensively studied topic for decades, its practical applications to the reduction of bridge vibrations due to moving vehicles is still a task full of challenge. So far, most of the previous research works on structural vibration control systems are concerned with vibrations of high-rise building, chimneys, towers, footbridges and so on. Therefore, there is a potential for further improvement of these devices to be applied in high-speed railway bridges.

Based on the above introduction, a comprehensive investigation on reducing the resonant response of high-speed railway bridges by using tuned mass dampers, semi-active tuned mass dampers, fluid viscous dampers and magnetorheological dampers is presented through an overview of structural vibration control in the following section.

1.2 Literature review of structural vibration control

In this section, a brief introduction and relevant literature review of different aspects of the presented subject are provided in a systematic way.

1.2.1 Tuned mass damper

The concept of a TMD was invented by Frahm in 1909 to reduce the rolling motion of ships. The solution for determining the optimal tuning frequency and the optimum damping of tuned mass dampers is described in Brock[17] and Den Hartog[18]. In this research, an undamped main structure subjected to a harmonic external force over a broad band of forcing frequencies was considered. Den Hartog used the fixed-point method for obtaining an approximate solution of the optimal parameters of the TMD that can minimize the displacement of the primary structure. An important assumption

used in this method is that structural damping is neglected. Recently, a method for computing exact closed-form solutions of optimal TMD parameters by minimizing the maximum of the transfer functions was presented by Nishihara and Asami[19].

In practical applications, tuned mass dampers have been successfully implemented in real structures to reduce their dynamic responses due to environmental loadings such as wind and earthquakes. Only few researchers have investigated the practical applications of TMD systems to the reduction of bridge vibrations due to moving vehicles.

For statically indeterminant bridges, such as continuous beam bridges, cable stayed bridges and suspension bridges, several natural frequencies are usually spaced closely. The response of the controlled bridges may be underestimated if the effects of modal control forces of TMDs may significantly increase the contributions of uncontrolled modes to the vibration of the main system, in which the contributions of its higher modes cannot be ignored. Jo *et al.*[20] studied a three-span steel box bridge with one TMD installed at the second midspan. The parameters of the TMD were optimized by Den Hartog's optimal criterion on the fundamental mode. This research indicated that the initial reducing effect of the forced vibration on the maximum displacement is only 2.6% but the free vibration is rapidly decreased.

Joshi and Jangid[21] extended the optimization algorithm for parameters of multiple tuned mass dampers to suppress the dynamic response of a base-excited structure in a specific mode. This research gave many interesting conclusions for the application of TMDs. Kitis[22] proposed an optimization algorithm for minimizing the dynamic response of a multi-degree of freedom system to sinusoidal loading over several excitation frequencies. It has also been applied to an undamped cantilever beam equipped with two TMDs excited harmonically at the free end and at the midpoint of the beam.

For multiple resonant structure systems, such as multi-span continuous beams, the optimal TMD design problem is much more complicated than that for the single-degree-of-freedom (SDOF) systems, as the mathematical model which includes not only the normal design variables, the damping and the stiffness, but also the locations and the number of the attached TMDs covering all the considered modes. Recently, Yau and Yang[2,3] studied the multiple resonant peaks of train-induced vibrations on cable stayed bridges and truss bridges. The authors proposed a *hybrid TMD system* that consists of several TMD subsystems, each of which is tuned for one dominant frequency of the main system. The optimal properties of each system are determined by two processes. Firstly, by minimizing the response peaks using Den Hartog's optimal procedure, the optimal properties of the TMDs are determined. Then, these properties are modified again to equalize the response peaks and include the structural damping effect of the main system. The result indicated that the proposed hybrid TMD system

can effectively suppress the main resonant peaks of the multi-span bridges subjected to the moving train loads at high speed. However, it can be seen that this method was developed from Den Hartog's classical theory in which only one TMD and one mode are considered. To approach the results for the case of multi-mode and multi-TMD problems, many procedures and approximate calculations were suggested. Because of these, the optimal parameters of TMDs can be deviated. Besides, some other drawbacks of this method can be seen that the number of TMDs, required to suppress multi-resonant vibrations, is quite large, at least n^2, where n is the number of resonant peaks of interest. For instance, for double-span continuous beams, the number of TMDs is at least 4. The positions of TMDs also must be fixed at the midspands. This is another drawback of this method because a strengthening of the structure at the midspans and high cost may be required.

Moreover, most studies on the vibration control of structures using passive TMDs assume that the structural properties are known. However, in practice the structural properties are not know exactly due to the effect of live loads, environmental parameters and various types of modeling uncertainties. Examples include uncertainties in the stiffness, mass, and damping of structural models arising from a varieties of reasons, such as inadequate modeling of the boundary conditions, degradation due to aging, fluctuations in structural mass as well as uncertainties in the member capacities, yield strengths and so on. The efficiency of TMDs can be drastically reduced if they are not tuned to the vibration mode they are designed to suppress. For such unexpected performance reductions, modeling uncertainties should be accounted for and TMDs must be designed to perform optimally over all possible values which the system parameters may be assumed. These will also be investigated in this dissertation.

1.2.2 Semi-active tuned mass damper

As discussed in the previous section, passive tuned mass dampers are simple, inexpensive and reliable but the effectiveness of TMD systems is restricted to its tuned frequency. Because the particular operating and environmental conditions often change with time called detuning effect[23], TMDs may become mistuned and lose their effectiveness. The use of multiple-tuned-mass-damper systems (MTMDs) whose parameters are optimized on an uncertain model mentioned in the previous section can be considered as a solution to reduce detuning effects. However, under severe vibrations in which structural parameters may be continuously varied in a large range, the effectiveness of MTMDs is also reduced significantly. Recently, many researchers are working towards developing passive tuned mass dampers with controllable or adjustable parameters such that their behavior can be tuned automatically by using modern control techniques. Active tuned mass damper systems (ATMD) are also one of the most common control device employed in full-scale civil engineering. Such research efforts

have led to the development of a variety of semi-active, active and adaptive tuned mass dampers.

Most active tuned mass damper systems developed so far consist of an active system element parallel to a resilient element that support reaction mass. The advantages of ATMDs over passive ones include more effective vibration suppression, broader bandwidth and higher control authority[24,25,26]. However, there is a serious challenge regarding the device that can provide required control forces. This should be considered before ATMDs can be used practically. Dyke[27] summarized some other challenges such as the system reliability and robustness, reduction capital cost and maintenance, eliminating reliance on external power and gaining acceptance of nontraditional technology.

The use of semi-active tuned mass dampers may be an promising solution to improve TMD systems and overcome ATMDs' drawbacks. Semi-active devices can combine the best features of both passive and active control systems and offer the greatest likelihood for near-term acceptance of control technology as a viable means of protecting civil engineering structural systems against earthquake, wind loading and traffic-induced loads. The attention received in recent years can be attributed to the fact that semi-active control devices offer the adaptability of active control devices without requiring the associated large power sources. In fact, many can operate on battery power (tens of watt)[28], which is critical during seismic events when the main power source to the primary structure may fail.

According to presently accepted definitions, a semi-active control device is one which cannot inject mechanical energy into the controlled structural system, but has properties that can be controlled to optimally reduce the responses of the system. Therefore, in contrast to active control devices, semi-active control devices do not have the potential to destabilize the structural system.

Based on the above introduction, some semi-active damping devices will be reviewed briefly including variable-stiffness devices, variable-orifice devices, tuned mass dampers with variable stiffness and tuned mass dampers with variable damping.

1.2.2.1 Variable-stiffness device

Conceived as a variable stiffness device, Kobori *et al.*[29] implemented a full scale variable orifice damper, using on-off mode, in a semi-active variable stiffness system to investigate semi-active control of the Kajima Research Institute building. Although variable-orifice dampers can be used for producing variable stiffness in an on-off mode as a very high stiffness device due to hydraulic fluid compressibility when the valve is

closed or a device with non stiffness when the valve is open. They cannot vary stiffness continuously between different stiffness states.

1.2.2.2 Variable-orifice device

The operating principle for variable orifice devices is to use a controllable, electromechanical, variable-orifice valve to alter the resistance to flow of a conventional hydraulic fluid damper. This kind of device has been widely used in many areas. The concept of applying this type of variable damping device to control the motion of bridges experiencing seismic motion was first proposed by Feng *et al.*[30], and studied analytically and experimentally by some researchers such as Kawashima and Unjoh[31], Sack and Patten[32]. Symans and Constantinou[33] have studies the application of variable fluid dampers for seismic response reduction of buildings and bridges. Jabbari and Bobrow[34] have studied an on-off controllable orifice hydraulic damper used as a resettable stiffness device.

1.2.2.3 Tuned Mass Dampers with variable stiffness

A tuned mass damper with variable stiffness can reduce structural vibration with time-varying frequency by tuning its natural frequency to track the excitation frequency. Generally, its operating principle is to adjust the natural frequency of a tuned mass damper through mechanical mechanism, variable magnetic element controlled by current, or using controllable new material. Recently, Nagarajaiah[1] proposed a model with capacity to continuously and independently vary stiffness. This system, shown in Fig. 1.1, consists of four spring elements arranged in a plane rhombus configuration with pivot joints at the vertices. A linear electromechanical actuator configures the aspect ratio of the rhombus configuration of this device. The aspect ratio changes between the fully closed configuration corresponding to joints 1 and 2 in closest positions and the open configuration corresponding to joints 3 and 4 in closest positions. These changes lead to maximum and minimum stiffness. Besides, a semi-active control algorithm is also developed based on real-time frequency tracking of excitation signal by short time Fourier transform in this work. The results showed that in the case that the fundamental frequency changes due to damage or deterioration of the main structure then TMD might off-tune; hence, it will lose its effectiveness significantly, whereas, the TMD system with variable stiffness is still robust.

Xu *et al.*[35] also developed a mechanical semi-active vibration absorber with an optimum variable step-size control strategy. This system is composed of two spring poles and an absorber mass. Its natural frequency varies as the span of the springs. This control strategy is made up by two stages: the roughly tuning stage and the optimization stage. Some experiments were conducted to evaluate the dynamic properties and

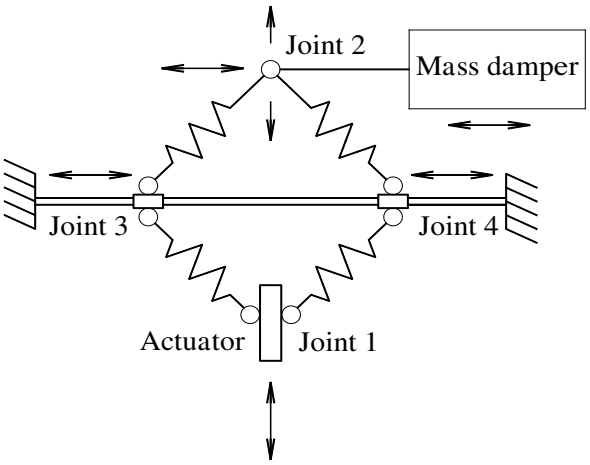

Figure 1.1: Model of semi-active variable stiffness[1]

vibration attenuation performance of the semi-active vibration absorber.

It can be seen that for the above mechanical mechanism systems, their disadvantages are their complicated structures and slow reaction because of the motion adjustment of the spring systems to adapt the change of frequency. Therefore, they might not be suitable for applications required a rapid reaction, especially in high-speed railway bridges.

For the adjustment to the spring stiffness through variable magnetic element controlled by current, Liu *et al.*[36] presented a newly designed electromagnetic vibration absorber, whose stiffness is on-line tunable. This system consists of a clamped-clamped aluminum beam and a permanent magnet that is embedded in the center of the beam and placed between two poles of a C-shaped electromagnet. By varying the current of the electromagnetic, the stiffness of the absorber can be adjusted instantaneously such that the absorber frequency can be tuned. The effective stiffness of the absorber is determined numerically and validated experimentally. The maximum spring force in this work is about some dozens Newton. However, to perform a practical implementation of this study, many issues need improving further to reach a larger force and stable operation required in most practical structures.

1.2.2.4 Tuned Mass Dampers with variable damping

Variable damping is produced by semi-active tuned mass dampers as described in some previous research. The use of piezoelectric friction dampers as an alternative to exist-

ing methods to control floor vibrations was presented by Jiang *et al.*[37]. The friction force can be controlled actively by applying a small amount of external energy to change the normal force between the friction surfaces. The controllable normal force is provided by two low voltage piezoelctric actuators. The experiments showed that piezoelectric actuators can respond to the control signal quickly and accurately.

In recent years, a class of novel intelligent materials such as electrorheological (ER) fluid and magnetorheological (MR) fluid whose dynamics characteristics change rapidly and can be controlled easily in the presence of an applied magnetic field controlled by input current or voltage has been applied to the variable damping element of tuned mass dampers. Because of their peculiar property, ER and MR fluids have been applied to various components such as shock absorbers and engine mounts for vehicles, clutches, valves, *etc*. As the key operation modes for ER and MR fluids are similar and the mathematical model utilized to describe dynamic behavior of ER and MR devices are also similar. One of successful applications of MR and ER fluids is to produce MR and ER dampers. These dampers can be used individually or combined with other dampers to reduce structural vibration. Hikada *et al.* constructed a variable damping dynamic absorber using ER fluid (STMD-ER), and its performance was verified with a three-story structural model[38]. An adaptive neural network control system was also introduced for tuning the damping property of the dynamic absorber corresponding to the vibration frequencies to be reduced. Additionally, a combination of a traditional tuned mass damper and a MR damper (STMD-MR damper) was also used to mitigate the structural response of high-rise buildings under earthquake excitation[39,40,41]. To date, MR dampers are one of the typical devices for MR fluid's commercial applications. They can offer large range of damping force capacity, high reliable operation, and robustness in a reliable fail-safe manner with very low power requirements, and then they become one of the most potential damping devices when combining with other mechanical components such as STMD-MR dampers.

Moreover, it is well-known that a successful semi-active control system depends on two important issues which are the selected semi-active device and its controller[42]. Concerning the design of controllers, the mathematical modeling of MR dampers has become a problem full of challenge because of its complicated behavior. Therefore, it can be seen that although the earliest work for modeling the dynamic behavior of MR and ER dampers can be found in 1987[43], a significant number of papers continue to appear in this area. It is due to the fact that no mathematical model is perfect, which is not only characterize the dynamic behavior accurately, but also be easily to be used. Especially, the effectiveness of STMD-MR dampers applied to railway bridges has not been investigated significantly in previous works. It is believable that this type of devices could be an interesting solution to mitigate the excessive vibrations that these structures may experiment under high-speed traffic.

1.2.2.5 Control methodology

As mentioned, the key of the active and semi-active systems is their control algorithm. Research efforts in active structural control have focussed on a variety of control algorithms based on different control design criteria. Basically, in the realization of an actuator-based structural control system, there are at least two different types of control strategies. The first type requires an accurate explicit mathematical model of the dynamics of the structure to be controlled. These methods are termed as the model-based methods with examples including the linear quadratic regulator (LQR) method [44], the H_2/LQG method[45], the H_∞ method[45] *etc*. Here, the mathematical information regarding the structure is used for calculation of control forces. The other type of control strategy can be classified as the non-model-based or the intelligent control methods with examples including neural network controllers, fuzzy controllers, *etc*. These controllers can be considered as adaptive or self organizing systems that learn through interaction with the environment with little a priori knowledge about the structure to be controlled. Some control algorithms are presented as follows:

Linear quadratic regulator control
The linear quadratic regulator control[44] is one of most popular control techniques that can be applied to many control systems. In this control method, the plant is assumed to be linear system in the state space form and the performance index is a quadratic function of the plant states and control inputs. One of salient advantages of the LQR control is that it leads to linear control laws that are easy to implement and analyze.

Pole assignment
A feasible control strategy is to choose the control gain in such a way that the eigenvalues of the system matrix take a set of values prescribed by the designer. Control algorithms developed based on this procedure are generally referred to as pole assignment techniques. Successful application of these algorithms thus requires judicious placement of the closed-loop eigenvalues on the part of the designer as well as a good understanding of the uncontrolled structural modal behavior[44,46]. Pole assignment algorithms have been studied extensively in the general control literature. Their application to the study of civil engineering structural control has been fruitful when only a few vibration modes contribute significantly to the structural response. In these cases, attention needs only to be paid to these selected modes and a more clear choice of the close-loop eigenvalues can be made. Additionally, the method of pole assignment offers a convenient base for comparison when, for example, relative merits of various control implementation devices are evaluated.

Fuzzy control
Fuzzy control is based on fuzzy logic which is much closer in spirit to human think-

ing and natural language than traditional logical systems[47]. The fuzzy logic controller based on fuzzy logic provides a means of converting a linguistic control strategy based on expert knowledge into an automatic control strategy. In particular, the methodology of the fuzzy logic controller appears very useful when the processes are too complex for analysis by conventional quantitative techniques or when the available sources of information are interpreted qualitatively, inexactly, or uncertainly. Battaini *et al.*[48] designed a fuzzy controller, which was initially designed using three bell-shape membership functions for each input variables and five for the output signal. The advantage of this approach is its inherent robustness and its ability to handle the non-linear behavior of the structure. Moreover, the computations for driving controller are quite simple and can easy be implemented into a fuzzy chip. Schurter *et al.*[49] described a new approach for reduction of environmental induced vibration in constructed facilities by way of a neuro-fuzzy technique. Effectiveness of the fuzzy proposed by the authors is dependent on defining a correlation between acceleration of a vibrating building and a control signal applied to an installed MR dampers. This correlation is defined by means of a fuzzy-mapping that is implemented according to the neuro network architecture of ANFIS toolbox provided by MATLAB®.

H_∞ *norm control*
The H_∞ control theory considers the worst case of external disturbances to design the optimal controller to achieve the desired performance. It can address the controller design problem in its general configuration of non-collocated disturbance and control inputs, and non-collocated performance and control outputs. Many books and papers have been published addressing different aspects of H_∞ controller design and explain the basic issues of the method[45]. The H_∞ model also addresses the issues of robustness due to model uncertainties, and is applicable to the single-input-single-output (SISO) systems as well as multiple-input-multiple-output (MIMO) systems.

H_2 *norm control*
The H_2 norm control method is a special case of the H_∞ one but, at the same time, it is a generalization of the LQR method[45]. It minimizes the H_2 norm similarly to the LQR index, but its two-input-two-output structure (disturbance and control inputs are not collocated and performance and sensor outputs are not collocated either) is similar to the H_∞ controller.

Based on the control methods listed above, a design procedure can be developed. The very first step in designing a semi-active damping systems is to take a decision according to which method the semi-active damping systems should be optimized. An optimization with respect to LQR control, Fuzzy control and H_2 norm control is recommended for structures that are excited by loads having mainly a wide band stochastic character such as wind loads, earthquake loads. For loads exhibiting mainly periodical

time components such as loads generated by human activities like walking, running, jumping, dancing *etc* or machines, an optimization with respect to H_∞ norm control is recommended.

It might be known that high-speed train loads can be considered as an approximately periodic load because the regularly spaced axles build an excitation frequency matching the frequency of a harmonic point load. Therefore, to reduce resonant structural response the development of the H_∞ optimization algorithm to control MR dampers in high-speed railway bridges is very promising. Moreover, the excitation frequency band can be limited because of the maximum speed of trains in practice. Thus, the modal truncation method and the independent modal space control method might be used to reduce the order of controllers in the optimization process.

1.2.3 Fluid viscous damper

The fluid viscous damper (FVD) has been successfully implemented in real structures to improve their dynamic performance under different sources of excitation. It was first used in 1897 in the 75 mm French artillery rifle and after that, in systems of aerospace and military hardware. Since 1990, these devices have been commonly applied to civil structures for seismic protection[11,50,51]. Numerous experimental and analytical investigations on FVDs have focused on reducing vibrations of high-rise buildings, chimneys, towers, footbridges and so on.

The first studies documented by Museros and Martinez-Rodrigo[12,52,53] are concerned with reducing excessive vertical vibrations of high-speed railway bridges experiencing resonance situations by using a double beam system. This system includes auxiliary beams installed underneath bridge decks and FVDs to connect the auxiliary beams to the bridge decks. The solution proposed by the previously mentioned authors could be installed and maintained in existing railway bridges without interfering with everyday rail traffic keeping the lines in operation. On the other hand, FVDs can control the structure vibrations in a wide frequency range, while retrofitting bridge decks with single or multiple tuned mass dampers, proposed by a few authors in the last years [3,54,55,56] leads to the structure vibration control at particular frequencies of operation. Furthermore, the above researchers derived analytical closed-form expressions for calculating the optimal damper constants of FVDs that minimize the bridge maximum response at resonance. They also analyzed the mitigation of torsional vibrations in double-track and skewed structures. The theory for these studies is based on the feature of "fixed-point" frequency. It means that when structural damping is neglected in the primary system, the family of response curves passes through one invariant point on the amplitude-frequency plane, irrespective of the value of the damping constants. The damping ratio of FVDs is taken to be optimal when the response curves pass through

either invariant point with a horizontal tangent. The results indicated that the proposed FVD system could effectively control the maximum response at resonance of bridges, that are subjected to moving loads of trains at high speed. However, it can be seen that the proposed analytical approach did not take the structural damping in consideration.

Recently, researchers have begun to focus on FVDs exhibiting a nonlinear force-velocity relation. Experimental testing by Seleemah and Constantinou[11,57] showed that a suitable mathematical model of the behavior of nonlinear viscous fluid dampers can be described by relating the force and the relative velocity through a fractional power law. For seismic applications, this parameter typically has a value range from 0.2 to 2. Furthermore, the above researchers proved that nonlinear FVDs are advantageous because of their ability to limit peak damper forces at large structural velocities while still providing sufficient supplemental damping. Besides, Symans[11] also suggested a formula to linearize the above nonlinear FVD model. However, it cannot be used directly in the objective functions to find optimal damping coefficients because it depends on the relative displacement amplitude of the main system. This is a challenge about nonlinear FVDs. Recently, to solve this problem, Diotallevi *et al.*[58] also proposed a method in which a new dimensionless parameter, called damper index, not related to the maximum displacement in Symans' formula, is introduced but only for some particular structures, especially buildings equipped with nonlinear fluid viscous dampers.

Also concerning the optimal parameters of FVDs, Kargahi and Ekwueme[59] presented an optimization technique through a flow chart to select damper properties of FVDs. The results are obtained by using an iterative procedure that modifies the overall building damping to match that from the expected response in the dampers. Although an optimization problem is solved, deriving an explicit objective function in this case is almost impossible. Lavan and Levy[60] proposed an approach for the optimal design of viscous dampers in framed structures under earthquake excitations. An objective function was also suggested in this research. The results were obtained by using an iteration procedure of the gradient based optimization. However, it can be seen clearly that this solution is only for some particular cases.

Based on the above introduction, it can be found that although FVDs have been used widely, it is still very attractive to researchers. The reason for this is that optimization problems for FVDs are quite complicated, in which finding their solutions for different FVD models is very different. Thus, the problems about FVDs are often full of challenges.

1.2.4 Semi-active magnetorheological damper in double-beam system

As presented in the above section, semi-active magnetorheological dampers have attracted researchers' attention recently. However, the effectiveness of MR dampers applied to railway bridges has not been investigated significantly in previous works. In a recent research, Jiang and Christenson[61] proposed the use of MR dampers to reduce the dynamic response of existing highway bridges. The authors derived an algorithm to optimize the control forces and performed initial experimental tests to validate some simulations. The results showed that the effectiveness of MR dampers was limited and the displacement response of the bridge beam was only reduced about 17%. This might be due to the fact that the MR dampers were installed quite far from the antinodes of the controlled mode shapes and the control algorithm to drive the MR dampers was not robust enough in this research.

It might be known that the use of double-beam system is very convenient to install damping devices near the antinodes of beam bridge structures. Thus, based on some experiment from previous studies, a new combination of MR dampers and a double-beam system will be investigated in this thesis. This could be an interesting solution to mitigate the excessive transverse vibrations that these structures may experiment under high-speed traffic.

1.3 Objectives of the dissertation

Through the literature survey, it can be seen that there are more or less limitations existing in the previous works. Therefore, there is a potential to improve further some of them.

By considering the amount of research that has been done, this work is aimed at further exploring the issues involved in the structural vibration control of high-speed railway bridges. Through this research, the following objectives are expected as:

1. Tuned mass damper

    - A new approach to optimize multiple tuned mass damper systems will be derived. To overcome some drawbacks in the previous research, the parameters of TMDs will be optimized directly and simultaneously on different modes contributing significantly to the multi-resonant peaks on an uncertain model to explore the different possible combinations of parameters.
    - The proposed objective function should be able to consider positions of TMDs along the beam length, include structural damping and reduce the

minimum number of TMDs in multi-mode problems but it must ensure that the structural response is still minimized. It is expected that the proposed approach can make the multiple-TMD systems more effective and robust when compared to the previous method.

2. Semi-active tuned mass damper

   - An optimization methodology for semi-active tuned mass damper systems will be proposed based on the H_∞ optimization criteria and the *DK-iteration* procedure with norm-bounded uncertainties in frequency domain. The use of this algorithm will generate various combinations of control gains and state variables in order to improve the tracking ability of MR dampers.
   - Besides, the optimization process should be able to consider uncertain models to reduce detuning effects, and include individual and simultaneous contribution of modes for analyzing multi-span beams.
   - The Bouc-Wen model will be adopted here, and its inverse model will be built with the adaptive neuro-fuzzy inference system technique to predict input voltages.

3. Fluid viscous damper

   - A new approach to improve the previous method will be derived. The proposed method will choose an objective function based on the H_∞ norm associated with loads exhibiting mainly periodical time components. This function should be able to take into account structural damping properties and minimize simultaneously the structural response associated with multiple modes.
   - Analytical closed-form expressions for the above optimization problem are expected because they are very useful in practical design. The perturbation method will be used to find the closed-form formulae for this optimization problem. The results should be validated by the previous method and the numerical optimization method.
   - Nonlinear problems to determine the optimal parameters of nonlinear fluid viscous dampers which may be an interesting solution in applications where high force levels are expected in the dampers are also explored further.

4. Magnetorheological damper in double-beam system

   - A new combination of MR dampers and a double-beam system will be investigated in this dissertation. This combination is very promising to suppress the resonant structural vibrations of beams under high-speed trains.

- In order to make MR dampers more effective and robust, the H_∞ control algorithm based on linear matrix inequality techniques will be derived to determine the desired control force. An uncertain time-delay model with weight functions as a loop shaping procedure should be introduced in the feedback controller to improve the tracking ability of the magnetorheological damping forces.
- The effectiveness of magnetorheological dampers controlled by the proposed scheme, along with the effects of the uncertain and the time-delay parameters on the models, will also be evaluated and compared to the performance of fluid viscous dampers in similar applications reported in previous research through numerical simulations.

5. Finally, the dampers presented above will be compared together based on their performance in which their abilities to reduce the resonant vibration of primary structures are considered.

1.4 Dissertation organization

In the previous sections, some key issues that will be addressed in this research were identified through an introduction to the structural vibration control, and the objectives of this work were clarified. The rest parts of the dissertation are arranged as follows:

Chapter 2 will derive a mathematical model describing the dynamics of the primary structure, dampers and moving loads. After that, the optimization problem for the parameters of multi-TMD systems retrofitted into the bridge structures is derived. The solutions of the proposed method are obtained by using the *DK-iteration* procedure. To evaluate the proposed method, some numerical simulations are presented and compared to the previous method.

Chapter 3 deals with the optimization problem of semi-active tuned mass damper systems. A design approach for the robust H_∞ static state feedback control with an uncertain model is derived to determine the desired control forces. The *DK-iteration* procedure is used to obtain the feasible solution to the problem. The Bouc-Wen model is adopted, and its inverse model is built with the adaptive neuro-fuzzy inference system technique to predict input voltages. Finally, the numerical simulations and comparison with the traditional TMD damper are presented to evaluate the effectiveness of STMD-MR dampers controlled by the proposed algorithm.

Chapter 4 will develop the H_∞ optimization to find the optimal damping parameters of FVDs implemented in high-speed railway bridges. The proposed method can

include structural damping properties, minimize simultaneously structural response at multiple modes and also be extended to nonlinear problems to determine the optimal parameters of nonlinear fluid viscous dampers. Especially, the closed-form formulae are also found based on the perturbation method.

Chapter 5 studies a new combination of MR dampers and a double-beam system. An H_∞ control algorithm to drive magnetorheological damping forces of MR dampers is derived by using standard linear matrix inequality techniques. Finally, the effectiveness of magnetorheological dampers controlled by the proposed scheme, along with the effects of the uncertain and the time-delay parameters on the models, are evaluated and compared to the performance of fluid viscous dampers in similar applications reported in previous research through numerical simulations.

Chapter 6 compares the effectiveness of the dampers presented above based on their performance in which their abilities to treat the resonant vibrations of the primary structures are considered. Here, the relative strength and weaknesses of the dampers will be clarified.

Chapter 7 summarizes the works that have been presented in this dissertation. The main contributions of this research are outlined. Finally, some recommendations for future work are suggested.

Chapter 2

Tuned Mass Damper

2.1 Introduction

In this chapter, the practical applications of TMD systems to reduce the resonant vibration of beam bridges due to high-speed trains will be investigated. In order to optimize the parameters of TMDs, a mathematical model describing the dynamics of the structure should be first set up. Then, the objective function is derived on an uncertain model. Unlike the previous research, the parameters of TMDs are optimized directly and simultaneously on different modes contributing significantly to the multi-resonant peaks in beam bridges under high-speed trains to explore the different possible combinations of parameters and make the TMDs more effective and robust. The solutions of the proposed method are obtained by using a unique procedure based on the *DK-iteration* algorithm with norm-bounded uncertainties[62] for the H_∞ optimization criteria. The reason for choosing the H_∞ optimization is that the train excitation is mainly periodic. It means that the resonant structural response can happen on one or some certain frequencies. Moreover, the H_∞ optimization can minimize the response peaks around the resonant frequencies. Meanwhile, the H_2 optimization focuses on minimizing the dynamic energy of the system, and thus it is more suitable for the systems excited by stochastic loads containing a wide frequency band such as wind loads and earthquake. Finally, to evaluate the obtained results, some numerical simulations using finite element method are presented and compared to the previous method[2].

2.2 Problem formulation

2.2.1 Dynamic modeling of train and structural system

In general, train loads may be simulated by using three models: moving force models, moving mass models and moving suspension mass systems as shown in Fig. 2.1. Each

of them may lead to slightly different structural response and natural frequencies because of the interaction between moving trains and bridges.

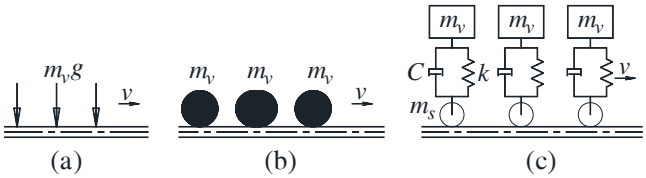

Figure 2.1: Train load models: (a) moving load model, (b) moving mass model and (c) moving suspension mass model

However, the previous studies[12,23] indicate that the use of the different train models leads to a change in resonant frequencies about 2.5%. Moreover, on the safety side, it is well known that the train-bridge interaction leads to a smaller reduction of the bridge vertical acceleration response at resonance. For these reasons, the railway excitation will be simulated by means of moving loads in this work. In particular, the high speed train model HSLM-A8, one of the high speed passenger train models in accordance with the requirements of the European Technical Specification - Annex A2[63], is used as a prototype of a moving train in what follows.

The retrofit system configuration considered consists of a main beam with TMDs and a series of vehicles as shown in Figs. 2.2 and 2.3. All required properties of the train are given in Table 2.1 and Fig. 2.3. The train loads are applied at the centerline of single-track bridges with straight decks and move along the longitudinal direction at a constant speed.

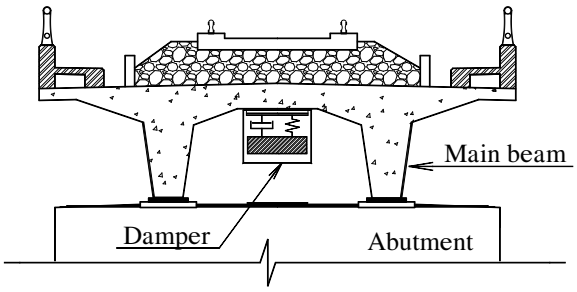

Figure 2.2: Retrofit configuration for concrete girder bridge

The equations of motion can be derived by using standard techniques[64] as

$$\begin{cases} \frac{\partial^2}{\partial x^2}\left[EI_B\frac{\partial^2 Z_B(x,t)}{\partial x^2}\right]+m_B\frac{\partial^2 Z_B(x,t)}{\partial t^2}+c_B\frac{\partial Z_B(x,t)}{\partial t}=F_v(x,t)+F_T(x,t) \\ m_{s_j}\ddot{Z}_{sj}+c_{sj}\left(\dot{Z}_{sj}-\dot{Z}_{Bj}\right)+k_{sj}\left(Z_{sj}-Z_{Bj}\right)=0;\ j=1...N_T \end{cases} \tag{2.1}$$

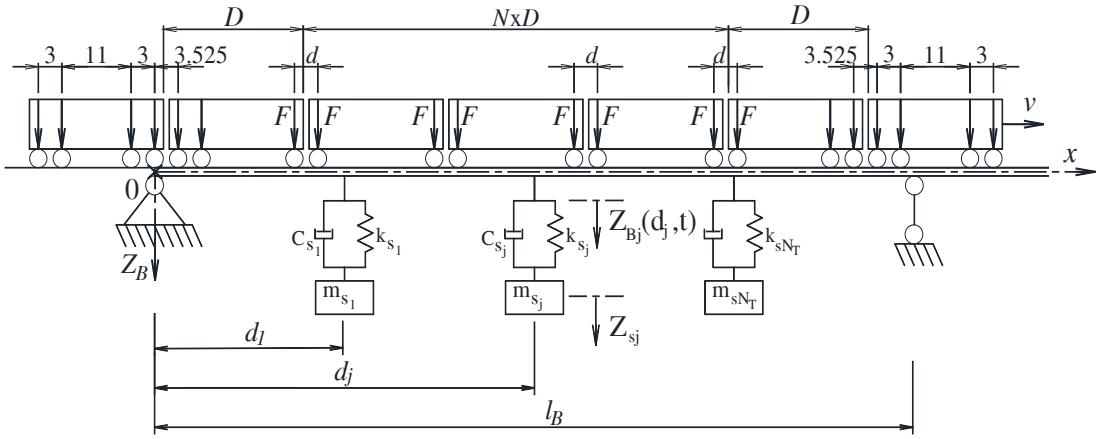

Figure 2.3: Vehicle-bridge system with TMDs

Table 2.1: Properties of the HSLM-A8 high-speed train[8]

Universal train	Number of intermediate coaches, N	Coach length D (m)	Bogie axle spacing, d (m)	Point force F (kN)
A8	12	25	2.5	190

where EI_B, Z_B, m_B and c_B are the stiffness, the vertical displacement, the mass and the viscous damping per unit length of the beam, respectively; $F_v(x,t)$ is the total vertical force of the train applied to the beam; $F_T(x,t)$ is the total force generated by the TMDs; N_T is the total number of TMDs; m_{s_j}, c_{sj}, k_{sj} and Z_{sj} are the mass, damping coefficient, stiffness and displacement of the jth TMD, respectively.

$F_v(x,t)$ is determined by

$$F_v(x,t) = \sum_{i=1}^{N_v} \delta\left[x-(vt-a_i)\right] F_i \mathrm{H}\left(t-t_i\right) \tag{2.2}$$

where N_v is the total number of axles; F_i is the gravity force of the ith wheel-axle set; v is the speed of the train; a_i is the longitudinal distance from the ith wheel-axle set to the first wheel-axle set; t_i is the time when the ith wheel-axle reaches the bridge. The remaining parameters are shown in Fig. 2.3; $\delta\left(x-a\right)$ and $\mathrm{H}\left(t-t_i\right) = \mathrm{H}_0\left(t-t_i\right) - \mathrm{H}_0\left(t-t_i-v/l_B\right)$ are the Dirac delta and Heaviside function defined as

$$\int_{-\infty}^{+\infty} \delta(x-a) f(x)\mathrm{d}x = f(a) \text{ and } H_0(x-a) = \begin{cases} 1, x \geq a \\ 0, x < a \end{cases} \tag{2.3}$$

$F_T(x,t)$ is determined as follows

$$F_T(x,t) = \sum_{j=1}^{N_T} \delta\left(x - d_j\right)\left[k_{s_j}\left(Z_{s_j} - Z_{B_j}\right) + c_{s_j}\left(\dot{Z}_{sj} - \dot{Z}_{Bj}\right)\right] \tag{2.4}$$

where d_j is the distance from the left end of the beam ($x = 0$) to the jth TMD, and l is the total length of the beam. The remaining parameters are described in Fig. 2.3.
An analytical solution of the equations of motion (2.1) is usually impossible. Hence, the numerical methods are most suitable for determining the response of the retrofitted systems under the moving loads. In this work, the finite element method and the average acceleration method for multiple-degree-of-freedom (MDOF) systems are used to solve Eqs. (2.1).

2.2.2 Transfer function and *DK-iteration* algorithm

In this section, the transfer function and the objective function are derived to optimize TMDs' parameters. In Eqs. (2.1), the displacement of the main beam $Z_B(x,t)$ may be expressed in series as

$$Z_B(x,t) = \sum_{i=1}^{N_B} \phi_{Bi}(x) q_{Bi}(t) = \Phi_B^{\mathrm{T}}(x)\mathbf{q}_B(t) \tag{2.5}$$

where

$$\Phi_B^{\mathrm{T}} = \left\{ \begin{array}{cccc} \phi_{B1} & \phi_{B2} & \ldots & \phi_{BN_B} \end{array} \right\}; \quad \mathbf{q}_B^{\mathrm{T}} = \left\{ \begin{array}{cccc} q_{B1} & q_{B2} & \ldots & q_{BN_B} \end{array} \right\}$$

where N_B is the number of modes, considered for the main beam; q_{Bi} is the generalized coordinate of the main beam corresponding to the ith mode, ϕ_{Bi}.

When Eqs. (2.5) are introduced in Eqs. (2.1), and multiplication by the ith normal mode of the main beam is carried out, the ith modal equations of motion are obtained. Then, the orthogonality properties of the normal modes will now be used to transform the equations of motion into modal space, and Eqs. (2.1) is rewritten

$$\left\{ \begin{array}{c} m_{Bi}\ddot{q}_{Bi}(t) + c_{Bi}\dot{q}_{Bi}(t) + k_{Bi}q_{Bi}(t) = F_{vi}(t) + F_{Ti}(t); \quad i = 1 \ldots N_B \\ m_{s_j}\ddot{Z}_{sj} + c_{sj}\left(\dot{Z}_{sj} - \dot{Z}_{Bj}\right) + k_{sj}\left(Z_{sj} - Z_{Bj}\right) = 0; \; j = 1 \ldots N_T \end{array} \right. \tag{2.6}$$

where m_{Bi}, c_{Bi} and k_{Bi} are the ith modal mass, damping coefficient and stiffness of the main beam, respectively. The ith modal force induced by the TMDs are expressed as

$$F_{Ti} = \sum_{j=1}^{N_T} \phi_{Bi}(d_j)\left[k_{s_j}\left(Z_{s_j} - Z_{B_j}\right) + c_{s_j}\left(\dot{Z}_{sj} - \dot{Z}_{Bj}\right)\right] \tag{2.7}$$

and the ith modal external force F_{vi} can be determined as

$$F_{vi} = \int_0^{l_B} \sum_{k=1}^{N_v} F_k \delta\left[x-(vt-a_k)\right] \mathrm{H}(t-t_k)\phi_{Bi}(x)\mathrm{d}x = \sum_{k=1}^{N_v} F_k \mathrm{H}(t-t_k)\phi_{Bi}(vt-a_k) \quad (2.8)$$

In general, the modal TMD force F_{Ti} can make Eqs. (2.6) coupled again because it depends on all the modal coordinates. However, in the previous research presented by Gawronski[45] showed that *"the structural transfer function at the ith resonant frequency is approximately equal to the ith modal transfer function at its resonant frequency"*. It means that the contribution of the modes different with the ith mode to the structural transfer function at the ith resonant frequency can be neglected. Additionally, the target of the presented method is to derive a structural transfer function and then, minimize it in the system's resonant frequency range to determine the optimal parameters of TMDs. Therefore, the above approximation is adopted during the optimization process in this work. Then, for the ith mode, Eqs. (2.6) can be rewritten approximately as

$$\begin{cases} m_{Bi}\ddot{q}_{Bi} + c_{Bi}\dot{q}_{Bi} + k_{Bi}q_{Bi} = F_{vi} + F_{Ti};\ \ i = 1...N_B \\ m_{s_j}\ddot{Z}_{sj} + c_{sj}\left[\dot{Z}_{sj} - \phi_{Bi}(d_j)\dot{q}_{Bi}\right] + k_{sj}\left[Z_{sj} - \phi_{Bi}(d_j)q_{Bi}\right] \approx 0;\ \ j = 1...N_T \end{cases} \quad (2.9)$$

and

$$F_{Ti} \approx \sum_{j=1}^{N_T} \phi_i(d_j)\left\{k_{s_j}\left[Z_{s_j} - \phi_{Bi}(d_j)q_{Bi}\right] + c_{s_j}\left[\dot{Z}_{sj} - \phi_{Bi}(d_j)\dot{q}_{Bi}\right]\right\} \quad (2.10)$$

Then, Eqs. (2.9) are decoupled. By substituting Eq. (2.10) into Eqs. (2.9), the equations of motion becomes

$$\begin{cases} m_{Bi}\ddot{q}_{Bi} + c_{Bi}\dot{q}_{Bi} + k_{Bi}q_{Bi} = F_{vi} + \Phi_{Fi}\mathbf{K}\mathbf{C}_{2i}\mathbf{x}_i;\ \ i = 1...N_B \\ \ddot{\mathbf{v}}_s = \mathbf{B}_v\mathbf{K}\mathbf{C}_{2i}\mathbf{x}_i \end{cases} \quad (2.11)$$

where Φ_{Fi}, $\mathbf{K}$, $\mathbf{C}_{2i}$, $\mathbf{x}_i$, $\mathbf{v}_s$ and $\mathbf{B}_v$ are $1\times N_T$, $N_T \times 2N_T$, $2N_T \times (2N_T+2)$, $(2N_T+2)\times 1$, $N_T \times 1$ and $N_T \times N_T$ matrices, respectively. They are given as follows:

$$\Phi_{Fi} = \begin{Bmatrix} \phi_{Bi}(d_1) \\ \phi_{Bi}(d_2) \\ \cdots \\ \phi_{Bi}(d_{N_T}) \end{Bmatrix}^{\mathrm{T}};\ \mathbf{v}_s = \begin{Bmatrix} Z_{s1} \\ Z_{s2} \\ \cdots \\ Z_{sN_T} \end{Bmatrix};\ \mathbf{x}_i = \begin{Bmatrix} q_{Bi} \\ \mathbf{v}_s \\ \dot{q}_{Bi} \\ \dot{\mathbf{v}}_s \end{Bmatrix};$$

$$\mathbf{K} = \begin{bmatrix} k_{s1} & c_{s1} & 0 & 0 & \ldots & 0 & 0 \\ 0 & 0 & k_{s2} & c_{s2} & \ldots & 0 & 0 \\ \ldots & \ldots & \ldots & \ldots & \ldots & \ldots & \ldots \\ 0 & 0 & 0 & 0 & \ldots & k_{sN_T} & c_{sN_T} \end{bmatrix};\ \mathbf{B}_v = \begin{bmatrix} -\frac{1}{m_{s1}} & 0 & \ldots & 0 \\ 0 & -\frac{1}{m_{s2}} & \ldots & 0 \\ \ldots & \ldots & \ldots & \ldots \\ 0 & 0 & \ldots & -\frac{1}{m_{sN_T}} \end{bmatrix};$$

$$\mathbf{C}_{2i} = \left[\begin{array}{cccccc|cccccc} -\phi_{Bi}(d_1) & 1 & 0 & 0 & \dots & 0 & 0 & 0 & 0 & 0 & \dots & 0 \\ 0 & 0 & 0 & 0 & \dots & 0 & -\phi_{Bi}(d_1) & 1 & 0 & 0 & \dots & 0 \\ -\phi_{Bi}(d_2) & 0 & 1 & 0 & \dots & 0 & 0 & 0 & 0 & 0 & \dots & 0 \\ 0 & 0 & 0 & 0 & \dots & 0 & -\phi_{Bi}(d_2) & 0 & 1 & 0 & \dots & 0 \\ \dots & \dots & \dots & \dots & \dots & \dots & \dots & \dots & \dots & \dots & \dots & 0 \\ -\phi_{Bi}(d_{N_T}) & 0 & 0 & 0 & \dots & 1 & 0 & 0 & 0 & 0 & \dots & 0 \\ 0 & 0 & 0 & 0 & \dots & 0 & -\phi_{Bi}(d_{N_T}) & 0 & 0 & 0 & \dots & 1 \end{array}\right]$$

By setting a vector $\mathbf{q}_i = \left\{ \begin{array}{cc} q_{Bi} & \mathbf{v}_s \end{array} \right\}^{\mathrm{T}}$, Eqs. (2.11) can be expressed in matrix form as follows

$$\mathbf{M}_{qi}\ddot{\mathbf{q}}_i + \mathbf{C}_{qi}\dot{\mathbf{q}}_i + \mathbf{K}_{qi}\mathbf{q}_i = \mathbf{B}_{di}F_{vi} + \mathbf{B}_{qi}\mathbf{u}_i \tag{2.12}$$

where $\mathbf{M}_{qi}$, $\mathbf{C}_{qi}$ and $\mathbf{K}_{qi}$ are the $N_{T1} \times N_{T1}$ matrices given by

$$\mathbf{M}_{qi} = \left[\begin{array}{cc} m_{Bi} & \mathbf{0}_{1,N_T} \\ \mathbf{0}_{N_T,1} & \mathbf{I}_{N_T,N_T} \end{array}\right];\ \mathbf{C}_{qi} = \left[\begin{array}{cc} c_{Bi} & \mathbf{0}_{1,N_T} \\ \mathbf{0}_{N_T,1} & \mathbf{0}_{N_T,N_T} \end{array}\right];\ \mathbf{K}_{qi} = \left[\begin{array}{cc} k_{Bi} & \mathbf{0}_{1,N_T} \\ \mathbf{0}_{N_T,1} & \mathbf{0}_{N_T,N_T} \end{array}\right];$$

$$\mathbf{B}_{di} = \left\{ \begin{array}{c} 1 \\ \mathbf{0}_{N_T,1} \end{array} \right\};\ \mathbf{B}_{qi} = \left\{ \begin{array}{c} \Phi_{Fi} \\ \mathbf{B}_v \end{array} \right\};\ \mathbf{u}_i = \mathbf{K}\mathbf{C}_{2i}\mathbf{x}_i$$

and $N_{T1} = N_T + 1$.

If the beam properties are changed, the model becomes uncertain. Then, three physical properties can be assumed that their values are within certain known intervals and can be expressed as

$$m_{Bi} = \overline{m}_{Bi}(1 + p_m\delta_m);\ c_{Bi} = \overline{c}_{Bi}(1 + p_c\delta_c);\ k_{Bi} = \overline{k}_{Bi}(1 + p_k\delta_k). \tag{2.13}$$

where $\overline{m}_{Bi}$, $\overline{c}_{Bi}$ and $\overline{k}_{Bi}$ are the so-called nominal values of m_{Bi}, c_{Bi} and k_{Bi}, respectively; δ_m, δ_c and δ_k represent the uncertain parameters and satisfy $|\delta_i| \leq 1$ with $i = m, c$ and k; p_m, p_c and p_k are constants whose values determine coefficients of variation of the beam properties.

The main idea to establish an TMD optimization problem with uncertain parameters in this work is based on methods and concepts from the robust control literature, especially the *DK-iteration* procedure[62]. In order to be able to approach the *DK-iteration* algorithm, the uncertain parameters are collected together in a block-diagonal matrix of stable perturbations and "pulled out". This process is presented as follows.

The mass matrix of $\mathbf{M}_{qi}$ in eq. (2.12) may be represented as a linear fractional transformation (LFT)[62] in δ_m as

$$\mathbf{M}_{qi}^{-1} = \left[\begin{array}{cc} \frac{1}{\overline{m}_{Bi}} & \mathbf{0}_{1,N_T} \\ \mathbf{0}_{N_T,1} & \mathbf{I}_{N_T,N_T} \end{array}\right] - \left[\begin{array}{c} p_m \\ \mathbf{0}_{N_T,1} \end{array}\right] \delta_m \left(1 + p_m\delta_m\right)^{-1} \left[\begin{array}{cc} \frac{1}{\overline{m}_{Bi}} & \mathbf{0}_{1,N_T} \end{array}\right] = \mathscr{F}\left(\mathbf{M}_{mi}, \delta_m\right) \tag{2.14}$$

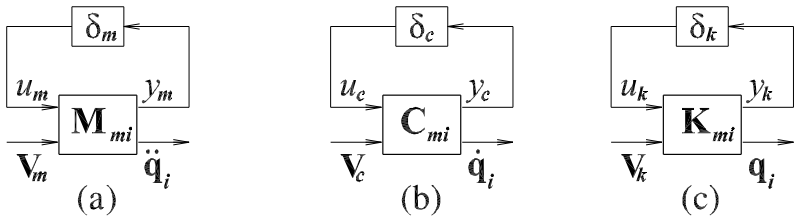

Figure 2.4: Representation of uncertain parameters as LFTs

where $\mathscr{F}$ denotes a linear fraction transformation and $\mathbf{M}_{mi}$ is given as

$$\mathbf{M}_{mi} = \left[\begin{array}{c|c} \mathbf{M}_{i1} & \mathbf{M}_{i2} \\ \hline \mathbf{M}_{i3} & \mathbf{M}_{i4} \end{array}\right] \text{ with } \mathbf{M}_{i1} = -p_m;\ \mathbf{M}_{i2} = \left[\begin{array}{cc} \frac{1}{\overline{m}_{Bi}} & \mathbf{0}_{1,N_T} \end{array}\right];$$

$$\mathbf{M}_{i3} = \left[\begin{array}{c} -p_m \\ \mathbf{0}_{N_T,1} \end{array}\right]_{N_T1\times 1} \text{ and } \mathbf{M}_{i4} = \left[\begin{array}{cc} \frac{1}{\overline{m}_{Bi}} & \mathbf{0}_{1,N_T} \\ \mathbf{0}_{N_T,1} & \mathbf{I}_{N_T,N_T} \end{array}\right]$$

Similarly, the matrix $\mathbf{C}_{qi}$ may be represented as LFT in δ_c

$$\mathbf{C}_{qi} = \mathscr{F}(\mathbf{C}_{mi}, \delta_c) \quad \text{and} \quad \mathbf{C}_{mi} = \left[\begin{array}{c|c} 0 & \mathbf{C}_{i20} \\ \hline \mathbf{C}_{i3} & \mathbf{C}_{i4} \end{array}\right] \tag{2.15}$$

where

$$\mathbf{C}_{i20} = \left[\begin{array}{cc} \overline{c}_{Bi} & \mathbf{0}_{1,N_T} \end{array}\right];\ \mathbf{C}_{i3} = \left[\begin{array}{c} p_c \\ \mathbf{0}_{N_T,1} \end{array}\right];\ \mathbf{C}_{i4} = \left[\begin{array}{cc} \overline{c}_{Bi} & \mathbf{0}_{1,N_T} \\ \mathbf{0}_{N_T,1} & \mathbf{0}_{N_T,N_T} \end{array}\right]$$

and the matrix $\mathbf{K}_{qi}$ may be represented as LFT in δ_k

$$\mathbf{K}_{qi} = \mathscr{F}(\mathbf{K}_{mi}, \delta_k) \quad \text{and} \quad \mathbf{K}_{mi} = \left[\begin{array}{c|c} 0 & \mathbf{K}_{i2} \\ \hline \mathbf{K}_{i3} & \mathbf{K}_{i4} \end{array}\right] \tag{2.16}$$

where

$$\mathbf{K}_{i2} = \left[\begin{array}{cc} \overline{k}_{Bi} & \mathbf{0}_{1,N_T} \end{array}\right];\ \mathbf{K}_{i3} = \left[\begin{array}{c} p_k \\ \mathbf{0}_{N_T,1} \end{array}\right];\ \mathbf{K}_{i4} = \left[\begin{array}{cc} \overline{k}_{Bi} & \mathbf{0}_{1,N_T} \\ \mathbf{0}_{N_T,1} & \mathbf{0}_{N_T,N_T} \end{array}\right]$$

All these linear fraction transformations are depicted by the block diagrams in Fig. 2.4. With the above substitutions, the equations relating all "inputs" to corresponding "output" around the uncertain parameters can now be obtained as

For the LFT in Fig. 2.4a,

$$\left\{\begin{array}{c} y_m \\ \ddot{\mathbf{q}}_i \end{array}\right\} = \mathbf{M}_{mi}\left\{\begin{array}{c} u_m \\ \mathbf{V}_m \end{array}\right\};\ u_m = \delta_M y_m;\ \mathbf{V}_m = \mathbf{B}_{di}F_{vi} + \mathbf{B}_{qi}\mathbf{u}_i - \mathbf{V}_c - \mathbf{V}_k; \tag{2.17}$$

for the LFT in Fig. 2.4b,

$$\left\{ \begin{array}{c} y_c \\ \dot{\mathbf{q}}_i \end{array} \right\} = \mathbf{C}_{qi} \left\{ \begin{array}{c} u_c \\ \mathbf{V}_c \end{array} \right\};\ u_c = \delta_c y_c; \tag{2.18}$$

and for the LFT in Fig. 2.4c,

$$\left\{ \begin{array}{c} y_k \\ \mathbf{q}_i \end{array} \right\} = \mathbf{K}_{qi} \left\{ \begin{array}{c} u_k \\ \mathbf{V}_k \end{array} \right\};\ u_k = \delta_k y_k. \tag{2.19}$$

By combining Eqs. (2.12), (2.17), (2.18) and (2.19) and eliminating the variables $\mathbf{V}_m$, $\mathbf{V}_c$ and $\mathbf{V}_k$, the sate space equations governing the system dynamic behavior are given by

$$\left\{ \begin{array}{l} \dot{\mathbf{x}}_i = \mathbf{A}_{1mi}\mathbf{x}_i + \mathbf{D}_{1mi}\mathbf{w}_{\Delta i} + \mathbf{B}_{1mi}F_{vi} + \mathbf{B}_{2mi}\mathbf{u}_i \\ \mathbf{z}_i = \mathbf{C}_{1i}\mathbf{x}_i + \mathbf{D}_{11i}F_{vi} + \mathbf{D}_{12i}\mathbf{u}_i \\ \mathbf{z}_{\Delta i} = \mathbf{A}_{1zi}\mathbf{x}_i + \mathbf{D}_{1zi}\mathbf{w}_{\Delta i} + \mathbf{B}_{1zi}F_{vi} + \mathbf{B}_{2zi}\mathbf{u}_i \\ \mathbf{u}_i = \mathbf{K}\mathbf{C}_{2i}\mathbf{x}_i \end{array} \right. \tag{2.20}$$

where

$$\mathbf{x}_i = \left\{ \begin{array}{c} q_{Bi} \\ \mathbf{v}_s \\ \dot{q}_{Bi} \\ \dot{\mathbf{v}}_s \end{array} \right\};\ \mathbf{w}_{\Delta i} = \left\{ \begin{array}{c} u_m \\ u_c \\ u_k \end{array} \right\};\ \mathbf{z}_{\Delta i} = \left\{ \begin{array}{c} y_m \\ y_c \\ y_k \end{array} \right\};$$

the matrices of $\mathbf{A}_{1mi}$, $\mathbf{D}_{1mi}$, $\mathbf{B}_{1mi}$, $\mathbf{B}_{2mi}$, $\mathbf{A}_{1zi}$, $\mathbf{D}_{1zi}$, $\mathbf{B}_{1zi}$ and $\mathbf{B}_{2zi}$ are presented as

$$\mathbf{A}_{1mi} = \left[\begin{array}{cc} \mathbf{0}_{N_{T1},N_{T1}} & \mathbf{I}_{N_{T1},N_{T1}} \\ -\mathbf{K}_{m2i} & -\mathbf{C}_{m2i} \end{array} \right];\mathbf{D}_{1mi} = \left[\begin{array}{c} \mathbf{0}_{N_{T1},3} \\ \mathbf{P}_{mck2i} \end{array} \right];\mathbf{B}_{1mi} = \left[\begin{array}{c} \mathbf{0}_{N_{T1},1} \\ \mathbf{B}_{d2i} \end{array} \right];\mathbf{B}_{2mi} = \left[\begin{array}{c} \mathbf{0}_{N_{T1},N_T} \\ \mathbf{B}_{q2i} \end{array} \right];$$

$$\mathbf{A}_{1zi} = \left[\begin{array}{cc} -\mathbf{K}_{mi} & -\mathbf{C}_{mi} \\ \mathbf{0}_{1,N_{T1}} & \mathbf{C}_{i20} \\ \mathbf{K}_{i2} & \mathbf{0}_{1,N_{T1}} \end{array} \right];\mathbf{D}_{1zi} = \left[\begin{array}{c} \mathbf{P}_{mcki} \\ \mathbf{0}_{1,3} \\ \mathbf{0}_{1,3} \end{array} \right];\mathbf{B}_{1zi} = \left[\begin{array}{c} \mathbf{B}_{dmi} \\ 0 \\ 0 \end{array} \right];\mathbf{B}_{2zi} = \left[\begin{array}{c} \mathbf{B}_{qmi} \\ \mathbf{0}_{1,N_T} \\ \mathbf{0}_{1,N_T} \end{array} \right];$$

$$\mathbf{P}_{mck2i} = \left[\begin{array}{ccc} \mathbf{M}_{i3} & -\mathbf{P}_{c2i} & -\mathbf{P}_{k2i} \end{array} \right];\mathbf{P}_{mcki} = \left[\begin{array}{ccc} \mathbf{M}_{i1} & -\mathbf{P}_{cmi} & -\mathbf{P}_{kmi} \end{array} \right];$$

$$\mathbf{P}_{c2i} = \mathbf{M}_{i4}\mathbf{C}_{i3};\mathbf{P}_{k2i} = \mathbf{M}_{i4}\mathbf{K}_{i3};\mathbf{B}_{d2i} = \mathbf{M}_{i4}\mathbf{B}_{di};$$

$$\mathbf{C}_{m2i} = \mathbf{M}_{i4}\mathbf{C}_{i4};\mathbf{K}_{m2i} = \mathbf{M}_{i4}\mathbf{K}_{i4};\mathbf{B}_{q2i} = \mathbf{M}_{i4}\mathbf{B}_{qi};$$

$$\mathbf{P}_{cmi} = \mathbf{M}_{i2}\mathbf{C}_{i3};\mathbf{P}_{kmi} = \mathbf{M}_{i2}\mathbf{K}_{i3};\mathbf{C}_{mi} = \mathbf{M}_{i2}\mathbf{C}_{i4};\mathbf{K}_{mi} = \mathbf{M}_{i2}\mathbf{K}_{i4};$$

$$\mathbf{B}_{dmi} = \mathbf{M}_{i2}\mathbf{B}_{di};\mathbf{B}_{qmi} = \mathbf{M}_{i2}\mathbf{B}_{qi}$$

In Eqs. (2.20), $\mathbf{z}_i$ is a controlled output that is considered as a design objective in the H_∞ optimization. In practice, the design of railway bridges satisfies not only the limit acceleration requirement but also the limit displacement of the main beam[8]. Thus, the controlled output is defined as $\mathbf{z}_i = [\ddot{q}_{Bi}\ \ \alpha q_{Bi}]^{\mathrm{T}}$, where the scalar weighting α is used

to control trade-off between the acceleration and the displacement of the beam in the optimization process, then the matrices of $\mathbf{C}_{1i}$, $\mathbf{D}_{11i}$ and $\mathbf{D}_{12i}$ in the controlled output $\mathbf{z}_i$ can be expressed as

$$\mathbf{C}_{1i} = \begin{bmatrix} -\frac{\bar{k}_e}{m_e} & \mathbf{0}_{1\times N_T} & -\frac{\bar{c}_e}{m_e} & \mathbf{0}_{1\times N_T} \\ \alpha & \mathbf{0}_{1\times N_T} & 0 & \mathbf{0}_{1\times N_T} \end{bmatrix};\ \mathbf{D}_{11i} = \begin{bmatrix} \frac{1}{m_e} \\ 0 \end{bmatrix};\ \mathbf{D}_{12i} = \begin{bmatrix} \frac{\Phi_{Fi}}{m_e} \\ 0 \end{bmatrix} \tag{2.21}$$

and the transfer function from $\mathbf{w}_{ui} = \begin{Bmatrix} \mathbf{w}_{\Delta i} \\ F_{vi} \end{Bmatrix}$ to $\mathbf{z}_{ui} = \begin{Bmatrix} \mathbf{z}_{\Delta i} \\ z_i \end{Bmatrix}$ is derived as follows

$$\mathbf{T}_{wzi} = \frac{\mathbf{z}_{ui}}{\mathbf{w}_{ui}} = \mathbf{C}_i \left(s\mathbf{I} - \mathbf{A}_i\right)^{-1} \mathbf{B}_{1ui} + \mathbf{D}_{11ui} \tag{2.22}$$

where $\mathbf{I}$ is an identity matrix with the size of $(2N_T+2)\times(2N_T+2)$;
$\mathbf{A}_i = \mathbf{A}_{1mi} + \mathbf{B}_{2mi}\mathbf{K}\mathbf{C}_{2i}$; $\mathbf{B}_{1ui} = \begin{bmatrix} \mathbf{D}_{1mi} & \mathbf{B}_{1mi} \end{bmatrix}$;
$\mathbf{C}_i = \mathbf{C}_{1ui} + \mathbf{D}_{12ui}\mathbf{K}\mathbf{C}_{2i}$;
$\mathbf{C}_{1ui} = \begin{bmatrix} \mathbf{A}_{1zi} \\ \mathbf{C}_{1i} \end{bmatrix}$; $\mathbf{D}_{11ui} = \begin{bmatrix} \mathbf{B}_{1zi} & \mathbf{B}_{1zi} \\ \mathbf{0}_{1\times 3} & 0 \end{bmatrix}$; $\mathbf{D}_{12ui} = \begin{bmatrix} \mathbf{B}_{2zi} \\ \mathbf{0}_{1\times N_T} \end{bmatrix}$;

In this work, the *DK-iteration* procedure[62] is used to find the controller $\mathbf{K}$ that minimizes the peak values of the transfer function over frequencies of interest, namely

$$\min_{\mathbf{K}} \left(\min_{\mathbf{D}_i \in \mathscr{D}} \left\| \mathbf{D}_i \mathbf{T}_{wzi} \mathbf{D}_i^{-1} \right\|_\infty \right) < \gamma \tag{2.23}$$

where γ is an upper bound constant; $\mathscr{D}$ is a set of matrices $\mathbf{D}_i$ which commute with Δ (i.e. satisfy $\mathbf{D}_i\Delta = \Delta\mathbf{D}_i$; $\Delta = \mathrm{diag}[\delta_m; \delta_c; \delta_k]$). $\mathbf{D}_i$ is a block-diagonal scaling matrix to make γ tighter.

In the case of the multi-mode problems, by using the assumption that the structural transfer function at the ith resonant frequency is approximately equal to the ith modal transfer function at its resonant frequency[45], then index (2.23) can be rewritten as follows

$$\min_{\mathbf{K}} \left(\min_{\mathbf{D}_1 \in \mathscr{D}} \left\| \alpha_1 \mathbf{D}_1 \mathbf{T}_{wzi} \mathbf{D}_1^{-1} \right\|_\infty ; \ldots ; \min_{\mathbf{D}_{N_B} \in \mathscr{D}} \left\| \alpha_{N_B} \mathbf{D}_{N_B} \mathbf{T}_{wzN_B} \mathbf{D}_{N_B}^{-1} \right\|_\infty \right) < \gamma \tag{2.24}$$

where N_B is the number of the considered modes; the factor $\alpha_{i(=1,\ldots,N_B)}$ is to control the trade-off between the influences of modes in the optimization process.

By alternating between minimizing index (2.24) with respect to either $\mathbf{K}$ or $\mathbf{D}_i$ (while holding the other fixed), the result can be obtained. To start the iterations, one selects an initial stable rational matrix $\mathbf{D}_i$ with appropriate structure. The identity matrix is an

initial choice in this work. Then, the *DK-iteration* algorithm proceeds as follows:
1. **K-step.** Minimize index (2.24) with fixed $\mathbf{D}_i$ by using the Nelder-Mead Simplex algorithm.
2. **D-step.** Find $\mathbf{D}_i$ by minimizing index (2.24) with fixed $\mathbf{K}$.
3. Compare $\mathbf{D}_i$ with the previous $\mathbf{D}_i$. Stop if they are close, otherwise, replace the previous $\mathbf{D}_i$ with the latest $\mathbf{D}_i$ and return to step 1.

2.3 Numerical verification and discussion

Based on the theoretical derivations described in section 2.2.2, numerical investigations will be performed. Besides, the optimal properties of TMDs will also be determined by using the previous multiple-mode optimal procedure for multi-span beams proposed by Yau and Yang[2,3]. The result of this procedure may be considered as a criterion to evaluate the effectiveness of the presented method.

The structural parameters and modal properties of the considered bridge systems are listed in Table 2.2 and Fig. 2.5. They are modeled as girder bridges with constant cross section. The TMDs are supposed to be installed underneath the girders. The high speed train, HSLM-A8, with the parameters listed in Table 2.1 is used as external load acting on the bridges.

Table 2.2: Properties of the main beams[9,10]

Beam	l_B (m)	m_B (kg/m)	ζ_B (%)	ω_1	ω_2	ω_3
Simply supported beam	30	2.5×10^4	1.0	20.0	80.5	183.8
Double-span continuous beam	20	3.4×10^4	2.5	21.1	33.0	84.9

Note: l_B is the length of each span; m_B and ζ_B are the mass per unit length and the damping ratio of the beam, respectively; $\omega_i(\mathrm{rad/s})$ is the ith natural frequency of the beams.

Effectiveness of multiple tuned mass dampers and influence of uncertain parameters

The simply-supported beam retrofitted with TMDs is analyzed in this case. The TMDs have a total mass of 7521 kg, approximately equal to 2% of the kinetically equivalent mass of the first mode. The corresponding optimal parameters of the TMDs based on the optimal design procedures developed above are calculated and listed in Table 2.3. Then, the magnitude of the transfer function (TF) versus frequency is presented in Fig. 2.6. This function can represent the maximum acceleration response in frequency domain. It can be seen that the magnitude of transfer function is reduced significantly

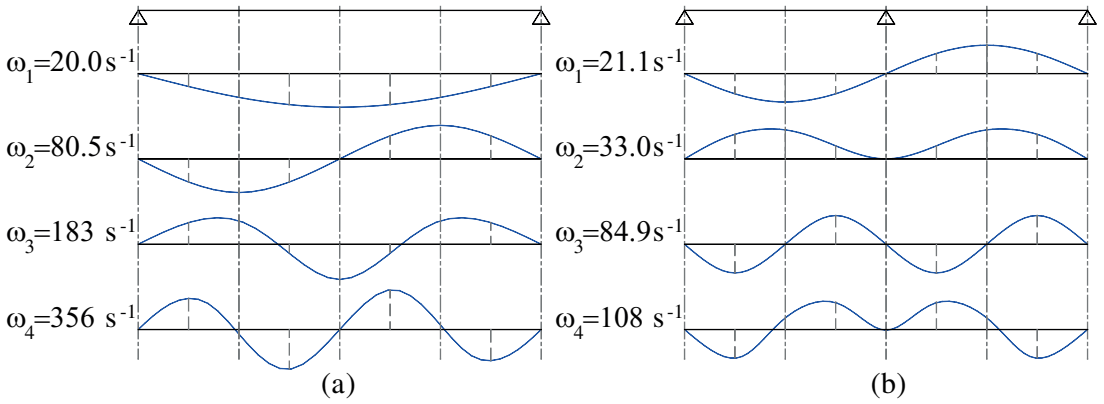

Figure 2.5: Mode shapes of (a) the simply supported beam, (b) the two-span beam

in the vicinity of the resonance frequency. Especially, as one would expect, the response decreases with increasing the number of TMDs whose total mass is equal to the mass of a single TMD. However, if this number is increased beyond a certain value (2 TMDs), only little improvement is observed.

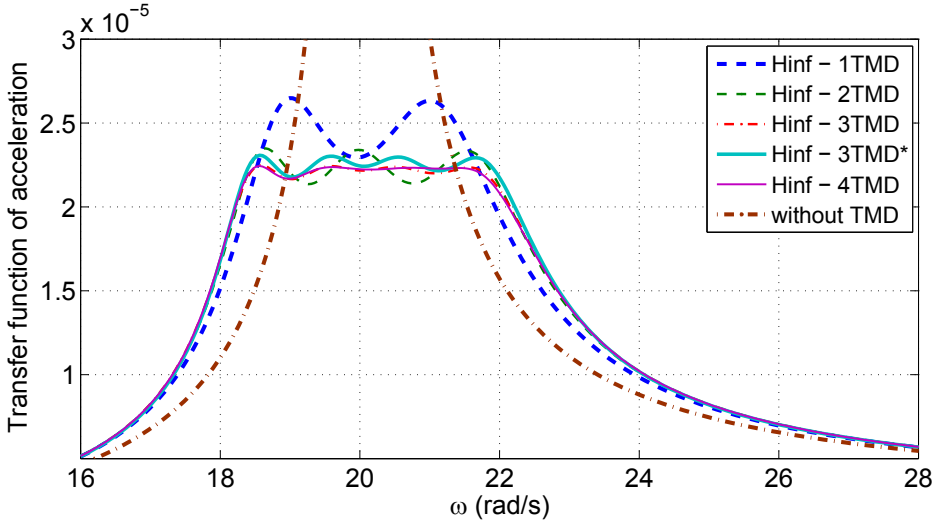

Figure 2.6: Transfer function of acceleration versus frequency

In addition, it is well-known that the optimal locations for the placement of TMDs are at the places where the controlled mode shape values are maximal[23]. However, many TMDs installed at the same section of the beam may reduce the bridge's load bearing capacity. Therefore, the presented method also takes into account the different locations of TMDs installed along the beam axis in the multi-mode objective function to retain best effectiveness of TMDs. Fig. 2.6 shows that the effectiveness of the 3-TMDs*

Table 2.3: Optimal parameters of TMDs

Type	No.	x_s/l_B	m_s (kg)	ζ_s (%)	η_s (%)	k_s (N/m)	c_s (Ns/m)
1 TMDs	1	1/2	7521.0	0.087	0.990	2.967×10^6	2.587×10^4
2 TMDs	1	1/2	3760.5	0.059	1.039	1.632×10^6	9.213×10^3
	2	1/2	3760.5	0.055	0.954	1.378×10^6	7.877×10^3
3 TMDs	1	1/2	2507.0	0.055	1.056	1.126×10^6	5.845×10^3
	2	1/2	2507.0	0.047	0.941	8.943×10^5	4.488×10^3
	3	1/2	2507.0	0.053	0.996	1.002×10^6	5.344×10^3
3 TMDs*	1	2/5	2507.0	0.048	1.059	1.130×10^6	5.110×10^3
	2	2/4	2507.0	0.044	0.943	8.970×10^5	4.192×10^3
	3	3/5	2507.0	0.046	0.999	1.007×10^6	4.682×10^3
4 TMDs	1	1/2	1880.3	0.054	1.063	8.548×10^5	4.362×10^3
	2	1/2	1880.3	0.043	0.938	6.655×10^5	3.021×10^3
	3	1/2	1880.3	0.055	0.981	7.278×10^5	4.099×10^3
	4	1/2	1880.3	0.058	1.015	7.799×10^5	4.412×10^3

Note: x_s is the distance of the sth TMD to the first point of beam; l_B is the span length; m_s is the sth TMD mass; ζ_s and η_s are the damping and frequency ratio of the sth TMD, respectively; k_s and c_s are the stiffness and the damping coefficient of the sth TMD.

group containing three TMDs installed at the different sections $(2/5l_B;\ 2/4l_B;\ 3/5l_B)$ still remains acceptable when compared to the 3-TMDs group installed at the same section $(1/2l_B)$, although the distance between the consecutive two TMDs in the 3-TMDs* group is increased to 3 m in Table 2.3.

To evaluate the influence of the uncertain coefficients when the parameters of TMD systems do not tune to the right frequencies, the maximum response of the acceleration transfer function versus incorrectly tuned frequency width ratio $\Delta\omega = \frac{\omega_B^{\text{actual}} - \omega_B^{\text{design}}}{\omega_B^{\text{actual}}}$ is presented in Fig. 2.7, where ω_B^{actual} is the actual structural frequency, and ω_B^{design} is the structural frequency used to design the TMD systems. For the case of the chosen uncertain parameters $p_k = 0.2$, $p_c = 0$ and $p_m = 0.01$, the optimal parameters of TMDs may be obtained by minimizing index (2.24) and then the maximum structural response is shown in Fig. 2.7a, and for the case of the certain model corresponding to $p_k = 0$, $p_c = 0$ and $p_m = 0$, the maximum response is shown in Fig. 2.7b. It shows that the TMD systems, whose parameters are optimized on the certain model, are more effective under the nominal condition ($\Delta\omega = 0$) but is more sensitive to uncertainty ($\Delta\omega \neq 0$), whereas the curves of the structural responses in the case of TMDs systems whose parameters optimized on the uncertain model in Fig. 2.7a are flatter under the uncertain condition ($\Delta\omega \neq 0$) but less effective in the case that $\Delta\omega$ is equal to zero. It means that they are less sensitive to detuning effect. In general, the use of a multiple tuned mass damper system whose parameters are optimized on an uncertain model may reduce detuning effects, although it will lose some control effectiveness in the case of no detuning or the nominal condition ($\Delta\omega = 0$).

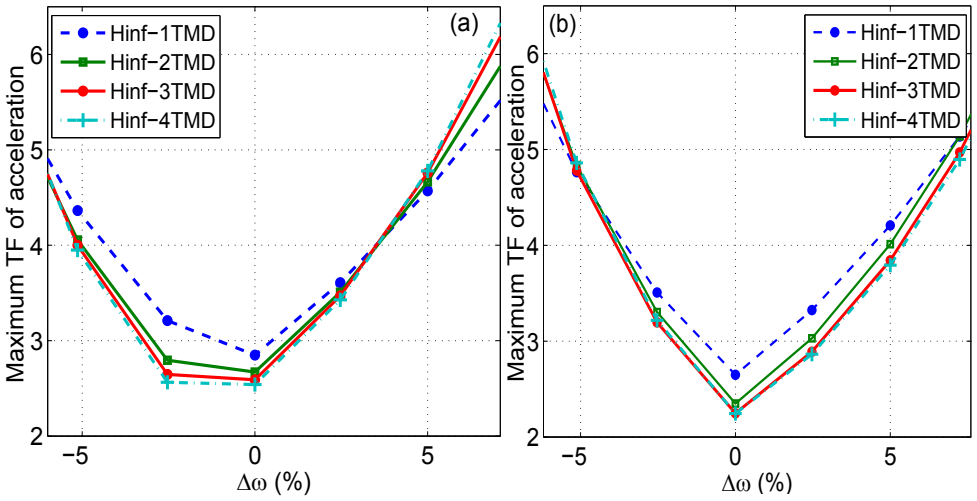

Figure 2.7: Influence of uncertain parameters on maximum structural response: (a) uncertain model: $p_k = 0.2$, $p_c = 0$ and $p_m = 0.01$; (b) certain model: $p_k = 0$, $p_c = 0$ and $p_m = 0$

Optimization of TMDs' parameters retrofitted into multi-resonant structure

In this section, the double-span continuous beam with the physical properties given in Table 2.2 is considered as a prototype of a multi-resonant structure. A TMD system consists of two TMDs, each of which is installed at each of the midspans of the beam.

In some previous research[2,3], the authors showed that the resonant phenomenon only happens if the external load frequency is near the frequency of the first mode or the second mode. The higher modes contribution to the response amplitudes is significant when the speed of the train is extremely high. Therefore, the TMD systems will be employed to reduce the first and second resonant peaks of the main structure. Their total mass is also approximately equal to 2% of the kinetically equivalent mass of the first mode. The optimal parameters of the TMDs calculated by minimizing the performance index in (2.24), called the H_∞ optimization method, are shown in Table 2.4. Fig. 2.8 shows the peak values of the transfer functions in the frequency range of interest. As it may be seen, the contribution of different modes in the optimization process can lead to the different optimal results and the different peak values of the response. The first resonant peak value of the transfer function with the TMDs optimized only for the first mode (TMDs-1) is significantly smaller than the second resonant peak value. In contrast, the first resonant peak value of the transfer function with the TMD systems optimized for the second mode (TMDs-2) is much larger than the second resonant peak value. In the case that the simultaneous contribution of both of the modes (TMDs-both) has been considered in the optimization process, the response curve of the transfer function lies between the curves with the TMDs optimized for the individual modes, and this case can be considered as the best result because both of the peak values of the transfer function corresponding to the first and second modes are reduced simultaneously and significantly.

By using the finite element method (FEM) and the central difference method to model and analyze the interaction of the train-TMDs-beam system, the displacements and acceleration at the second midspan in time domain corresponding to the resonant speed of the train are given in Figs. 2.9a and b, respectively. It can be observed in these diagrams that the TMDs are very effectively reducing the response at resonance. The maximum dynamic displacements and acceleration at the second midspan without TMDs are 15.3 mm and 11.49 m/s^2 and with TMDs are 8.07 mm and 6.02 m/s^2, respectively. The vibrations are reduced by 46.3 % for displacement and 40.1 % for acceleration. From these simulation results, one can conclude that the TMDs optimized by the presented method are very effective to suppress resonance response due to high-speed train passages.

For comparison, the previous method proposed by Yau and Yang[2,3] called the DHOP

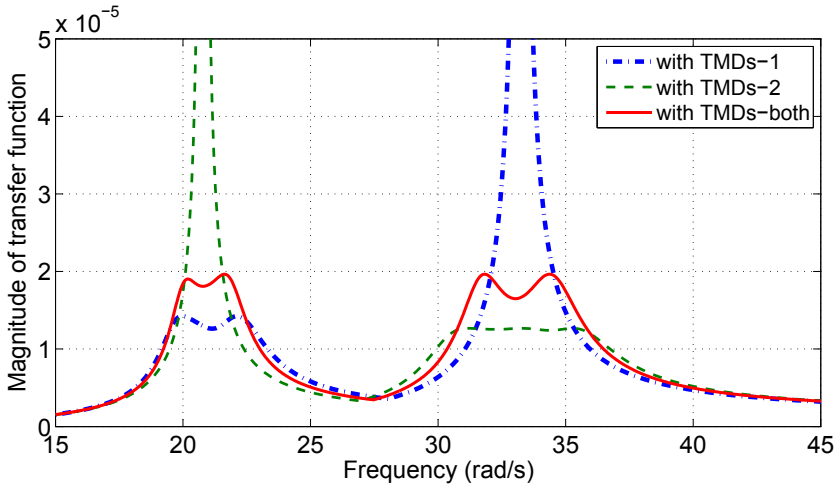

Figure 2.8: Variation of the acceleration transfer function versus the TMDs groups and load frequency

Table 2.4: Optimal parameters of the 4-TMDs group in the two-span beam obtained by the presented method (H_∞ optimization method)

Type	No.	x_s/L	m_s (kg)	ζ_s (%)	η_s	k_s (N/m)	c_s (Ns/m)
4 TMDs	1	1/4	3408.8	5.8	1.007	1.542×10^6	0.844×10^4
	2	1/4	3408.8	5.9	1.549	3.656×10^6	1.308×10^4
	3	3/4	3408.8	5.3	0.968	1.427×10^6	0.743×10^4
	4	3/4	3408.8	6.0	1.572	3.759×10^6	1.356×10^4

Note: x_s is the distance of the sth TMD to the first point of beam; L is the total length of bridge; ζ_s and η_s are the optimal damping and frequency ratio of the sth TMD, where $\eta_s = \omega_s/\omega_{B1}$; ω_{B1} is the first frequency of the beam; ω_s, k_s and c_s are the frequency, the stiffness and the damping of the sth TMD.

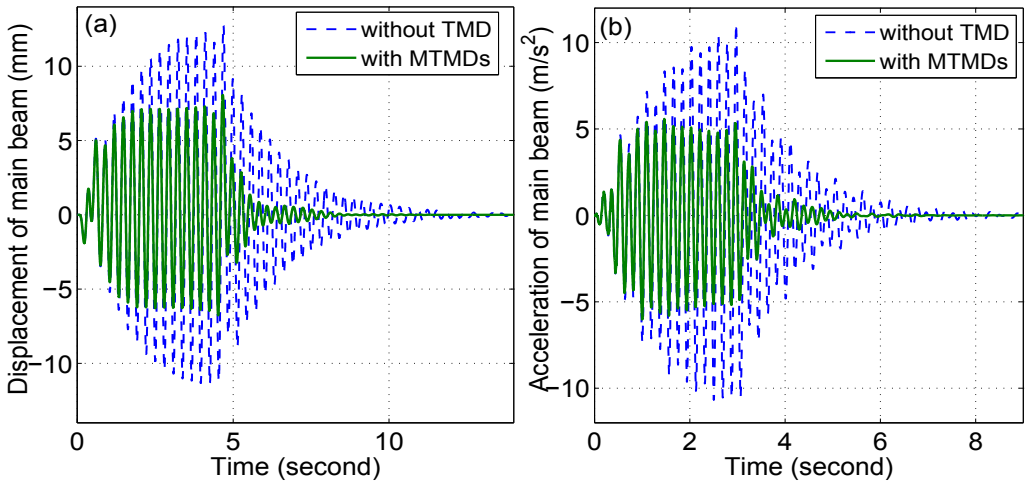

Figure 2.9: (a) Dynamic vertical displacements of the two-span continuous beam at the second midspan; (b) dynamic vertical acceleration of the two-span continuous beam at the second midspan

method, are applied to optimize the parameters of the TMDs. This method uses a *hybrid TMD system* that consists of several TMD subsystems, each of which is tuned for one dominant frequency of the main system. The optimal properties of each system are determined by two processes. Firstly, by minimizing and equalizing the response peaks using Den Hartog's optimal procedure, the optimal properties of the TMDs are determined. After that, these properties are modified again to include the damping effect of the main structure. It can be seen that for the double-span continuous beam this method requires at least 4 TMDs. The TMDs are also installed at the same positions and with the same total mass as described before. They are grouped into two hybrid TMD systems as shown in Fig. 2.10. A hybrid TMD system combines two subsystems, with one tuned to the first mode and the other to the second mode. The optimal parameters calculated for $TMD_{1,1}$, $TMD_{1,2}$, $TMD_{2,1}$ and $TMD_{2,2}$ of the hybrid systems are listed in Table 2.5.

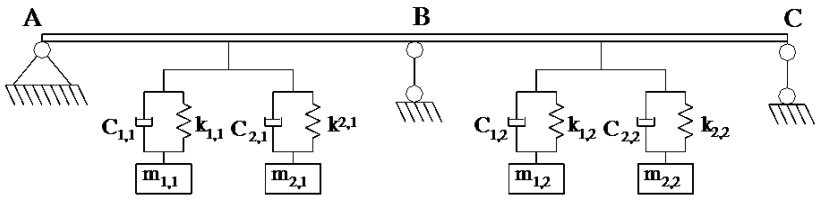

Figure 2.10: Arrangement of hybrid TMD systems[2,3]

Table 2.5: Optimal parameters of the hybrid system in the two-span beam obtained by the previous method (DHOP method)

Hybrid system	No.	x_s/L	m_s (kg)	ζ_s (%)	η_s	k_s (N/m)	c_s (Ns/m)
1	$TMD_{1,1}$	1/4	4010.4	6.53	0.988	1.750×10^6	1.094×10^4
	$TMD_{2,1}$	1/4	2807.2	3.91	1.556	3.038×10^6	0.721×10^4
2	$TMD_{1,2}$	3/4	4010.4	6.53	0.988	1.750×10^6	1.094×10^4
	$TMD_{2,2}$	3/4	2807.2	3.91	1.556	3.038×10^6	0.721×10^4

As illustrated in Fig. 2.11 and Table. 2.6, the calculated vertical displacements at the second midspan of the two-span system obtained by the methods are almost the same. Meanwhile, the acceleration obtained by using the H_∞ optimization method could be reduced to 14% when compared to that obtained by the previous method. It is concluded that the improvement by applying the presented method is obtained. This improvement is because for the presented method, the TMDs parameters can optimized simultaneously on different modes contributing significantly to the multi-resonant peaks to find the different possible combinations of parameters and make the TMDs more effective while for the previous method, the TMDs can be only optimized individually on different modes and an extra procedure was implemented to control the

Table 2.6: Maximum response of the beam obtained by the methods

Method	N_T	d (mm)	a (m/s^2)
Without TMD		15.344	11.490
Previous method (DHOP)	4 TMDs	8.239	6.888
Presented method (H_∞)	4 TMDs	8.283	6.020
	2 TMDs	8.947	5.924
$\Delta = \frac{a_{\text{DHOP}} - a_{H_\infty}}{a_{H_\infty}}$	4 TMDs		14.285%

Note: N_T is the total number of TMDs retrofitted into the beam; d and a are the maximum displacement and the maximum acceleration of the beam, respectively.

trade off between the first mode and the second mode. It can be seen that the second process of the previous method can make the optimal parameters of TMDs be deviated. The presented method can fulfill this gap to lead to a better result as expected.

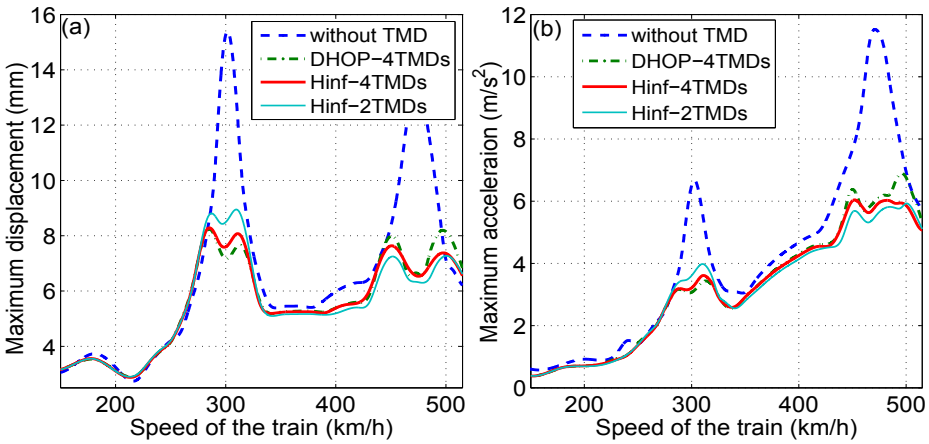

Figure 2.11: Variation of the maximum structural response versus speed of the train: (a) maximum displacement; (b) maximum acceleration

Additionally, the use of the H_∞ method can reduce the necessary number of TMDs meanwhile it still ensures that the structural response is acceptable when compared to the TMDs hybrid system obtained by the previous method. Fig. 2.11 shows that the results obtained by using the 2-TMDs system is not significantly different with that obtained by the others. It should be noticed that the previous method must use at least 4 TMDs ($n^2 = 2^2 = 4$, where $n = 2$ is the number of resonant peaks of interest) to reduce the resonant responses in double-span continuous beams and also to guarantee that the total masses of TMDs on each of the spans are equal.

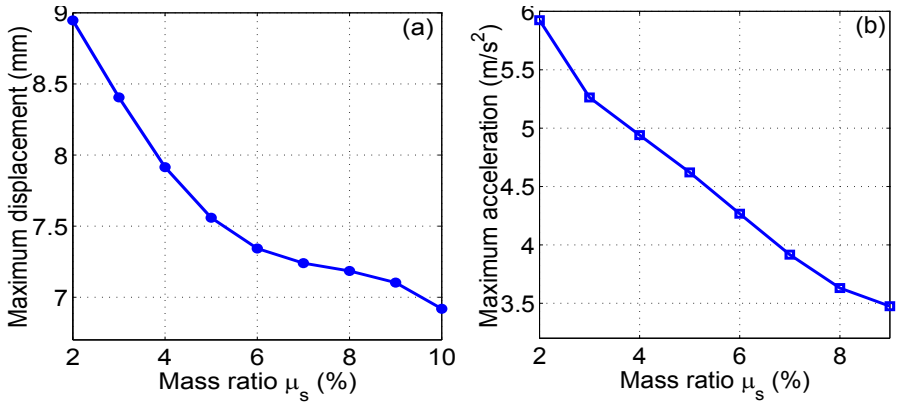

Figure 2.12: Variation of the maximum structural response versus total mass ratio: (a) maximum displacement; (b) maximum acceleration

Fig. 2.12 presents the variation of response of the mean beam at the second midspan. As the mass ratio increases, the maximum response of the primary structure decreases significantly. To guarantee one of the important requirements in standard for bridge design[8], in which the maximum deck vertical acceleration under the rail track does not exceed the maximum value 3.5 m/s^2, the mass ratio should be chosen at least 8 %. This value is large and the TMDs system can overload the bridge bearing ability. This is one of the drawbacks of TMDs. In this case, another damping system more effective should be considered.

2.4 Conclusions

In this study, a new approach for the determination of the optimal parameters of tuned mass dampers retrofitted into high-speed railway bridges is developed. Based on the theoretical and numerical simulation results, the following conclusions may be drawn:

- The proposed approach has led to a more effective TMDs system on multi-modes structures when compared to the previous method. The performance of the methodology is demonstrated for multi-span railway bridges.

- The simulation results also show that the H_∞ optimization method can reduce the number of TMDs in multi-mode cases meanwhile it still ensures that the structural response is acceptable compared with the previous method.

- Finally, the optimization of multiple tuned mass dampers on an uncertain model is also another advantage in this work. It can reduce detuning effect in a narrow frequency band around the fundamental frequency of the main system.

Chapter 3

Semi-active Tuned Mass Damper

3.1 Introduction

As mentioned, tuned mass dampers have many advantages such as efficiency to reduce resonant response, mechanic simplicity, low cost and a reliable damping device. However, as a passive damper, the performance of TMDs is limited. The very narrow band of suppression frequencies, the ineffective reduction of non-stationary vibration, and the sensitivity problem due to detuning effects are the drawbacks of TMDs. The use of multi-tuned mass damper systems, whose parameters are optimized on an uncertain model as derived in the previous chapter, can improve detuning effects but it is only effective in a quite narrow frequency band. To overcome these problems, semi-active tuned mass dampers (STMD) in which the damping element of TMDs is replaced with a magnetorheological damper. In this chapter, in order to make MR dampers more effective and robust, a design approach for the robust H_∞ static state feedback control with an uncertain model is derived here. Additionally, concerning the models of magnetorheological dampers, it might be known that one of the most accurate mathematical models to describe the hysteretic diagram of MR dampers is the Bouc-Wen model[7], due to its extremely versatile characteristics. Thus, this model is adopted, and its inverse model is built with the adaptive neuro fuzzy inference system (ANFIS) technique to predict command voltages in this work. By implementing the ANFIS inverse model into the H_∞ controller, a semi-active H_∞ controller is proposed finally. An optimization algorithm based on the *DK-iteration* procedure is used to obtain a feasible solution to the problem. Finally, the numerical simulations and comparison with the traditional TMD dampers are presented to evaluate the effectiveness of STMD dampers controlled by the proposed algorithm.

3.2 Magnetorheological fluid and MR damper

3.2.1 Typical properties of magnetorheological fluid

Magnetorheological (MR) fluids typically consist of microsized, magnetically polarizable particles such as iron particles dispersed in a carrier medium[65]. These materials demonstrate dramatic changes in their rheological behavior in response to a magnetic field. MR fluids have attracted considerable interest recently because they can provide a simple and rapid response interface between electronic control and mechanical systems[66]. Normally, MR fluids are free-flowing liquids having a consistency similar to that motor oil. However, in the presence of an applied magnetic field, the particles acquire a dipole moment aligned with the external field that causes particles to form linear chains parallel to the field as shown in figure 3.1. This phenomenon can solidify the suspension and restrict the fluid movement. Consequently, yield stress is developed. The degree of change is related to the magnitude of the applied magnetic field and can occur in only a few milliseconds[4].

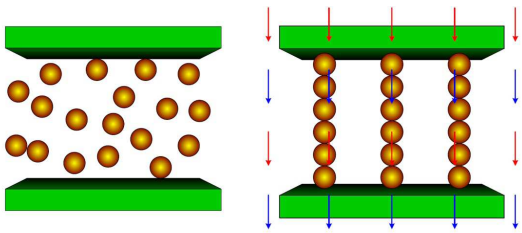

Figure 3.1: MR fluid without and with magnetic field[4]

A yield stress of nearly 100 kPa can be obtained for MR fluids with magnetic suspensions containing carbonyl iron powder[67]. MR fluid can operate at temperatures from -40 to 150^0C with only slight variations in yield stress. From practical perspective, MR devices can be powered directly from common, low power sources (some tens watt)[28]. Further, standard electrical connectors, wires and feedthroughs can be reliably used, even in mechanically aggressive and dirty environments, without fear of dielectric breakdown.

3.2.2 Dynamic modeling of MR dampers

Various devices have been developed to utilize the above special material properties of MR fluids, and MR damper device is one of them. MR dampers are a controllable damping device based on the controllable property of the critical yield stress of MR fluids when exposed to a magnetic field and this phenomenon is defined as MR effect.

An applied magnetic field can turn MR fluid into a semi-solid within a few milliseconds. Thus, when no voltage is supplied to the coil wrapped around the piston head, the MR damper behaves as an ordinary viscous damper. On the other hand, when voltage is sent through the coil generating a magnetic field, the MR fluid becomes semi-solid. This phase change increases the yield stress of the MR fluid dramatically. A description of several widely used models of MR dampers are briefly introduced and their abilities to reproduce the hysteresis behavior of MR dampers can be found in the previous research by Spencer[7]. However, major drawbacks that hinder MR damper

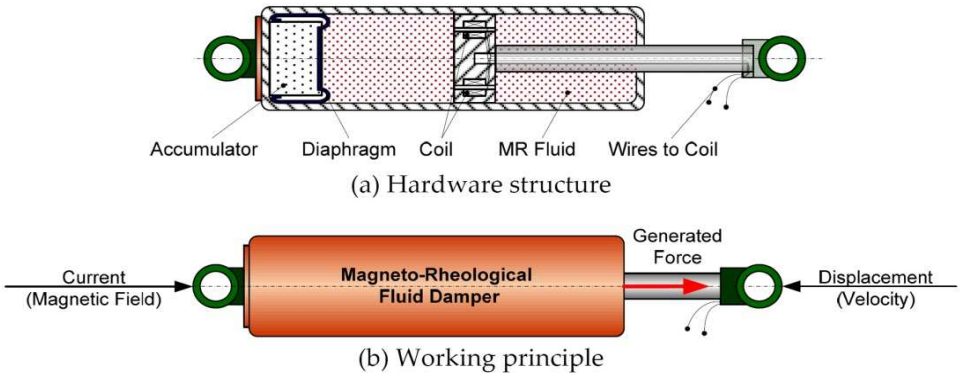

Figure 3.2: General configuration of a MR fluid damper[4]

applications are their high-nonlinear force-displacement and hysteretic force-velocity characteristics. Therefore, one of the challenges involved in creating high efficiencies for MR fluid damper applications, especially in damping control field is to develop an accuracy model that can take full advantages of the unique features of this device and to design proper control algorithm in order to improve the system working performances.

With modeling technologies of MR fluid dampers, both parametric and non-parametric models have been built by researchers to describe MR fluid damper behaviors. Parametric models based on mechanical idealizations have been proposed such as Bingham model, Bouc-Wen model, phenomenological model, *etc*. For non-parametric methods, a set of numerical equations are utilized to interpolate the dynamic behavior of MR dampers, such as fuzzy model, scheduling gain fuzzy inference model, polynomial model, *etc*. Some typical MR fluid damper modeling methodologies can be revised as follows.

3.2.2.1 Bingham model

The stress-train behavior of the Bingham visco-plastic model[68] is often used to describe the behavior of MR fluid. In this model, the plastic viscosity is defined as slope

of the measured shear stress versus shear strain rate data. This model consists of a

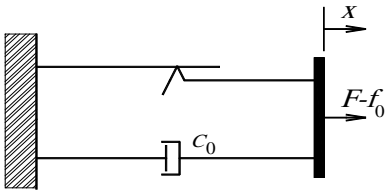

Figure 3.3: Bingham model of MR damper[4]

Coulomb friction element placed in parallel with a viscous damper as depicted as figure 3.3. Here, the force F generated by the device depends on nonzero piston velocity $\dot{x}$, damping coefficient c_0, the friction force related to the fluid yield stress and an offset in the force f_0 to account for the nonzero mean observed in the measured force due to the presence of the accumulator.

Some previous results experimentally obtained by this model showed that although the force-time and force-displacement behavior were reasonably modeled, the predicted force-velocity relation was not captured, especially for velocity that were near zero. Hence, Gamota *et al.* developed an extension of the Bingham model, which is given by the viscoelastic-plastic model shown in figure 3.4.

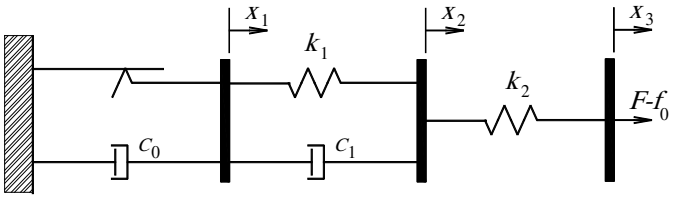

Figure 3.4: Extended Bingham model of MR damper[4]

This model can present the force-displacement behavior of the damper better the Bingham model. However, the governing equations described the extended model are extremely stiff, making them difficult to deal with numerically. Therefore, the Bingham model or extended Bingham model are normally employed in case there is a significant need for a simple model.

3.2.2.2 Bi-viscous model

By assuming that the MR fluid is plastic in both the pre-yield and the post-yield conditions, the nonlinear bi-viscous model developed by Stanway *et al.*[5] was used to model the hysteretic behavior of MR dampers shown in figure 3.5. The study showed that the nonlinear force-velocity behavior could be adequately predicted. However, the model

does not adequately account for the variations in the excitation and response conditions, since the identified damping rates are applicable in the vicinity of a specific excitation and response.

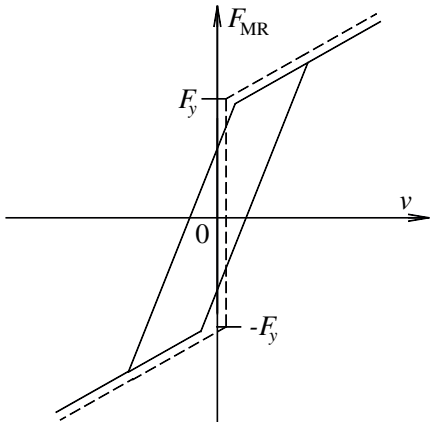

Figure 3.5: Hysteresis behavior of nonlinear bi-viscous model[5]

3.2.2.3 Schematic identification

The parameters in the parametric dynamic models for MR dampers should be identified using experiment data to make the hysteresis loop agree with experimental data[6]. The principle of the parameter estimation for the parametric dynamic models for MR dampers in the sense of optimization can be illustrated by Fig. 3.6.

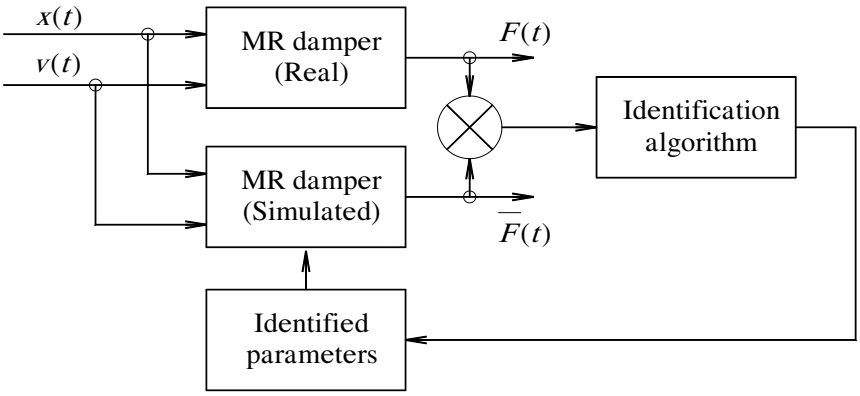

Figure 3.6: Schematic of the identification for MR dampers[6]

Parameter estimation essentially is a multi-dimensional numerical optimization problem, where decision variables are parameters of the parametric dynamic models for MR dampers and the optimization algorithm is used to adjust model parameters.

3.2.2.4 Non-parametric model

A non-parametric method based on intelligent techniques, for example, is an effective solution to estimate directly MR fluid damper behavior with high precision. Chang *et al.*[69] proposed a non-parametric model using multilayer perception neural network with optimization method for a satisfactory representation of a damper behavior. Schurter *et al.*[70] investigated the modeling of MR fluid dampers with an adaptive neuro-fuzzy inference system. The fuzzy structure was simple for modeling; nevertheless, the training model process relied on input and output information on MR fluid dampers and took much computation time.

3.2.2.5 Bouc-Wen model

The Bouc-Wen model hysteresis operator was initially formulated by Bouc[71] as an analytical description of a smooth hysteretic model and later generalized by Wen. This hysteresis model possesses an appealing mathematical simplicity and is able to represent a large class of hysteresis behavior. It is also well-known that this model is the most accurate and has been used extensively for modeling hysteretic systems. Thus, the Bouc-Wen model will be utilized to simulate large-scale MR dampers in this work.

In order to model the hysteretic behavior of MR dampers, Spencer *et al.*[7] adopted the Bouc-Wen hysteretic operator to present the hysteretic behavior of MR dampers and the schematic of the proposed Bouc-Wen model for MR dampers is shown in figure 3.7.

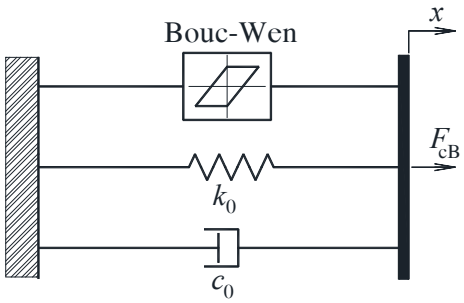

Figure 3.7: Bouc-Wen model[7]

The Bouc-Wen model is based on a phenomenological model[7], which is described by the following equation

$$F_{cB} = c_0\dot{x} + k_0(x - x_0) + \alpha z \tag{3.1}$$

where c_0 and k_0 are the viscous damping constant and the stiffness coefficient, respectively; x_0 stands for the initial displacement.

The evolutionary variable z is governed by

$$\dot{z} = -\gamma |\dot{x}| z |z|^{n-1} - \beta \dot{x} |z|^n + A\dot{x} \tag{3.2}$$

By tuning the parameters γ, β, α and A, this model is able to simulate the dynamic response of a variety of hysteretic materials for MR dampers.

For large-scale dampers in civil engineering[7,72,73], the optimal identified equations for α and c_0 as functions of the input voltages u are written as

$$\alpha(u) = \alpha_a + \alpha_b u; \;\; c_0(u) = c_{0a} + c_{0b} u \tag{3.3}$$

and the rest of the identified parameters are given in Table 3.1.

Table 3.1: Model parameters identified for a large-scale damper

Parameter	Value	Unit	Parameter	Value	Unit
A	6		n	2	
γ	30	cm^{-2}	x_0	18.6	cm
β	30	cm^{-1}	k_0	10	N/cm
c_{0a}	800	Ns/cm	c_{0b}	300	Ns/cm
α_a	2.1	kN/cm	α_b	34	kN/cm

3.2.3 Inverse model of MR damper for control force

An inverse model of MR dampers as one part of a damping force control scheme is a model that predicts a control input voltage signal for a given displacement, velocity and force. The predicted input voltage, which is input to MR dampers, is used to produce the desired force, which is the purpose of the control strategy. However, the corresponding inverse model is difficult to obtain due to its strong nonlinearity and complexity. For some other forward models, including the polynomial model[74], sigmoid function-based model[75], modified LuGre model[76], and simplified phenomenological model[77], their inverse dynamic model can be analytically determined. Moreover, neural networks[78] and the adaptive neuro-fuzzy inference system (ANFIS)[79] are also developed the inverse MR damper models because of their strong nonlinearity disposing ability. Among these methods, the neuro-network and ANFIS methods can accurately predict the input voltage of the MR dampers. For this reason, the adaptive neuro-fuzzy inference system technology, as implemented in the Fuzzy Logic Toolbox in MATLAB® [80], is used to build the inverse model in this thesis. There are two primary advantages of the ANFIS model when compared to conventional arithmetic methods. Firstly, it reduces the difficulties of modeling and analyzing complex

systems. Secondly, it is suitable to incorporate the qualitative aspects of human experience within its mapping laws.

ANFIS uses a hybrid learning algorithm[79] that combines the back propagation gradient descent and least square methods to create a fuzzy inference system whose membership functions are iteratively adjusted according to a given set of input and output data.

Data for training and checking process is obtained from the mathematical model of MR dampers presented in the previous subsection. Limits of displacement and input current are dependent upon the specific application of the dampers. A flowchart to calculate the input voltage signals $u(t)$ is proposed in figure 3.8. The predicted voltage signal is based on the current and previous history of measured velocity $v(t)$, $v(t-1)$, the desired control forces $F_{MR}(t)$, $F_{MR}(t-1)$ and the previous input voltage signal $u(t-1)$.

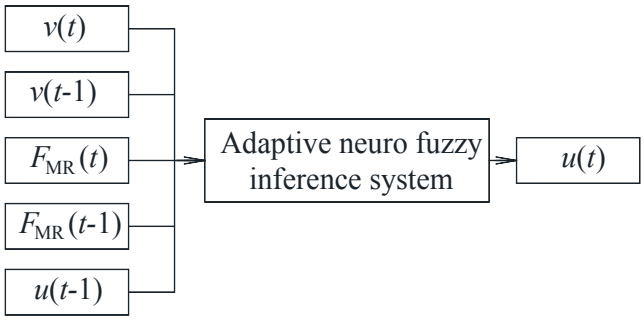

Figure 3.8: Flowchart of inverse model for MR damper using ANFIS

To ensure the creation of a valid model, the data used for training must thoroughly cover the spectrum of operation at conditions in which the dampers have to operate. For this reason, the training data contains a displacement signal with amplitudes in the range of ± 40 mm with frequency contents between $0-6$ Hz approximately as shown in Fig. 3.9. Band-limited signals are used for training. A sampling rate of 1000 Hz is chosen to produce 40000 samples with a total time of 40 seconds.

Similarly, the voltage signal ranges between 0 and 15 V within a frequency band of $0-6$ Hz, respectively. Fig. 3.10 shows a time history of the voltage with the limiting amplitude and the corresponding power spectral density with a frequency band of interest.

Then, the MR damping forces are determined by solving the system of differential

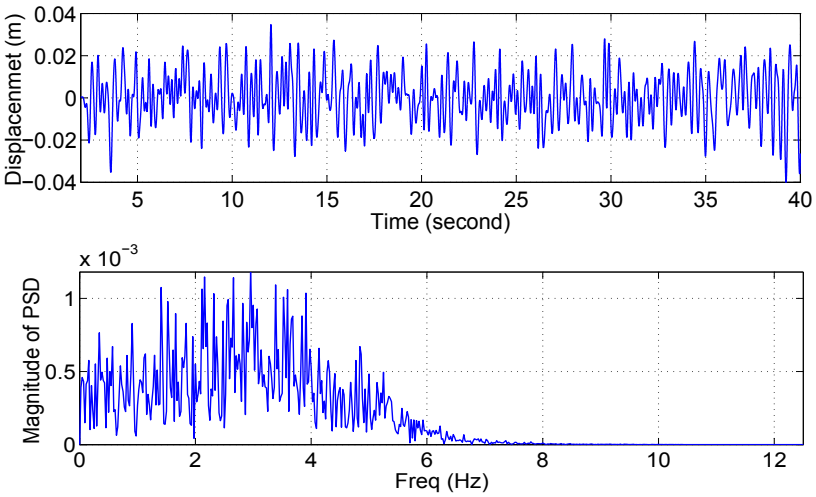

Figure 3.9: Input displacement signal versus time and its power spectra density

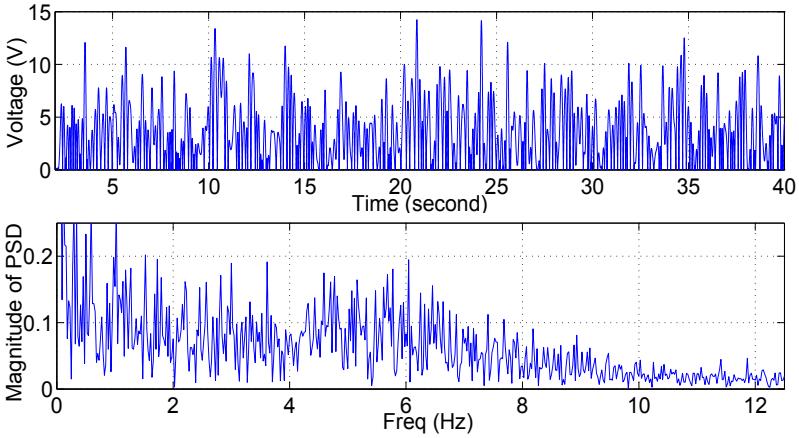

Figure 3.10: Input voltage signal versus time and its power spectra density

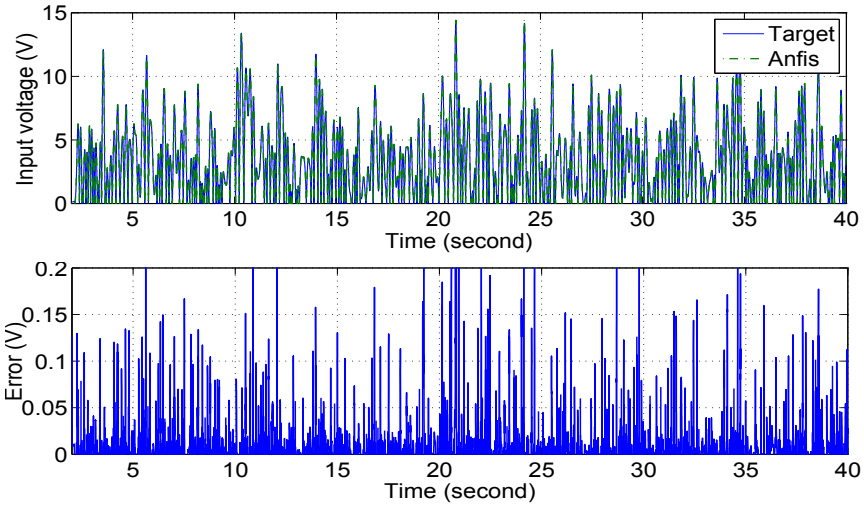

Figure 3.11: Input voltage for validation

Eqs. (3.6) for a simulation time of 40 seconds for the described input voltage and displacement data.

Of the 40000 original data sets, 14000 are used as training data while the remaining data is used for evaluation purposes. After several trials, the best results as indicated in Figs. 3.11 are obtained. It can be detected that the behavior of the ANFIS model matches very well that of the mathematical model.

3.2.4 Constraints of MR dampers

Optimal control forces can be obtained by using various control algorithms, such as the Linear Quadratic Regulator (LQR), the Linear Quadratic Gaussian (LQG), the Robust Optimal Control (H_∞) and the Instantaneous Optimal Prediction Control. Basically, there is no restriction on what type of control algorithm should be used. But there are two intrinsic constraints due to the characteristics of MR dampers, namely, the passivity constraint and the limitation constraint.

Passivity constraint: for active control, forces can be produced in any of the four quadrants in the force-velocity graph, while semi-active damping devices can almost only generate forces in the first and third quadrants. This means that the MR force and the piston's velocity have the same sign at time t.

Limitation constraint: In addition to the passivity constraint, MR dampers have an upper and a lower limit of the force, which depend on the motion of the piston.

On the basis of the two constraints above, if the optimal control force can be attained by the MR damper, implying that it satisfies both of the constraints, the ANFIS model may be employed to obtain the optimal input voltage corresponding to the desired damper force. Otherwise, the input voltage should be set to either zero or the maximal achievable level.

3.3 Problem formulation

3.3.1 Dynamic modeling of structural system

The modeling of the bridge-semiactive tuned mass damper-train load system is shown in Fig. 3.12. The HSLM-A8 train load model presented in Section 2.2.1 are also applied here.

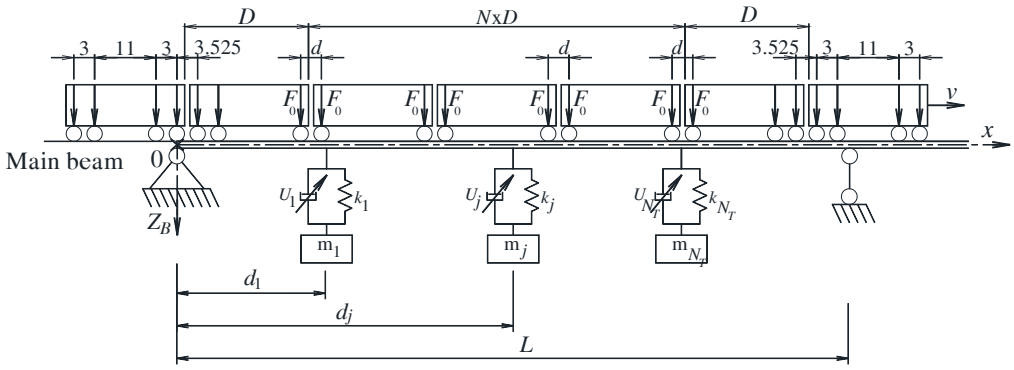

Figure 3.12: Vehicle-bridge system with STMDs

The equations of motion can be derived by using standard techniques[64] as

$$\begin{cases} \frac{\partial^2}{\partial x^2}\left[EI_B\frac{\partial^2 Z_B(x,t)}{\partial x^2}\right]+m_B\frac{\partial^2 Z_B(x,t)}{\partial t^2}+c_B\frac{\partial Z_B(x,t)}{\partial t}=F_v(x,t)+F_T(x,t) \\ m_{s_j}\ddot{Z}_{sj}+k_{sj}\left(Z_{sj}-Z_{Bj}\right)+F_{MRj}=0;\ \ j=1,...,N_T \end{cases} \tag{3.4}$$

where EI_B, Z_B, m_B and c_B are the stiffness, the vertical displacement, the mass and the viscous damping per unit length of the beam, respectively; N_T is the total number of STMDs; m_{s_j}, k_{sj} and Z_{sj} are the mass, the spring stiffness and the displacement of the jth STMD, respectively; F_{MRj} is the force of the jth MR damper.

$F_v(x,t)$ is the total vertical force of the train applied to the beam, and it is described in Eq. (2.2).

$F_T(x,t)$ is the total force generated by the STMDs determined as follows

$$F_T(x,t)=\sum_{j=1}^{N_T}\delta\left(x-d_j\right)\left[k_{s_j}\left(Z_{s_j}-Z_{B_j}\right)+F_{MRj}\right] \tag{3.5}$$

where d_j is the distance from the left end of the beam $(x=0)$ to the jth STMD. The remaining parameters are described in figure 3.12.

3.3.2 Control algorithm

The main idea of the STMD model is that the damping element in the tuned mass damper systems presented in chapter 2 is replaced with an MR damper. Therefore, the spring stiffness parameter of STMDs is determined by using Eq. (2.24). This section will focus on generating an algorithm to control the MR damper in the STMD system.

By substituting the displacement of the main beam Z_B expressed in series as shown

in Eq. (2.24) into Eqs. (3.4) and using the orthogonality property of the normal modes, then they result

$$\begin{cases} m_{Bi}\ddot{q}_{Bi}(t)+c_{Bi}\dot{q}_{Bi}(t)+k_{Bi}q_{Bi}(t)=F_{vi}(t)+F_{Ti}(t); & i=1...N_B \\ m_{s_j}\ddot{Z}_{sj}+k_{sj}\left(Z_{sj}-Z_{Bj}\right)+u_j=0; & j=1...N_T \end{cases} \tag{3.6}$$

where m_{Bi}, c_{Bi} and k_{Bi} are the ith modal mass, damping coefficient and stiffness of the main beam, respectively. The modal external force F_{vi} is described in Eq. (2.8). The MR force F_{MRj} has been replaced by the active control force u_j. The ith modal force induced by the STMDs are expressed

$$F_{Ti}=\sum_{j=1}^{N_T}\phi_{Bi}(d_j)\left[k_{s_j}\left(Z_{s_j}-Z_{B_j}\right)+u_j\right] \tag{3.7}$$

As mentioned in section 2.2.2, the modal STMD force F_{Ti} can make Eqs. (3.6) coupled because it depends on all the modal coordinates. Therefore, the assumption of the fact that the structural transfer function at the ith resonant frequency is approximately equal to the ith modal transfer function at its resonant frequency is also adopted here. Therefore, for the ith mode, Eqs. (3.6) can be rewritten approximately as

$$\begin{cases} m_{Bi}\ddot{q}_{Bi}+c_{Bi}\dot{q}_{Bi}+k_{Bi}q_{Bi}=F_{vi}+F_{Ti}; & i=1...N_B \\ m_{s_j}\ddot{Z}_{sj}+k_{sj}\left[Z_{sj}-\phi_{Bi}(d_j)q_{Bi}\right]+u_j\approx 0; & j=1...N_T \end{cases} \tag{3.8}$$

and

$$F_{Ti}\approx\sum_{j=1}^{N_T}\phi_{Bi}(d_j)\left\{k_{s_j}\left[Z_{s_j}-\phi_{Bi}(d_j)q_{Bi}\right]+u_j\right\} \tag{3.9}$$

Additionally, the modal active control forces u_j also can lead to a couple system of differential Eqs. (3.8). However, if each modal active control force is designed to depend on q_{Bi}, Z_{sj}, $\dot{q}_{Bi}$ and $\dot{Z}_{sj}$ alone, then

$$u_j=G_{j1}q_{Bi}+G_{j2}Z_{sj}+G_{j3}\dot{q}_{Bi}+G_{j4}\dot{Z}_{sj} \tag{3.10}$$

where G_{j1}, G_{j2}, G_{j3} and G_{j4} are the control gains of the jth MR damper. More commonly, this design procedure is called independent modal space control (IMSC)[81].

Now, the set of Eqs. (3.8) are decoupled.

If $j=1:N_T$, the second equation in (3.8) is given in matrix form as

$$\ddot{\mathbf{v}}_s=\mathbf{B}_v\mathbf{S}_v+\mathbf{B}_v\mathbf{u}_i=\mathbf{B}_v\mathbf{S}_{v0}\mathbf{v}_s-\mathbf{B}_v\mathbf{S}_{v1}q_{Bi}+\mathbf{B}_v\mathbf{u}_i \tag{3.11}$$

where $\mathbf{S}_v = \mathbf{S}_{v0}\mathbf{v}_s - \mathbf{S}_{v1}q_{Bi}$; $\mathbf{u}_i = \mathbf{K}\mathbf{C}_2\mathbf{x}_i$; $\mathbf{C}_2$ is an identity matrix with the size of $2N_T \times (2N_T + 2)$, and the other matrices are expressed as follows:

$$\mathbf{B}_v = \begin{bmatrix} -\frac{1}{m_{s1}} & 0 & \dots & 0 \\ 0 & -\frac{1}{m_{s2}} & \dots & 0 \\ \dots & \dots & \dots & \dots \\ 0 & 0 & \dots & -\frac{1}{m_{sN_T}} \end{bmatrix}; \ \mathbf{v}_s = \begin{Bmatrix} Z_{s1} \\ Z_{s2} \\ \dots \\ Z_{sN_T} \end{Bmatrix}; \ \mathbf{x}_i = \begin{Bmatrix} q_{Bi} \\ \mathbf{v}_s \\ \dot{q}_{Bi} \\ \dot{\mathbf{v}}_s \end{Bmatrix};$$

$$\mathbf{S}_{v0} = \begin{bmatrix} k_{s1} & 0 & 0 & \dots & 0 \\ 0 & k_{s2} & 0 & \dots & 0 \\ \dots & \dots & \dots & \dots & \dots \\ 0 & 0 & 0 & \dots & k_{sN_T} \end{bmatrix}; \ \mathbf{S}_{v1} = \begin{Bmatrix} k_{s1}\phi_{Bi}(d_1) \\ k_{s2}\phi_{Bi}(d_2) \\ \dots \\ k_{sN_T}\phi_{Bi}(d_{N_T}) \end{Bmatrix};$$

$$\mathbf{K} = \left[\begin{array}{ccccc|ccccc} G_{11} & G_{12} & 0 & \dots & 0 & G_{13} & G_{14} & 0 & \dots & 0 \\ G_{21} & 0 & G_{22} & \dots & 0 & G_{23} & 0 & G_{24} & \dots & 0 \\ \dots & \dots & \dots & \dots & 0 & \dots & \dots & \dots & \dots & \dots \\ G_{N_T1} & 0 & 0 & \dots & G_{N_T2} & G_{N_T3} & 0 & 0 & \dots & G_{N_T4} \end{array}\right]$$

The modal active control force F_{Ti} is also rewritten in matrix form as

$$F_{Ti} = \Phi_{Fi}\mathbf{S}_{v0}\mathbf{v}_s - \Phi_{Fi}\mathbf{S}_{v1}q_{Bi} + \Phi_{Fi}\mathbf{u}_i \tag{3.12}$$

where

$$\Phi_{Fi} = \begin{Bmatrix} \phi_{Bi}(d_1) \\ \phi_{Bi}(d_2) \\ \dots \\ \phi_{Bi}(d_{N_T}) \end{Bmatrix}^{\mathrm{T}}$$

By inserting Eq. (3.12) into Eqs. (3.8) and replacing the second equation in Eqs. (3.8) with Eq. (3.11), it results

$$\begin{cases} m_{Bi}\ddot{q}_{Bi} + c_{Bi}\dot{q}_{Bi} + (k_{Bi} + \Phi_{Fi}\mathbf{S}_{v1})q_{Bi} - \Phi_{Fi}\mathbf{S}_{v0}\mathbf{v}_s = F_{vi} + \Phi_{Fi}\mathbf{u}_i \\ \ddot{\mathbf{v}}_s - \mathbf{B}_v\mathbf{S}_{v0}\mathbf{v}_s + \mathbf{B}_v\mathbf{S}_{v1}q_{Bi} = \mathbf{B}_v\mathbf{u}_i \end{cases} \tag{3.13}$$

Let $\mathbf{q}_i = \begin{Bmatrix} q_{Bi} & \mathbf{v}_s \end{Bmatrix}^{\mathrm{T}}$, Eqs. (3.13) can be expressed in matrix form as follows

$$\mathbf{M}_{qi}\ddot{\mathbf{q}}_i + \mathbf{C}_{qi}\dot{\mathbf{q}}_i + \mathbf{K}_{qi}\mathbf{q}_i = \mathbf{B}_{di}F_{vi} + \mathbf{B}_{qi}\mathbf{u}_i \tag{3.14}$$

where

$$\mathbf{M}_{qi} = \begin{bmatrix} m_{Bi} & \mathbf{0}_{1,N_T} \\ \mathbf{0}_{N_T,1} & \mathbf{I}_{N_T,N_T} \end{bmatrix}; \ \mathbf{K}_{qi} = \begin{bmatrix} (k_{Bi} + \Phi_{Fi}\mathbf{S}_{v1}) & -\Phi_{Fi}\mathbf{S}_{v0} \\ \mathbf{B}_v\mathbf{S}_{v1} & -\mathbf{B}_v\mathbf{S}_{v0} \end{bmatrix};$$

$$\mathbf{C}_{qi} = \begin{bmatrix} c_{Bi} & \mathbf{0}_{1,N_T} \\ \mathbf{0}_{N_T,1} & \mathbf{0}_{N_T,N_T} \end{bmatrix};\ \mathbf{B}_{di} = \begin{Bmatrix} 1 \\ \mathbf{0}_{N_T,1} \end{Bmatrix};\ \mathbf{B}_{qi} = \begin{Bmatrix} \Phi_{Fi} \\ \mathbf{B}_v \end{Bmatrix};\ \mathbf{u}_i = \mathbf{K}\mathbf{C}_{2i}\mathbf{x}_i$$

and $N_{T1} = N_T + 1$

If an uncertain model is considered, then three structural parameters, m_{Bi}, c_{Bi} and k_{Bi} can be assumed that their values are within certain known intervals and can be expressed as

$$m_{Bi} = \overline{m}_{Bi}(1 + p_m\delta_m);\ c_{Bi} = \overline{c}_{Bi}(1 + p_c\delta_c);\ k_{Bi} = \overline{k}_{Bi}(1 + p_k\delta_k) \tag{3.15}$$

where $\overline{m}_{Bi}$, $\overline{c}_{Bi}$ and $\overline{k}_{Bi}$ are the so-called nominal values of m_{Bi}, c_{Bi} and k_{Bi}, respectively; δ_m, δ_c and δ_k represent the uncertain parameters and satisfy $|\delta_i| \leq 1$ with $i = m, c$ and k; p_m, p_c and p_k are constants whose values determine coefficients of variation of the beam properties.

Similarly to the above TMD optimization problem with the uncertain mode presented in section 2.2.2, the *DK-iteration* procedure[62] is also used here to find the control gain matrix $\mathbf{K}$ in Eq. (3.14) with the uncertain parameters in Eq. (3.15). Firstly, the uncertain parameters are collected in a block-diagonal matrix of stable perturbations and "pulled out". This process is presented in Fig. 2.4.

Then, in the form of linear fraction transformation[62], the matrices $\mathbf{M}_{qi}$, $\mathbf{C}_{qi}$ and $\mathbf{K}_{qi}$ can be rewritten as

$$\mathbf{K}_{qi} = \mathscr{F}(\mathbf{K}_{mi}, \delta_k) \quad \text{and} \quad \mathbf{K}_{mi} = \left[\begin{array}{c|c} 0 & \mathbf{K}_{i2} \\ \hline \mathbf{K}_{i3} & \mathbf{K}_{i4} \end{array}\right] \tag{3.16}$$

where

$$\mathbf{K}_{i2} = \begin{bmatrix} \overline{k}_{Bi} & \mathbf{0}_{1,N_T} \end{bmatrix};\ \mathbf{K}_{i3} = \begin{bmatrix} p_k \\ \mathbf{0}_{N_T,1} \end{bmatrix};\ \mathbf{K}_{i4} = \begin{bmatrix} \overline{k}_{Bi} + \Phi_{Fi}\mathbf{S}_{v1} & -\Phi_{Fi}\mathbf{S}_{v0} \\ \mathbf{B}_v\mathbf{S}_{v1} & -\mathbf{B}_v\mathbf{S}_{v0} \end{bmatrix}$$

and the other matrices $\mathbf{M}_{qi}$ and $\mathbf{C}_{qi}$ are described in Eqs. (2.14) and (2.15), respectively.

After some algebraic manipulations, the sate space equations governing the system dynamic behavior are given by

$$\begin{cases} \dot{\mathbf{x}}_i = \mathbf{A}_{1mi}\mathbf{x}_i + \mathbf{D}_{1mi}\mathbf{w}_{\Delta i} + \mathbf{B}_{1mi}F_{vi} + \mathbf{B}_{2mi}\mathbf{u}_i \\ \mathbf{z}_i = \mathbf{C}_{1i}\mathbf{x}_i + \mathbf{D}_{11i}F_{vi} + \mathbf{D}_{12i}\mathbf{u}_i \\ \mathbf{z}_{\Delta i} = \mathbf{A}_{1zi}\mathbf{x}_i + \mathbf{D}_{1zi}\mathbf{w}_{\Delta i} + \mathbf{B}_{1zi}F_{vi} + \mathbf{B}_{2zi}\mathbf{u}_i \\ \mathbf{u}_i = \mathbf{K}\mathbf{C}_{2i}\mathbf{x}_i \end{cases} \tag{3.17}$$

where the matrices in the above equation were determined as Eqs. (2.20).

Here, the minimized objectives in the H_∞ optimization are the acceleration and displacement of the main beam. Then, the controlled output is defined as $\mathbf{z}_i = [\ddot{q}_{Bi} \quad \alpha q_{Bi}]^{\mathrm{T}}$, where the scalar weighting α is used to control trade-off between the acceleration and the displacement in the optimization process. The matrices of $\mathbf{C}_{1i}$, $\mathbf{D}_{11i}$ and $\mathbf{D}_{12i}$ in the controlled output $\mathbf{z}_i$ are also expressed in Eq. (2.21)

Finally, the transfer function is derived as

$$\mathbf{T}_{wzi} = \mathbf{C}_i \left(s\mathbf{I} - \mathbf{A}_i\right)^{-1} \mathbf{B}_{1ui} + \mathbf{D}_{11ui} \tag{3.18}$$

where $\mathbf{A}_i$, $\mathbf{B}_{1ui}$, $\mathbf{C}_i$ and $\mathbf{D}_{11ui}$ are expressed in Eq. (2.22) and the optimization problem based on the *DK-iteration* procedure to find the control gain matrix $\mathbf{K}$ in the case of multi-mode problem as follows:

$$\min_{\mathbf{K}} \left(\min_{\mathbf{D}_1 \in \mathscr{D}} \left\| \alpha_1 \mathbf{D}_1 \mathbf{T}_{wzi} \mathbf{D}_1^{-1} \right\|_\infty ; \ldots ; \min_{\mathbf{D}_{N_B} \in \mathscr{D}} \left\| \alpha_{N_B} \mathbf{D}_{N_B} \mathbf{T}_{wzN_B} \mathbf{D}_{N_B}^{-1} \right\|_\infty \right) < \gamma \tag{3.19}$$

where γ is an upper bound constant; N_B is the number of the considered modes; the factor $\alpha_{i(=1\ldots N_B)}$ is to control the trade-off between the influences of modes in the optimization process; $\mathscr{D}$ is a set of matrices $\mathbf{D}$ which commute with Δ (i.e. satisfy $\mathbf{D}\Delta = \Delta\mathbf{D}$; $\Delta = \mathrm{diag}[\delta_m; \delta_c; \delta_k]$). $\mathbf{D}_i$ is a block-diagonal scaling matrix to make γ tighter.

Physical and modal coordinate

Modal coordinates are not physical coordinates and therefore cannot be measured directly. Since distributed sensors are not always available, discrete sensors are usually used. Suppose the displacements can be obtained at certain points x_i, $i = 1, \ldots, N_s$, where N_s discrete sensors are used, and the first N_B modal coordinates need to be determined. After some algebraic manipulations of Eq. (2.5), the modal coordinates of the main beam can be reformulated as

$$\mathbf{q}_B = \mathbf{D}_B^{-1} \mathbf{Z}_{Bs} \tag{3.20}$$

where $\mathbf{D}_B$ is the $N_s \times N_B$ modal matrix

$$\mathbf{D}_B = \left\{ \begin{array}{cccc} \Phi_B^{\mathrm{T}}(x_1) & \Phi_B^{\mathrm{T}}(x_2) & \ldots & \Phi_B^{\mathrm{T}}(x_{N_s}) \end{array} \right\}^{\mathrm{T}}$$

and $\mathbf{Z}_{Bs}$ is the $N_s \times 1$ actual response vector corresponding to the number of sensors N_s at the positions $x_1, x_2, \ldots x_{N_s}$ on the beam

$$\mathbf{Z}_{Bs} = \left\{ \begin{array}{cccc} Z_B(x_1) & Z_B(x_2) & \ldots & Z_B(x_{N_s}) \end{array} \right\}^{\mathrm{T}}$$

If $N_s \neq N_B$, the inverse matrix $\mathbf{D}_B^{-1}$ can be replaced by the pseudo-inverse matrix $\mathbf{D}_B^{+}$.

Similarly to the case of displacement, modal velocities and accelerations can be determined as

$$\dot{\mathbf{q}}_B = \mathbf{D}_B^{-1}\dot{\mathbf{Z}}_{Bs};\ \text{and}\ \ddot{\mathbf{q}}_B = \mathbf{D}_B^{-1}\ddot{\mathbf{Z}}_{Bs} \tag{3.21}$$

In fact, this procedure converts the discrete sensor measurements at particular points of the system into approximate continuous displacements, velocities and accelerations in modal space. Commonly, it is known as the modal filter for control of structures[82]. Besides, all the feedback control designs discussed above have one thing in common, namely they are all based on the assumption that the full state vector is available for measurement. Then, the current control vector is assumed as a function of the current state vector.

Indeed, it is not practical to measure the full state vector, but only some certain structural responses because using so many sensors can lead to a higher implementation cost as well as difficulty in measuring all the needed variables. Thus, the design of observers, such as the Kalman observer, the H_∞ observer and other nonlinear observer approaches[83] that introduce an algorithm permitting an estimate of a full state vector from some measured data with high accuracy and noise reduction is necessary. This topic has been discussed in many previous papers and lectures about control engineering[82,83] and thus, it is not presented here.

To this end, the semi-active H_∞ control system can be depicted in figure 3.13.

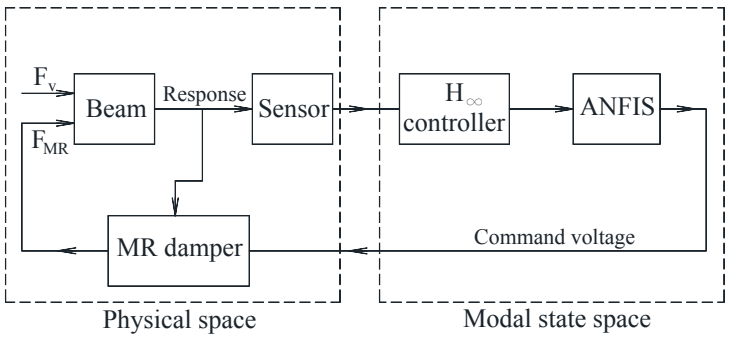

Figure 3.13: Structure of the semi-active controller for reducing the beam vibration with STMDs

3.4 Numerical simulation and discussion

In this section, the performance of the semi-active static output feedback H_∞ controller applied to the simply supported beam and the double-span continuous beam under the high-speed train HSLM-A8 is evaluated. The physical properties of the beams are listed in Table 2.2.

3.4.1 Simply supported beam

In simply supported bridges experiencing resonant situations, the maximum response will most likely be associated to the contribution of the fundamental mode[84]. Under this circumstance, the response of modes different from the resonant mode is practically negligible in the optimization process. The design objective of the controller is to find the control gain $\mathbf{G}_1 = [G_{11}\ G_{12}\ G_{13}\ G_{14}]$. Firstly, by setting the mass ratio μ_{s1}=2%, the spring stiffness k_{s1} is obtained from Eq. (2.23) and its value is 2.967×10^6 N/m. Then, after some iterations of the optimization process by solving index (3.19) for the certain model with and without the constraint of the upper bound of the actual MR force, corresponding to the cases called active 1 and active 2, the control gain vectors are obtained as presented in Table 3.2.

Table 3.2: Control gain vector

Type	$\mathbf{p} = [p_k\ p_c\ p_m]$	$\mathbf{G}_1 = [G_{11}\ G_{12}\ G_{13}\ G_{14}]$
Active 1	[0 0 0]	$10^5 \times [3.347\ \ -9.836\ \ -3.490\ \ 0.166]$
Active 2	[0 0 0]	$10^8 \times [-3.026\ \ 0.009\ \ 0.016\ \ 0.005]$
Active (uncertain model)	[0.1 0 0.05]	$10^5 \times [-8.183\ \ -7.376\ \ -3.468\ \ 0.259]$

The first result is presented in Fig. 3.14 showing the transfer function magnitude with and without the damper versus frequency. It may be seen that the control gain vector determined above can lead to the minimum response of the main system in frequency band of interest.

By implementing the obtained control gain vectors into the control system, the response of the main beam under the HSLM-A8 train load is analyzed in Fig. 3.15. Firstly, it can be found that the actual damping force generated by the MR damper can track the desired control force quite well except some deterioration ranges because of the constraints of the MR damper in which its force is only produced in the first and third quadrants of the hysteretic force-velocity plane meanwhile the desired force can be produced in any of the four quadrants. The upper and lower limits of the MR force are also its constraints. Moreover, Fig. 3.15 also proves that the phenomenon of the control spillover is not evident in this case.

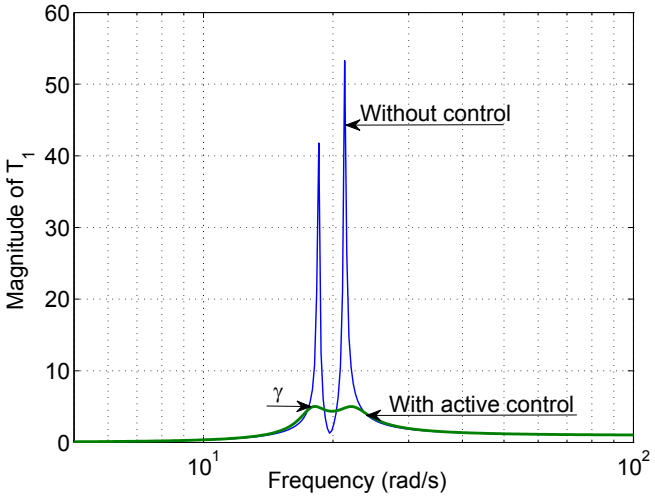

Figure 3.14: Magnitude of closed-loop transfer functions T_1 versus frequency

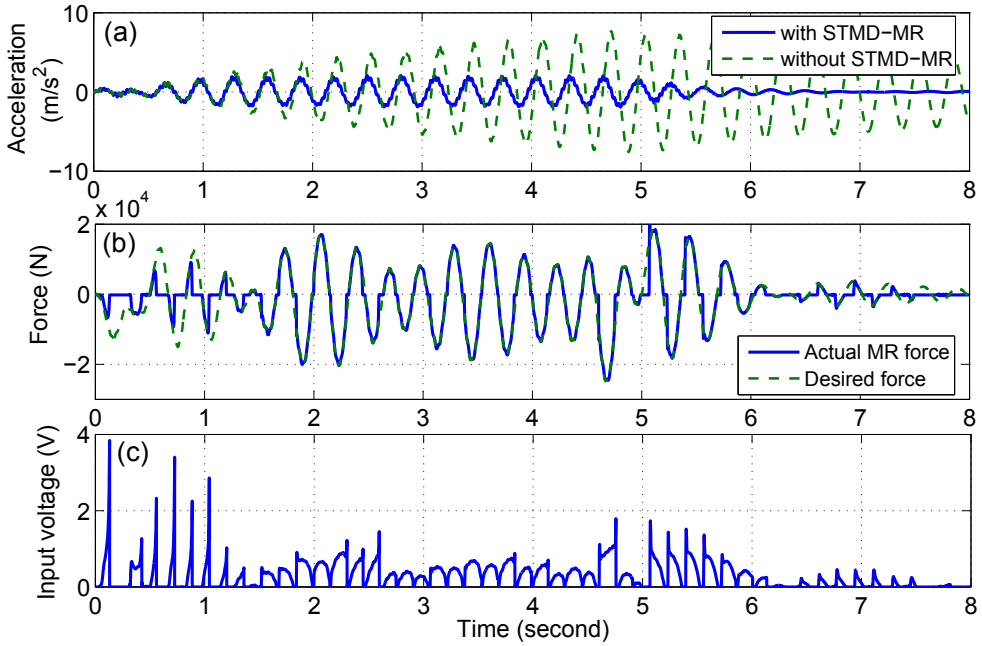

Figure 3.15: Response in time domain: (a) acceleration of the main beam with and without STMD versus time; (b) comparison of the actual STMD and the desired control force; (c) input voltage to STMD

Table 3.3: Maximum acceleration and displacement at midspan of the main beam under the train load

Response	Peak-to-peak value				
	W/o damper	Passive	Semi-active	Active 1	Active 2
a (m/s^2)	7.417	2.504	2.075	2.063	1.104
d (mm)	23.111	9.958	8.941	9.078	5.822

Considering frequency or speed domain, the accelerations at the main beam midspan are presented in Fig. 3.16a and Table 3.3. These results are obtained by using FEM to analyze the structural dynamic response with four cases including the beam without dampers, with one TMD (passive), with one STMD (semiactive), with one active damper (active 1) in which the optimization process considers the upper limit of the actual MR damper force according to the device ability, and finally also with one active damper (active 2) but neglecting the MR force limit. The maximum accelerations at the main beam midspan with the passive damper, the STMD and the active damper (active 1) decrease by about 67.3 %, 73.8% and 80.3%, respectively, when compared to the case without damper.

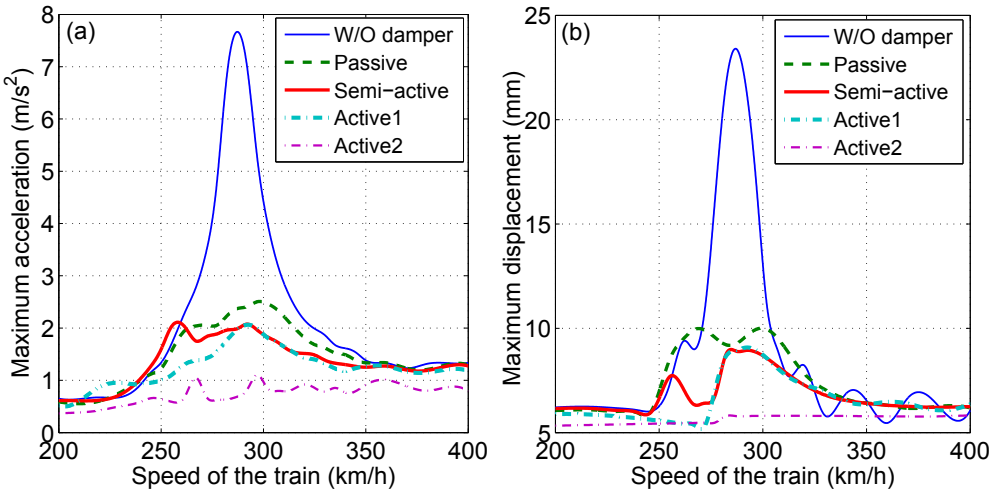

Figure 3.16: Response of the beam versus speed of the train: (a) acceleration; (b) displacement

Similarly to the case of acceleration, Fig. 3.16b and Table 3.3 also show that the displacements of the main beam under the train load are also reduced significantly. These results demonstrate the effectiveness of the active and semi-active dampers controlled by the proposed algorithm. Especially, in the case of the active-2 damper, the structural responses reduce dramatically. It shows that the desired active control force obtained by using the proposed optimization control algorithm is very effective. Thus, if it is possible to choose a MR damper in practice fulfilling the requirements of this desired

active force, the reduction in structural response of the beam will be improved much more. However, to date, it is known that commercial productions of MR dampers have still not been various. This is one of the drawbacks of designing damping systems using MR dampers in practice.

Detuning effect

It is well-known that optimal control gains used to generate the desired control forces are significantly affected by the controlled structure frequencies. Therefore, knowledge of the controlled primary structures is required in order to accurately calculate the control forces. However, structural property estimation and fabrication errors, the time-variant characteristics of the combined system may also make the primary frequencies tuned incorrectly. Thus, the optimization of the parameters of TMDs and MR dampers on an uncertain model proposed above is expected to be a solution to reduce their sensitivity to incorrect frequency tuning, and the dampers become more reliable and applicable for vibration control. To clarify the effectiveness of the present algorithm, a numerical simulation for the structure system with its properties in Table 2.2 is considered. Firstly, the uncertain parameters in Eq. (3.15) are set as follows: $p_k = 0.1$, $p_c = 0$ and $p_m = 0.05$, and then the control gain of the desired force may be obtained by minimizing index (3.19). The result is presented in Table 3.2.

The maximum response of the main beam with the STMD versus mistuned primary frequencies is shown in Fig. 3.17. It shows that when the original frequency of the main beam (ω_B) is tuned incorrectly by increasing ω_B to $(\omega_B + \Delta\omega)$, where $0 \leq \Delta\omega \leq 15\%$, the maximum acceleration of the main beam with the passive tuned mass damper increases significantly. This is equivalent to the attenuation of the effectiveness of the traditional tuned mass damper. Meanwhile, the semi-active damper controlled by the proposed algorithm shows very little influence although only a single STMD is used here. This can confirm that the present STMD model is much more effective and stable than the passive tuned mass damper even if the detuning effects happen.

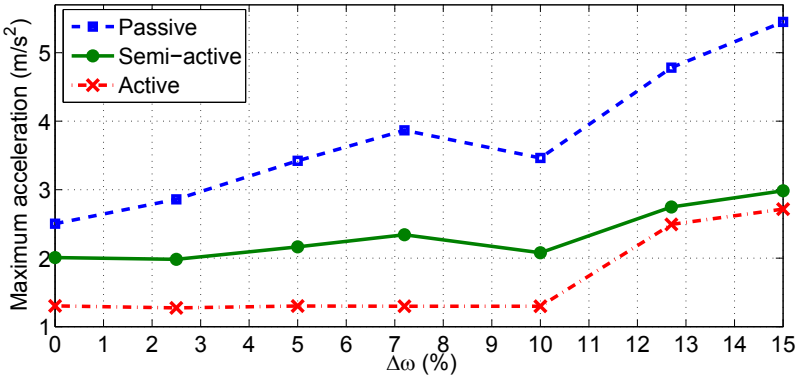

Figure 3.17: Maximum acceleration at midspan of the main beam versus detuned frequencies on the uncertain model

3.4.2 Multi-mode control of double-span continuous beam with STMDs

The dynamic performance of the double-span continuous bridge with STMDs, whose properties are included in Table 2.2, is evaluated in this section. The contribution of the first two modes of the beam vibration is now taken into account in the optimization process to predict the desired control forces. Besides, it can be shown that the optimal locations for the placement of STMDs, when the number of devices is intended to be minimum, are at the sections of maximum modal amplitude. For the two-span continuous beam, due to dominance of the first and second modes, optimal locations are the mid section of each span. Two STMDs are assumed to be placed at the locations $L/4$ and $3L/4$ where $L/2$ is the length of each span. The STMDs are employed to reduce simultaneously responses of the first two modes of the main structure under the circulation of the HSLM-A8 train in the range of high speed.

Firstly, the spring stiffness parameters of STMDs are also determined by minimizing index Eq. (2.23), and their obtained values are 2.933×10^6 N/m and 7.237×10^6 N/m, corresponding to the spring stiffness of the first and second STMD.

Then, by minimizing index (3.19), the control gains can be obtained as shown in Table 3.4. These control gains are implemented into the controller. The finite element method is also used to analyze the response of the system. As a result, the tracking ability of the first MR damper that follows its desired control force is shown in Fig. 3.19. In this case, an unexpected result happens. The actual damping force cannot track the desired control well and there are so many deterioration ranges. The reason for this is the limitation constraints of actual MR dampers mentioned in Section 3.2.4. It means that the desired control force with the control gains in Table 3.4 is almost generated in the second and fourth quadrants of the MR hysteresis while the MR damper only produces forces in the first and third quadrants as shown in Fig. 3.18.

Table 3.4: Control gain vectors in the control system

STMD	Location	$\mathbf{G} = [G_{i1}\ G_{i2}\ G_{i3}\ G_{i4}]$
1	$L/4$	$10^4 \times [1.527\ \ -2.756\ \ -1.651\ \ -0.171]$
2	$3L/4$	$10^4 \times [0.399\ \ 0.318\ \ 1.129\ \ 0.718]$

In order to improve the tracking ability of MR damper forces, after a trial-and-error process, a combination of the modal state vector and the control gains instead of the previous combination presented in Eq. (3.10) is proposed as

$$u_j = G_{j1}q_{Bi} + G_{j2}Z_{sj} - G_{j3}\dot{q}_{Bi} + G_{j3}\dot{Z}_{sj} = G_{j1}q_{Bi} + G_{j2}Z_{sj} + G_{j3}(\dot{Z}_{sj} - \dot{q}_{Bi}) \quad (3.22)$$

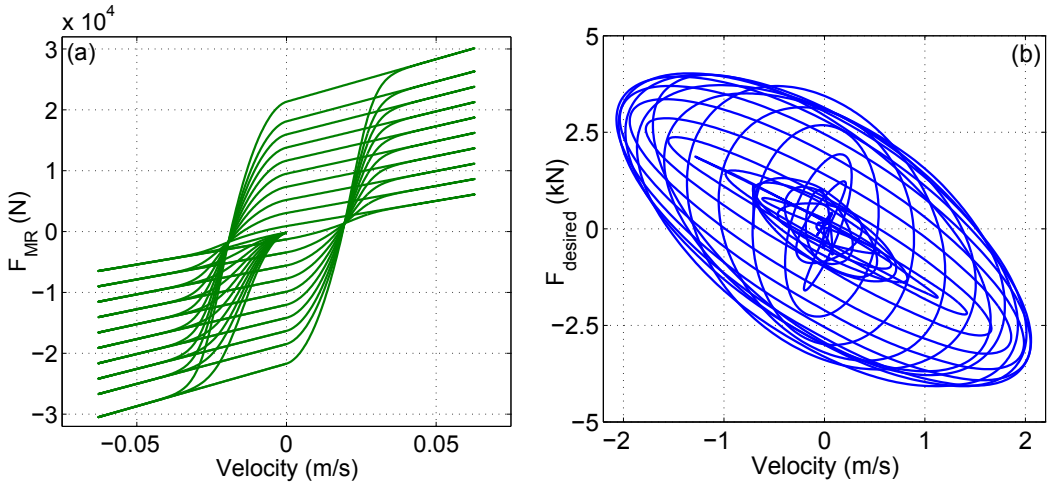

Figure 3.18: Hysteresis behavior of (a) the MR damper force for a 1Hz sinusoidal excitation and $u_j = 0.1 \rightarrow 2$ V; (b) the desired force to control the 1st MR damper with the optimal control gain $\mathbf{G}_1 = 10^4 \times [1.527 \ \ -2.756 \ \ -1.651 \ \ -0.171]$ in Table 3.4 ($v_{\text{train}} = 300$ km/h)

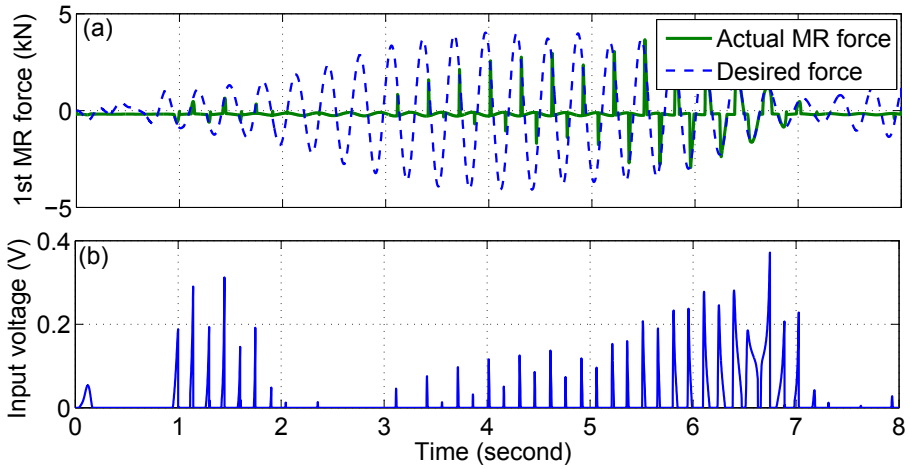

Figure 3.19: (a) Comparison of the 1st actual MR damper force and its desired control force with the optimal control gain $\mathbf{G}_1 = 10^4 \times [1.527 \ \ -2.756 \ \ -1.651 \ \ -0.171]$ ($v_{\text{train}} = 300$ km/h); (b) input voltage to the 1st MR damper

and the matrix $\mathbf{K}$ in Eq. (3.11) is rewritten as follows

$$\mathbf{K} = \left[\begin{array}{ccccc|ccccc} G_{11} & G_{12} & 0 & \ldots & 0 & -G_{13} & G_{13} & 0 & \ldots & 0 \\ G_{21} & 0 & G_{22} & \ldots & 0 & -G_{23} & 0 & G_{23} & \ldots & 0 \\ \ldots & \ldots & \ldots & \ldots & 0 & \ldots & \ldots & \ldots & \ldots & \ldots \\ G_{N_T1} & 0 & 0 & \ldots & G_{N_T2} & -G_{N_T3} & 0 & 0 & \ldots & G_{N_T3} \end{array}\right]$$

It might be known that the new combination in Eq. (3.22) can generate a desired control force less effective than that generated by Eq. (3.10). However, it is expected that the tracking ability of the actual MR force will be improved.

Similarly, by minimizing index in Eq. (3.19) with u_j in Eq. (3.22) instead of Eq. (3.10), the control gains can be obtained as shown in Table 3.5.

Table 3.5: Control gain vectors in the control system

STMD	Location	$\mathbf{G} = [G_{i1}\ G_{i2}\ G_{i3}]$
1	$L/4$	$10^4 \times [-3.993\ \ -4.954\ \ 2.070]$
2	$3L/4$	$10^4 \times [-2.005\ \ 9.012\ \ 2.740]$

Figs. 3.20 and 3.21 show the response of the main beam under the HSLM-A8 train load at the first and second midspans. Especially, the tracking ability of the MR dampers are improved. Besides, the structural resonant responses are reduced by 47% for acceleration and 37% for displacement as shown in Table 3.6. In Fig. 3.22, both of the resonant peaks of the acceleration and displacement curves are reduced significantly over the speed range of interest. Again, these results can show the effectiveness of the MR dampers controlled by the present algorithm in the case of the multi-mode control problem.

Table 3.6: Maximum acceleration and displacement at the second midspan of the main beam under the train load

Response	Peak-to-peak value		
	w/o damper	semi-active	active
a (m/s^2)	11.540	6.021	6.208
d (mm)	15.247	9.596	9.423

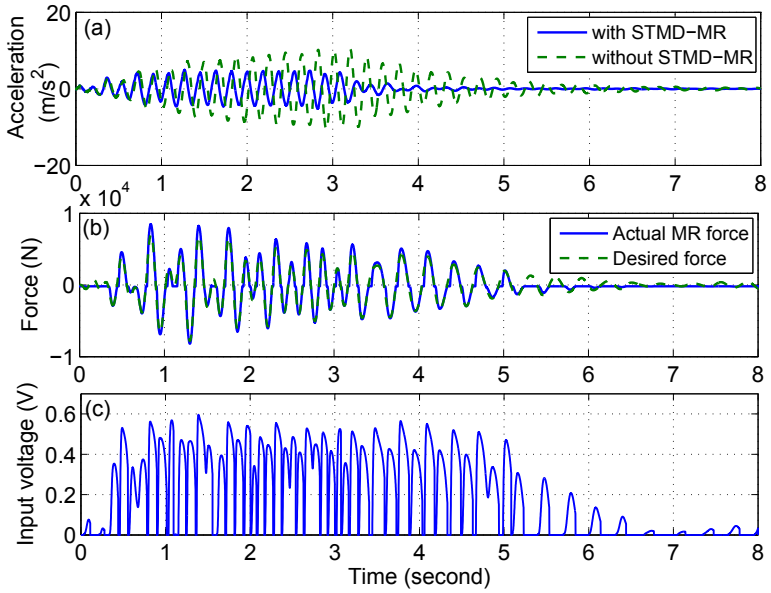

Figure 3.20: Response at the first midspan of the main beam in time domain: (a) acceleration without MR damper and with MR damper versus time; (b) comparison of the actual MR damper force and the desired control force; (c) input voltage to MR damper

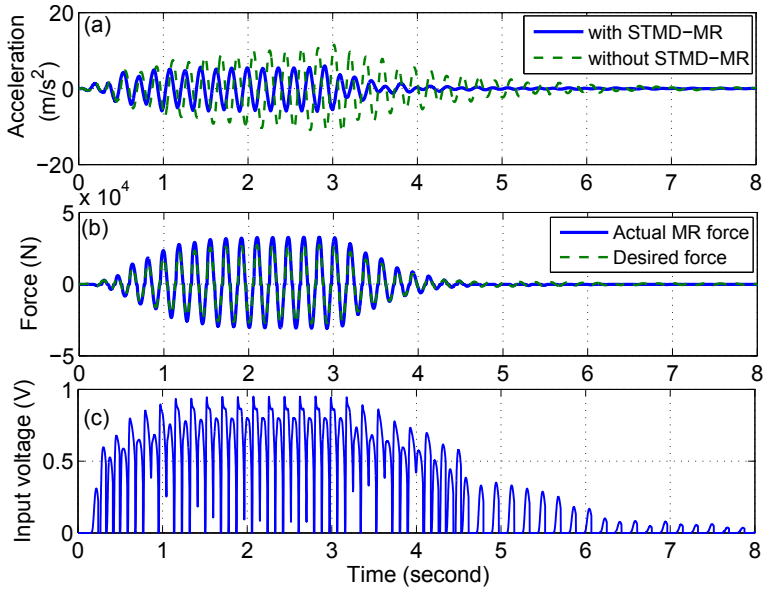

Figure 3.21: Response at the second midspan of the main beam in time domain: (a) acceleration without MR damper and with MR damper versus time; (b) comparison of the actual MR damper force and the desired control force; (c) input voltage to MR damper

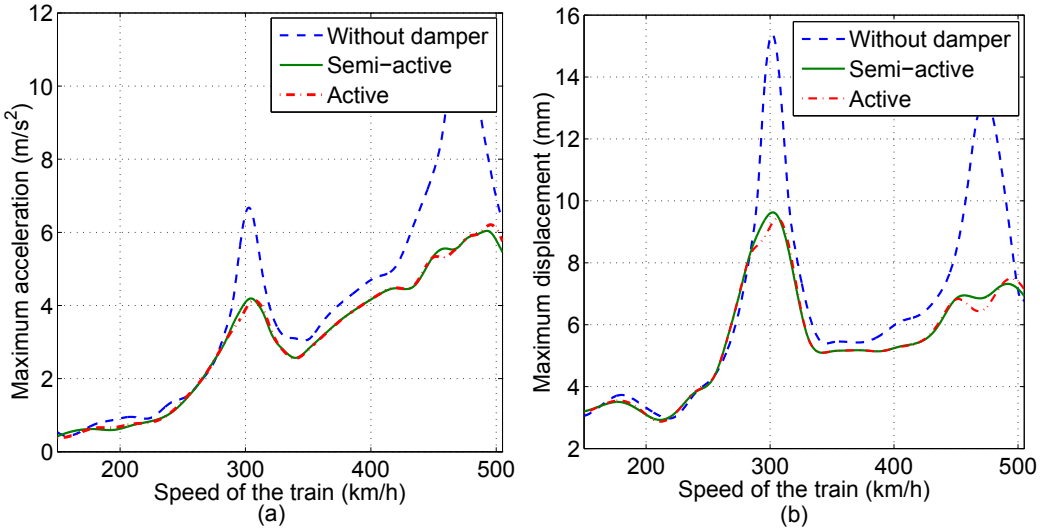

Figure 3.22: Response at the second midspan of the main beam versus train speed: (a) acceleration ; (b) displacement

3.5 Conclusions

Semi-active vibration control of railway bridges under the high-speed train has been investigated. The static output feedback H_∞ controller combined with the ANFIS inverse model of MR dampers proposed in this work can achieve compatible performance. Especially, the proposed control scheme, validated by the numerical simulations, can extend the band of suppression frequency and significantly reduce the detuning effect. This can show that the main drawback of the traditional TMD systems is overcome.

Moreover, the approach of the MR damper inverse model by using the ANFIS model in this study can provide the quite exact predictions about command voltage to control MR dampers effectively. This makes the control voltage versus time diagram smoother and avoids suddenly changing the MR forces.

Chapter 4

Fluid viscous damper

4.1 Introduction

As mentioned, although fluid viscous dampers (FVDs) have been used widely, a significant number of studies continues to appear in this area. It is due to the fact that optimization problems of FVDs are quite complicated, in which finding their solutions for FVD models corresponding to different applications is very different. Thus, no any solution for FVD problems is perfect, which cannot only give the optimal parameters of FVDs accurately, but also be easily to be used. In this chapter, a new approach is established based on H_∞ norm to find optimal damping parameters of FVDs implemented in high-speed railway bridges. The present method can include structural damping properties, minimize simultaneously structural response at multiple modes and also be extended to nonlinear problems to determine the optimal parameters of nonlinear fluid viscous dampers. Especially, the analytical closed-form expressions are also found based on the perturbation method[85] in some particular cases.

4.2 Fluid viscous damper linearization

Fluid viscous dampers operate on the principle of fluid flow through orifices either around or through the piston head. The dampers consist of a hollow cylinder filled with fluid typically being silicone[11]. The piston head orifice design can alter the flow characteristics with the fluid speed so that the output force is proportional to $|\dot{y}|^{\alpha}$, where $\dot{y}$ is the piston rod velocity and α is the predetermined coefficient. For α equal to unity, the damper may be described as an ideal linear viscous damper.

Some previous studies[11,57] showed that the energy dissipation characteristics of linear and nonlinear fluid dampers are different. If the damper is subjected to a harmonic relative displacement, the energy dissipation per cycle is determined in Table. 4.1.

Table 4.1: Energy dissipation per cycle,[11]

Exponent factor, α	2	1	0.5
$\frac{E_d}{F_{D\max}Y}$	2.667	3.142	3.496

Note: E_d is the energy dissipation per cycle; $F_{D\max}$ and Y are the maximum force and the displacement amplitude of the FVD, respectively.

As shown in Table 4.1, for the same level of maximum force and amplitude of motion, the energy dissipated per cycle increases as the α exponent decreases. Because of this, it is commonly used as a passive energy dissipation device for structures subjected to extremely high velocity shocks and the cases that need to limit the peak forces in FVDs.

For the optimization of the fluid viscous damper parameters, expressing the equations of motion in the modal space might be a convenient approach to objective functions. Therefore, converting nonlinear damper forces of FVDs into equivalent linear damper forces is used in this study. In 1998, Symans[11] suggested a formula for this linearization by using the equivalent energy method. Here, another approach to Symans' well-known formula by using the harmonic balance method[86] is derived as follows:

The damper force of a nonlinear FVD system may be expressed as

$$F_D(\dot{y}) = C_\alpha \, |\dot{y}|^\alpha \, \mathrm{sgn}(\dot{y})$$

where C_α, $\dot{y}$ and α are the damper coefficient, the damper velocity and the fractional power law, respectively.

What is needed is a means to obtain

$$F_D(\dot{y}) \simeq C_{eq}\dot{y} \tag{4.1}$$

where C_{eq} is the equivalent damping coefficient.

Choosing a trial output $y = Y\sin(\omega_0 t)$, the nonlinear form of $F_D(\dot{y})$ can be expanded as a Fourier series

$$F_D(\dot{y}) = F_D(Y\omega_0\cos(\omega_0 t)) = a_0 + \sum_{n=1}^{\infty} a_n \cos(n\omega_0 t) + \sum_{n=1}^{\infty} b_n \sin(n\omega_0 t) \tag{4.2a}$$

and the harmonic amplitude coefficients can be evaluated using the expressions

$$a_0 = \frac{1}{2\pi}\int_0^{2\pi} F_D(Y\omega_0\cos(\omega_0 t))\mathrm{d}(\omega_0 t) = \frac{1}{2\pi}\int_0^{2\pi} F_D(Y\omega_0\cos\theta)\mathrm{d}\theta \tag{4.2b}$$

$$a_n = \frac{1}{\pi}\int_0^{2\pi} F_D(Y\omega_0\cos(\omega_0 t))\cos(n\omega_0 t)\mathrm{d}(\omega_0 t) = \frac{1}{\pi}\int_0^{2\pi} F_D(Y\omega_0\cos\theta)\cos(n\theta)\mathrm{d}\theta \tag{4.2c}$$

$$b_n = \frac{1}{\pi}\int_0^{2\pi} F_D(Y\omega_0\cos(\omega_0 t))\sin(n\omega_0 t)\mathrm{d}(\omega_0 t) = \frac{1}{\pi}\int_0^{2\pi} F_D(Y\omega_0\cos\theta)\sin(n\theta)\mathrm{d}\theta \tag{4.2d}$$

where $\theta = \omega_0 t$

By retaining the fundamental of the periodic function $F_D(\dot{y})$ and restricting it to be an even function, $a_0 = b_1 = 0$ then

$$F_D(\dot{y}) = F_D(Y\omega_0\cos(\omega_0 t)) \simeq a_1\cos\theta = \frac{1}{\pi}\int_0^{2\pi} F_D(Y\omega_0\cos\theta)\cos\theta\mathrm{d}\theta\cos\theta \tag{4.3}$$

By substituting Eq. (4.3) into Eq. (4.1) and using the Gamma integral table[87] to calculate the integral $\int_0^{2\pi}\cos^{\alpha}\theta\cos\theta\mathrm{d}\theta$, then the equivalent damping of the system may be written as follows

$$C_{eq} = \frac{1}{\pi\omega_0 Y}\int_0^{2\pi}\cos\theta F_D(Y\omega_0\cos(\theta))\mathrm{d}\theta = \frac{1}{\pi\omega_0 Y}\int_0^{2\pi} C_\alpha Y^\alpha\omega_0^\alpha\cos^\alpha\theta\,\mathrm{sgn}(\dot{y})\cos\theta\mathrm{d}\theta \tag{4.4a}$$

$$C_{eq} = \frac{2}{\pi}C_\alpha Y^{(\alpha-1)}\omega_0^{(\alpha-1)}\frac{\Gamma(1+\frac{\alpha}{2})\Gamma(\frac{1}{2})}{\Gamma(\frac{3}{2}+\frac{\alpha}{2})} \tag{4.4b}$$

It should be noticed that in Eq. (4.4) the equivalent damping depends on the term Y, which is the displacement amplitude of the main system at the position of the FVD. Thus, optimal equivalent damping coefficients are almost impossible to find if Eq. (4.4) still contains $Y^{(\alpha-1)}$. Therefore, a procedure to eliminate Y in Eq. (4.4) is derived in the next sections before the equivalent damping coefficients are implemented into the objective functions to find the optimal values.

4.3 Problem formulation

4.3.1 Dynamic modeling of structural system

The system configuration considered consists of a main beam, an auxiliary beam with FVDs installed to connect both of the beams and a series of vehicles as shown in Figs. 4.2 and 4.1. The structural parameters and the modal properties of the systems are given in Table 2.2.

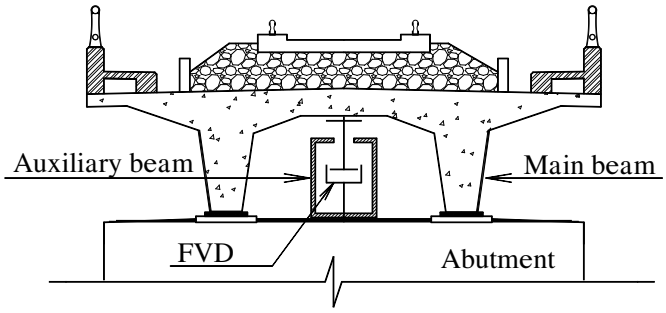

Figure 4.1: Retrofit configuration for concrete girder bridge

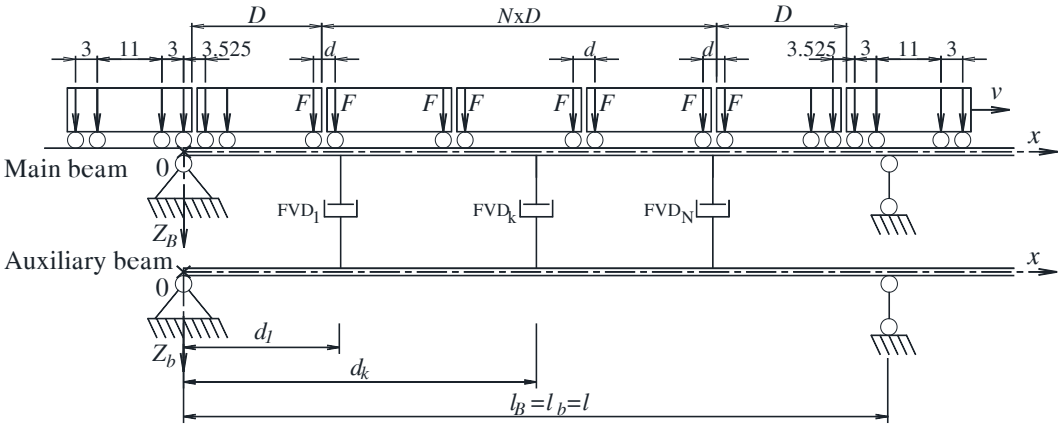

Figure 4.2: Train-bridge system with FVD

The auxiliary beams are steel box girders with a constant cross section inside which the FVDs are to be installed. The external dimensions of the auxiliary beam are $b \times h_b$ (width $\times$ height) and its wall thickness is e . The inertia moment is $I = (bh_b^3 - (b - 2e)(h_b - 2e)^3)/12$ and the mass per unit length is $\overline{m}_b = \rho_b(bh_b - (b-2e)(h_b-2e))$, where $\rho_b = 7850\ \mathrm{kg/m^3}$ is the mass density of steel. The width and the wall thickness of the auxiliary beam are considered as the functions of the beam height[53] as follows:

$$b = a \times h_b \text{ for } a = 0.6 \text{ and } e = e_0 + e_1 \times h_b + e_2 \times h_b^2$$

where $e_0 = 2.14 \times 10^{-2}$ (m), $e_1 = 7.86 \times 10^{-3}$ and $e_2 = 1.07 \times 10^{-2}$ (m^{-1})

Defining the beam geometry in this way allows performing parametric analysis in terms of just one parameter, h_b, which completely defines the element mass and the natural frequency.

The equations of motion can be derived by using standard techniques[64]:

$$\begin{cases} \frac{\partial^2}{\partial x^2}\left[EI_B\frac{\partial^2 Z_B(x,t)}{\partial x^2}\right] + \overline{m}_B\frac{\partial^2 Z_B(x,t)}{\partial t^2} + c_B\frac{\partial Z_B(x,t)}{\partial t} = F_v(x,t) - F_D(x,t) \\ \frac{\partial^2}{\partial x^2}\left[EI_b\frac{\partial^2 Z_b(x,t)}{\partial x^2}\right] + \overline{m}_b\frac{\partial^2 Z_b(x,t)}{\partial t^2} + c_b\frac{\partial Z_b(x,t)}{\partial t} = F_D(x,t) \end{cases} \tag{4.5}$$

where the coordinate origin of x is assumed to be at the left-hand end of each beam; $Z_{B(b)}$, $EI_{B(b)}$, $\overline{m}_{B(b)}$ and $c_{B(b)}$ are the vertical displacement, bending stiffness, mass and viscous damping per unit length of the main beam (the auxiliary beam), respectively; $F_v(x,t)$ is the total vertical force of the train applied to the main beam and $F_D(x,t)$ is the total force generated by FVDs. The force $F_v(x,t)$ is determined in Eq. (2.2).

The force $F_D(x,t)$ is determined as follows

$$F_D(t) = \sum_{i=1}^{N_D} \delta(x - d_i) C_\alpha^i \left|\dot{Z}_{Bi} - \dot{Z}_{bi}\right|^\alpha \operatorname{sgn}\left(\dot{Z}_{Bi} - \dot{Z}_{bi}\right) \tag{4.6}$$

where N_D is the total number of FVDs; d_i is the distance from the left end of the beam ($x = 0$) to the ith FVD; C_α^i is the damper coefficient of the ith FVD; sgn() is the signum function and α is the damper velocity exponent in the range from 0.2 to 2.

An analytical solution of the equations of motion (4.5) is usually impossible. Hence, the numerical methods are most suitable for determining the response of the retrofitted systems under the moving loads. In this thesis, the finite element method and the average acceleration method for nonlinear and multiple-degree-of-freedom systems (MDOF) are used to solve Eqs. (4.5).

4.3.2 Objective function

In equations of motion (4.5), the displacement of the main beam $Z_B(x,t)$ and the auxiliary beam $Z_b(x,t)$ may be expressed in series as

$$Z_B(x,t) = \sum_{i=1}^{N_B} \phi_{Bi}(x) q_{Bi}(t) = \Phi_B^{\mathrm{T}}(x)\mathbf{q}_B(t) \tag{4.7a}$$

$$Z_b(x,t) = \sum_{j=1}^{N_b} \phi_{bj}(x) q_{bj}(t) = \Phi_b^{\mathrm{T}}(x)\mathbf{q}_b(t) \tag{4.7b}$$

where

$$\Phi_{B(b)}^{\mathrm{T}} = \left\{ \begin{array}{cccc} \phi_{B1(b1)} & \phi_{B2(b2)} & \cdots & \phi_{BN_B(bN_b)} \end{array} \right\};$$
$$\mathbf{q}_{B(b)}^{\mathrm{T}} = \left\{ \begin{array}{cccc} q_{B1(b1)} & q_{B2(b2)} & \cdots & q_{BN_B(bN_b)} \end{array} \right\}$$

are the mode shape matrix and the modal coordinate vector; N_B and N_b are the number of modes, considered for the main and auxiliary beam, respectively; $q_{Bi(bj)}$ is the generalized coordinate of the main beam (the auxiliary beam) corresponding to the $i(j)$th mode, $\phi_{Bi(bj)}$.

If Eqs. (4.7) are introduced in Eq. (4.5), and multiplication by the ith(jth) normal mode of the main (auxiliary) beam is carried out, the ith(jth) modal equation of motions are obtained.

By assuming that the beams have the same length and are vertically aligned, the orthogonality properties of the normal modes will now be used to transform the equations of motion into modal space:

$$\left\{ \begin{array}{l} \ddot{q}_{Bi}(t) + 2\zeta_{Bi}\omega_{Bi}\dot{q}_{Bi}(t) + \omega_{Bi}q_{Bi}(t) = F_{vi}(t) - F_{DBi}(t); \quad i = 1...N_B \\ \ddot{q}_{bj}(t) + 2\zeta_{bj}\omega_{bj}\dot{q}_{bj}(t) + \omega_{bj}q_{bj}(t) = F_{Dbj}(t); \quad j = 1...N_b \end{array} \right. \tag{4.8}$$

where $\omega_{Bi(bj)}$ and $\zeta_{Bi(bj)}$ are the ith(jth) circular frequency, and the modal damping ratio of the main beam (the auxiliary beam), respectively. The modal forces induced by the FVDs are expressed as

$$F_{DBi}(t) = \frac{1}{m_{Bi}} \sum_{k=1}^{N_D} \phi_{Bi}(d_k) C_{eqk} \left[\Phi_B^{\mathrm{T}}(d_k)\, \dot{\mathbf{q}}_B - \Phi_b^{\mathrm{T}}(d_k)\, \dot{\mathbf{q}}_b \right] = \tag{4.9}$$

$$= \frac{1}{m_{Bi}} \left[\sum_{k=1}^{N_D} \phi_{Bi}(d_k) C_{eqk} \Phi_B(d_k) \right]^{\mathrm{T}} \dot{\mathbf{q}}_B - \frac{1}{m_{Bi}} \left[\sum_{k=1}^{N_D} \phi_{Bi}(d_k) C_{eqk} \Phi_b(d_k) \right]^{\mathrm{T}} \dot{\mathbf{q}}_b$$

and

$$F_{Dbj}(t) = \frac{1}{m_{bj}} \sum_{k=1}^{N_D} \phi_{bj}(d_k) C_{eqk} \left[\Phi_B^{\mathrm{T}}(d_k)\, \dot{\mathbf{q}}_B - \Phi_b^{\mathrm{T}}(d_k)\, \dot{\mathbf{q}}_b \right] \tag{4.10}$$

$$= \frac{1}{m_{bj}} \left[\sum_{k=1}^{N_D} \phi_{bj}(d_k) C_{eqk} \Phi_B(d_k) \right]^{\mathrm{T}} \dot{\mathbf{q}}_B - \frac{1}{m_{bj}} \left[\sum_{k=1}^{N_D} \phi_{bj}(d_k) C_{eqk} \Phi_b(d_k) \right]^{\mathrm{T}} \dot{\mathbf{q}}_b$$

where d_k is the distance from the left support of the beams to the kth FVD and $m_{Bi(bj)}$ is the modal mass of the main beam (the auxiliary beam).

In the first approach, the system response is evaluated under the harmonic excitation in order to get some insight regarding the main beam response at resonance. Thus, $F_v(x,t)$ is considered a harmonic force with an amplitude p_0 acting in vertical direction at a fixed coordinate x_0. In this condition, F_v may be written as

$$F_v(x,t) = \delta(x-x_0)p_0 e^{i\omega t} \tag{4.11}$$

where $\delta(x-x_0)$ is the Dirac delta function.

Accordingly, the vertical force F_v for the ith mode of the main beam is given by

$$F_{vi}(t) = \frac{1}{m_{Bi}}\int_0^l \delta(x-x_0)p_0 e^{i\omega t}\phi_{Bi}(x)dx = \frac{1}{m_{Bi}}p_0 e^{i\omega t}\phi_{Bi}(x_0) \tag{4.12}$$

By setting the vector

$$\mathbf{Y}(t) = \left\{ \begin{array}{c} \mathbf{q}_B(t) \\ \mathbf{q}_b(t) \end{array} \right\}$$

and combining with Eqs. (4.8), (4.9), (4.10) and (4.12), the coupled equations of motion in modal space are given in matrix form as

$$\mathbf{M}\ddot{\mathbf{Y}} + [\mathbf{C} + \mathbf{C}_D]\dot{\mathbf{Y}} + \mathbf{K}\mathbf{Y} = \mathbf{F} \tag{4.13}$$

where $\mathbf{M}$ is the $(N_B+N_b)\times(N_B+N_b)$ identity matrix, and

$$\mathbf{C} = \left[\begin{array}{cc} \mathbf{C}_B & 0 \\ 0 & \mathbf{C}_b \end{array} \right]; \quad \mathbf{C}_D = \left[\begin{array}{cc} \mathbf{C}_D^{BB} & \mathbf{C}_D^{Bb} \\ \mathbf{C}_D^{bB} & \mathbf{C}_D^{bb} \end{array} \right]; \quad \mathbf{K} = \left[\begin{array}{cc} \mathbf{K}_B & \mathbf{0} \\ \mathbf{0} & \mathbf{K}_b \end{array} \right]; \quad \mathbf{F} = \left\{ \begin{array}{c} \mathbf{F}_B \\ \mathbf{F}_b \end{array} \right\}$$

$$\mathbf{C}_B = \left[\begin{array}{cccc} 2\zeta_{B1}\omega_{B1} & 0 & \ldots & 0 \\ 0 & 2\zeta_{B2}\omega_{B2} & \ldots & 0 \\ \ldots & \ldots & \ldots & \ldots \\ 0 & 0 & \ldots & 2\zeta_{BN_B}\omega_{BN_B} \end{array} \right];$$

$$\mathbf{C}_b = \left[\begin{array}{cccc} 2\zeta_{b1}\omega_{b1} & 0 & \ldots & 0 \\ 0 & 2\zeta_{b2}\omega_{b2} & \ldots & 0 \\ \ldots & \ldots & \ldots & \ldots \\ 0 & 0 & \ldots & 2\zeta_{bN_b}\omega_{bN_b} \end{array} \right]$$

The ijth element of the four submatrices $\mathbf{C}_D^{BB}$, $\mathbf{C}_D^{Bb}$, $\mathbf{C}_D^{bB}$ and $\mathbf{C}_D^{bb}$ is determined as

$$C_{D,ij}^{BB} = \frac{1}{m_{Bi}}\sum_{k=1}^{N_D}\phi_{Bi}(d_k)C_{eqk}\phi_{Bj}(d_k); \quad i = 1\ldots N_B \text{ and } j = 1\ldots N_B$$

$$C_{D,ij}^{Bb} = \frac{-1}{m_{Bi}} \sum_{k=1}^{N_D} \phi_{Bi}(d_k) C_{eqk} \phi_{bj}(d_k); \quad i = 1...N_B \text{ and } j = 1...N_b$$

$$C_{D,ij}^{bB} = \frac{-1}{m_{bi}} \sum_{k=1}^{N_D} \phi_{bi}(d_k) C_{eqk} \phi_{Bj}(d_k); \quad i = 1...N_b \text{ and } j = 1...N_B$$

$$C_{D,ij}^{bb} = \frac{1}{m_{bi}} \sum_{k=1}^{N_D} \phi_{bi}(d_k) C_{eqk} \phi_{bj}(d_k); \quad i = 1...N_b \text{ and } j = 1...N_b$$

$$\mathbf{K}_B = \begin{bmatrix} \omega_{B1}^2 & 0 & ... & 0 \\ 0 & \omega_{B2}^2 & ... & 0 \\ ... & ... & ... & ... \\ 0 & 0 & ... & \omega_{BN_B}^2 \end{bmatrix}; \quad \mathbf{K}_b = \begin{bmatrix} \omega_{b1}^2 & 0 & ... & 0 \\ 0 & \omega_{b2}^2 & ... & 0 \\ ... & ... & ... & ... \\ 0 & 0 & ... & \omega_{bN_b}^2 \end{bmatrix};$$

$$FF_B = \begin{Bmatrix} \frac{\phi_{B1}(x_0)}{m_{B1}} \\ \frac{\phi_{B2}(x_0)}{m_{B2}} \\ ... \\ \frac{\phi_{BN_B}(x_0)}{m_{BN_B}} \end{Bmatrix} p_0 e^{i\omega t} \text{ and } \mathbf{F}_b \text{ is the } N_b \times 1 \text{ zero vector.}$$

Eq. (4.13) in complex form is

$$\overline{\mathbf{Y}}(\omega) = \left[-\omega^2 \mathbf{M} + i\omega (\mathbf{C} + \mathbf{C}_D) + \mathbf{K}\right]^{-1} \overline{\mathbf{F}}(\omega) \tag{4.14}$$

In expanded form, Eq. (4.14) may be written as

$$\begin{Bmatrix} \overline{\mathbf{q}}_B(\omega) \\ \overline{\mathbf{q}}_b(\omega) \end{Bmatrix} = \begin{bmatrix} \mathbf{L}_B(\omega) & \mathbf{L}_{Bb}(\omega) \\ \mathbf{L}_b(\omega) & \mathbf{L}_{bB}(\omega) \end{bmatrix} \begin{Bmatrix} \overline{\mathbf{F}}_B(\omega) \\ 0 \end{Bmatrix} \tag{4.15}$$

where $\mathbf{L}_B, \mathbf{L}_b, \mathbf{L}_{bB}$ and $\mathbf{L}_{Bb}$ are the submatrices of $\left[-\omega^2 \mathbf{M} + i\omega (\mathbf{C} + \mathbf{C}_D) + \mathbf{K}\right]^{-1}$ with the sizes of $N_B \times N_B, N_b \times N_b, N_b \times N_B$ and $N_B \times N_b$, respectively.

$$\overline{\mathbf{F}}_B^{\mathrm{T}}(\omega) = \left\{ \frac{\phi_{B1}(x_0)}{m_{B1}} \quad \frac{\phi_{B2}(x_0)}{m_{B2}} \quad ... \quad \frac{\phi_{BN_B}(x_0)}{m_{BN_B}} \right\} p_0$$

Then, the modal response components of the main beam and the auxiliary beam are given as

$$\overline{\mathbf{q}}_B(\omega) = \mathbf{L}_B(\omega) \overline{\mathbf{F}}_B(\omega) \tag{4.16a}$$

$$\overline{\mathbf{q}}_b(\omega) = \mathbf{L}_b(\omega) \overline{\mathbf{F}}_B(\omega) \tag{4.16b}$$

The total displacement Z_B at coordinate x_0 is then obtained by superimposing all modal contributions:

$$Z_B(x_0,t) = \sum_{i=1}^{N_B} \phi_{Bi}(x_0) q_{Bi}(t) = \Phi_B^{\mathrm{T}}(x_0)\mathbf{q}_B(t) \tag{4.17}$$

By using the Fourier transform of Eq. (4.17) and combining with (4.16), then Eq. (4.17) is rewritten in frequency domain as

$$\overline{Z}_B(\omega) = \Phi_B^{\mathrm{T}}(x_0)\overline{\mathbf{q}}_B(\omega) = \Phi_B^{\mathrm{T}}(x_0)\mathbf{L}_B(\omega)\overline{\mathbf{F}}_B(\omega) \tag{4.18}$$

The transfer function for flexural displacement at coordinate x_0 of the main beam for all modal components may be set as

$$H_B(\omega) = \frac{\overline{Z}_B(\omega)}{p_0} = \frac{1}{p_0}\Phi_B^{\mathrm{T}}(x_0)\mathbf{L}_B(\omega)\overline{\mathbf{F}}_B(\omega) \tag{4.19}$$

The magnitude of transfer function $|H_B(\omega)|$ dominates the flexural displacement of the main beam in frequency domain. Thus, the FVDs are designed to suppress the resonant peaks of $|H_B(\omega)|$.

The objective function to optimize the FVDs coefficients is based on the H_∞ norm [45] as

$$\|H(\omega)\|_\infty = \sup_\omega |H_B(\omega)| \tag{4.20}$$

The H_∞ norm represents the maximum absolute value of the transfer function. In the optimization process, minimizing the H_∞ norm implies decreasing the maximum amplitude magnification of the system over all frequencies of interest.

4.3.3 Solution to H_∞ optimization

The H_∞ optimization is the minimization of the objective function over all frequencies of interest. Then, the performance index (4.20) may be rewritten as

$$\min_{\xi_D} \|H(\omega)\|_\infty = \min_{\xi_D} \sup_\omega |H_B(\omega)| \tag{4.21}$$

The solution of the optimization problem with the performance index (4.21) may be found by the analytical and numerical methods in some specific cases as follows.

4.3.3.1 Simply supported beam

It is assumed that all the dampers are equal and symmetrically distributed along the beam lengths. Also the harmonic force is applied at the mid-span section of the main

beam. In simply-supported bridges experiencing resonant situations, the maximum response will most likely be associated to the contribution of the fundamental mode[84]. Under these circumstances, the response of modes different from the resonant mode is practically negligible. For this reason, a harmonic excitation applied at mid-span is selected for the optimization process, as it captures the essence of the structural response in the worst scenario.

From Eqs. (4.9) and (4.10), a series of FVDs installed along the beam axis can be substituted by an equivalent FVD installed at midspan with a damping coefficient determined as follows

$$C_D = \sum_{k=1}^{N_D} C_{eqk}\phi^2(d_k) \text{ with } \phi(x) = \sin(\pi x/l) \tag{4.22}$$

Therefore, the following expressions will focus on analyzing the response of the system with an equivalent FVD installed between the mid-span sections of the beams.

By taking into account only the fundamental mode of both beams, Eq. (4.14) is rewritten as

$$\overline{\mathbf{Y}}(\omega) = \left[-\omega^2\mathbf{M} + \mathrm{i}\omega\left(\mathbf{C}+\mathbf{C}_D\right)+\mathbf{K}\right]^{-1}\overline{\mathbf{F}}(\omega) \tag{4.23}$$

where

$$\overline{\mathbf{Y}}(\omega) = \left\{\begin{array}{c}\overline{q}_B(\omega)\\ \overline{q}_b(\omega)\end{array}\right\};\quad \mathbf{M} = \left[\begin{array}{cc}1 & 0\\ 0 & 1\end{array}\right];\quad \mathbf{C} = \left[\begin{array}{cc}2\zeta_B\omega_B & 0\\ 0 & 2\zeta_b\omega_b\end{array}\right];$$

$$\mathbf{C}_D = \left[\begin{array}{cc}\frac{C_D}{m_B} & -\frac{C_D}{m_B}\\ -\frac{C_D}{m_b} & \frac{C_D}{m_b}\end{array}\right];\quad \mathbf{K} = \left[\begin{array}{cc}\omega_B^2 & 0\\ 0 & \omega_b^2\end{array}\right];\quad \overline{\mathbf{F}}(\omega) = \left\{\begin{array}{c}\frac{p_0}{m_B}\\ 0\end{array}\right\}$$

where $m_B = \overline{m}_B l/2$; $m_b = \overline{m}_b l/2$; $\omega_B = \omega_{B1}$; $\omega_b = \omega_{b1}$; $\zeta_B = \zeta_{B1}$ and $\zeta_b = \zeta_{b1}$
For the sake of conciseness, the following dimensionless ratios are used in what follows

$$\eta = \frac{\omega_b}{\omega_B};\quad \Omega = \frac{\omega}{\omega_B};\quad \mu = \frac{m_b}{m_B};\quad \xi_D = \frac{C_D}{2m_B\omega_B}$$

where η, Ω, μ and ξ_D are the frequency, excitation frequency, mass and supplemental damping ratio, respectively; ζ_B and ζ_b are the modal damping ratios of the main and auxiliary beams.
Then, the components of L_B and L_b in Eqs. (4.16) can be determined as

$$L_B(\omega) = \frac{\mu(\eta^2-\Omega^2)+2\mathrm{i}\Omega(\xi_D+\mu\eta\zeta_b)}{\omega_B^2(E+2\mathrm{i}\Omega F)} \tag{4.24a}$$

$$L_b(\omega) = \frac{2\mathrm{i}\Omega\xi_D}{\omega_B^2(E+2\mathrm{i}\Omega F)} \tag{4.24b}$$

where

$$E = \mu(1-\Omega^2)(\eta^2-\Omega^2)+4\Omega^2\left[\xi_D^2-(\zeta_B+\xi_D)(\mu\eta\zeta_b+\xi_D)\right]$$
$$F = (1-\Omega^2)(\mu\eta\zeta_b+\xi_D)+\mu(\zeta_B+\xi_D)(\eta^2-\Omega^2)$$

Similarly, the components of L_{aB} and L_{ab} in the case of the acceleration are found as

$$L_{aB}(\omega) = \frac{\mu(\eta^2-\Omega^2)\Omega^2+2\mathrm{i}\Omega^3(\xi_D+\mu\eta\zeta_b)}{(E+2\mathrm{i}\Omega F)} \tag{4.25a}$$

$$L_{ab}(\omega) = \frac{2\mathrm{i}\Omega^3\xi_D}{(E+2\mathrm{i}\Omega F)} \tag{4.25b}$$

In practice, the auxiliary beams could be made of steel with a hollow rectangular cross section. Then, FVDs can be installed in the auxiliary beams to minimize the occupied space under the bridge. Besides, because steel structural damping is very small about 0.5%, it is neglected in the optimization problem with the performance index (4.21).

Analytical solution to H_∞ ***optimization*** $(\zeta_B \neq 0, \zeta_b = 0)$

Eqs. (4.19) and (4.24) show that the transfer function H_B varies with the damping coefficient ζ_D and the load frequency ω. Because Ω is affine in ω, the optimization for the transfer function H_B implies finding the pair of values $(\zeta_D^{\mathrm{opt}}, \Omega)$ instead of $(\zeta_D^{\mathrm{opt}}, \omega)$. The H_∞ optimization in this case is achieved if the following equations are satisfied

$$\frac{\partial|H_B(\Omega,\xi_D)|^2}{\partial\xi_D} = 0 \tag{4.26a}$$

$$\frac{\partial|H_B(\Omega,\xi_D)|^2}{\partial\Omega^2} = 0 \tag{4.26b}$$

However, the analytical solution of Eqs. (4.26) is impossible to find. Therefore, a different approach to the solution of these equations may be pursued by applying the perturbation method[85]. It is assumed that ζ_B is small and referred to as a perturbation. In this case, a solution to Eqs. (4.26) is sought in the form of the power series in ε as follows

$$\xi_D = \xi_{D0}+\varepsilon\xi_{D1}+\varepsilon^2\xi_{D2}+\ldots = \sum_{i=0}^{\infty}\varepsilon^i\xi_{Di} \tag{4.27a}$$

$$\Omega^2 = \Omega_0^2+\varepsilon\Omega_1^2+\varepsilon^2\Omega_2^2+\ldots = \sum_{i=0}^{\infty}\varepsilon^i\Omega_i^2 \tag{4.27b}$$

where $\varepsilon = \zeta_B$ and the functions ξ_{Di} and Ω_i^2 are independent of the perturbation ε.

Moreover, it can be seen that if the structural damping is neglected ($\varepsilon = 0$), ξ_{D0} and Ω_0^2 become the exact solution of Eqs. (4.26). The solution of ξ_{D0} and Ω_0^2 is referred to as the zero-order approximation of Eqs. (4.26).

By substituting Eqs. (4.27) into Eqs. (4.26), collecting terms of like powers of ε and setting these terms equal to zero, the unknown coefficients in Eqs. (4.27) may be determined recursively.

Analytical solution to zero-order approximation

Because Ω_0 is positive and not located near the resonant frequency of the auxiliary beam, the selected root is extracted and given by

$$\Omega_0^2 = \frac{2+\mu\eta^2}{2+\mu}$$

Then, the value ξ_{D0} may be found as

$$\xi_{D0}^1 = \frac{\mu(1-\eta^2)\mathrm{i}}{\sqrt{\eta^2\mu^2+2\eta^2\mu+2\mu+4}} \text{ with } \mathrm{i}^2 = -1$$

$$\xi_{D0}^2 = -\frac{\mu\left(\eta^2-1\right)}{\sqrt{4+6\mu+2\mu+2\mu\eta^2+3\mu^2\eta^2+\mu^3\eta^2}}$$

$$\xi_{D0}^3 = -\frac{\mu(1-\eta^2)\mathrm{i}}{\sqrt{\eta^2\mu^2+2\eta^2\mu+2\mu+4}}$$

$$\xi_{D0}^4 = \frac{\mu\left(\eta^2-1\right)}{\sqrt{4+6\mu+2\mu+2\mu\eta^2+3\mu^2\eta^2+\mu^3\eta^2}}$$

Based on the condition that the FVD damping ratio is real and positive, the value of ξ_{D0} lies on the fourth root of ξ_{D0}^4.

Analytical solution to first-order and second-order approximation

Similarly, by equating the first-order and the second-order terms of ε to zero and substituting ξ_{D0} and Ω_0 into equations (4.26), the first-order solution may be obtained as follows

$$\Omega_1^2 = \frac{2\mu\sqrt{(\mu+2)(\mu+1)(\mu\eta^2+2)}}{(\mu+1)(\mu+2)^2} \tag{4.28a}$$

$$\xi_{D1} = -\frac{\mu\left(2\,\eta^4\mu+\mu^2\eta^4+2\,\eta^2-2\right)}{(\mu+2)\,(\mu\eta^2+2)\,(\mu\eta^2+1)} \tag{4.28b}$$

and the second-order approximations provide

$$\Omega_2^2 = \frac{8}{(\mu+2)^2} \tag{4.29a}$$

$$\xi_{D2} = \frac{2\left(\mu^2\eta^2+3\,\mu\eta^2+3\,\eta^2+\mu+1\right)\mu\sqrt{(\mu+2)(\mu+1)(\mu\eta^2+2)}}{(\mu+2)^2(\mu+1)^2(\mu\eta^2+2)^2} \tag{4.29b}$$

By substituting the terms obtained above into Eqs. (4.27) and returning the symbol ε to the original parameter ζ_B, then the second-order approximate solution may be presented as:

$$\begin{cases} \xi_D^{\text{opt}} = \xi_{D0} + \zeta_B\xi_{D1} + \zeta_B^2\xi_{D2} \\ \Omega^2 = \Omega_0^2 + \zeta_B\Omega_1^2 - \zeta_B^2\Omega_2^2 \end{cases} \tag{4.30}$$

Similarly, if the transfer function of the displacement $H_B(\omega)$ is replaced by that of the acceleration $H_{aB}(\omega)$, the analytical solution to the H_∞ optimization can also be found as follows.

For the zero-order approximation,

$$\Omega_0^2 = \frac{2+\mu\eta^2}{2+\mu} \tag{4.31a}$$

$$\xi_{D0} = \frac{(\eta+1)(\eta-1)\mu}{\sqrt{(\mu+2)(\mu\eta^2+2)(\mu\eta^2+1)}} \tag{4.31b}$$

For the first-order approximation,

$$\Omega_1^2 = \frac{2\sqrt{(\mu+2)(\mu\eta^2+2)(\mu\eta^2+1)}\mu\eta^2}{(\mu+2)^2(\mu\eta^2+1)} \tag{4.32a}$$

$$\xi_{D1} = -\frac{\mu\left(2\,\eta^4\mu+\mu^2\eta^4+2\,\eta^2-2\right)}{(\mu+2)(\mu\eta^2+2)(\mu\eta^2+1)} \tag{4.32b}$$

And for the second-order approximation,

$$\Omega_2^2 = \frac{4(\mu^2\eta^4+2\,\mu\eta^2+2)}{(\mu+2)^2(\mu\eta^2+1)} \tag{4.33a}$$

$$\xi_{D2} = -\frac{2\left(\mu^2\eta^4+\eta^4\mu+3\,\mu\eta^2+\eta^2+3\right)\sqrt{(\mu+2)(\mu\eta^2+2)(\mu\eta^2+1)}\mu}{(\mu+2)^2(\mu\eta^2+2)^2(\mu\eta^2+1)^2} \tag{4.33b}$$

***Analytical solution to the "fixed-point" method*[12]**

The detailed solution of the "fixed-point" method for the fundamental mode in primary structures retrofitted with linear FVD systems was derived by Museros and Martinez-Rodrigo[12]. The result of this method may be considered as a criterion to evaluate the effectiveness of the presented method. This study utilized the feature of "fixed-point" frequency. It means that when there is no damping in the primary system, $\zeta_B = \zeta_b = 0$, the family of response curves passes through one invariant point at the amplitude frequency plane irrespective of the value of the damping constant. The damping ratio of the equivalent FVD is taken to be the optimal when the response curves pass through either invariant point with a horizontal tangent provided as follows

$$\xi_D^{\text{opt}} = \frac{\mu\left(\eta^2 - 1\right)}{\sqrt{4 + 6\mu + 2\mu + 2\mu\eta^2 + 3\mu^2\eta^2 + \mu^3\eta^2}} \tag{4.34a}$$

$$C_D^{\text{opt}} = 2m_B\omega_B \frac{\mu\left(\eta^2 - 1\right)}{\sqrt{4 + 6\mu + 2\mu + 2\mu\eta^2 + 3\mu^2\eta^2 + \mu^3\eta^2}} \tag{4.34b}$$

However, if the primary system is damped, the useful "fixed-point" feature is lost. It means that the use of the "fixed-point" method to find optimal damping coefficients is impossible in this case.

Besides, it can be seen that the result (4.34) obtained by the "fixed-point" method[12] is a particular case of the presented result (4.30) if the structural damping ξ_D is equal to zero.

4.3.3.2 Double-span continuous beam

In this section, the problem of using linear FVD systems to reduce the multi-resonant response associated with the high frequencies of structures is presented. The double-span continuous beam may be considered as a prototype of a multi-resonant structure. For this structure, some results in some previous studies[2,88] showed that the first two modes mostly dominate the dynamic response of the beams at resonance under the action of high-speed trains. Therefore, modes higher than the first two modes are neglected in the optimization process but then the response of the beams has also been obtained numerically by using the finite element method to simulate the whole structure under the high-speed train HSLM-A8. Moreover, the above research also showed that at resonant speeds, the maximum displacement of the second span is larger than that of the first span. Therefore, the dynamic response at the second midspan of the main beam is analyzed here. By retrofitting two FVDs at each of the mid-span sections of the beams, then the transfer function of the system is generated as follows.

The mode shapes of the double-span continuous beam, presented by Fryba[89], are
- For antisymmetric vibration, the normal modes of the first and second span

$$\phi_n = \sin\left(\frac{n+1}{2l}\pi x\right) \quad n = 1,3,5,... \tag{4.35}$$

where l is the span length.

- For symmetric vibration, the normal modes of the first span have the form

$$\phi_n = \sin\left(\frac{\lambda_n}{l}x\right) - \frac{\sin\lambda_n}{\sinh\lambda_n}\sinh\left(\frac{\lambda_n}{l}x\right) \quad n = 2,4,6... \; ; \; 0 \le x \le l \tag{4.36}$$

and of the second span

$$\phi_n = \sin\left[\frac{\lambda_n}{l}(2l-x)\right] - \frac{\sin\lambda_n}{\sinh\lambda_n}\sinh\left[\frac{\lambda_n}{l}(2l-x)\right] \quad n = 2,4,6... \; ; \; l < x \le 2l \tag{4.37}$$

where the coordinate origin of x is assumed to be at the left-hand end of each beam; λ is determined by solving equation $\mathrm{tg}\lambda = \mathrm{tgh}\lambda$.

The mode-shape vectors at the coordinates of $l/2$ and $3l/2$ may be obtained as

$$\Phi_{B(b)}\left(\frac{l}{2}\right) = \begin{Bmatrix} \phi_{B1(b1)}\left(\frac{l}{2}\right) \\ \phi_{B2(b2)}\left(\frac{l}{2}\right) \end{Bmatrix} = \begin{Bmatrix} 1 \\ 1 \end{Bmatrix}; \quad \Phi_{B(b)}\left(\frac{3l}{2}\right) = \begin{Bmatrix} \phi_{B1(b1)}\left(\frac{3l}{2}\right) \\ \phi_{B2(b2)}\left(\frac{3l}{2}\right) \end{Bmatrix} = \begin{Bmatrix} -1 \\ 1 \end{Bmatrix}$$

Then, Eq. (4.14) is rewritten as

$$\overline{\mathbf{Y}}(\omega) = \left[-\omega^2\mathbf{M} + \mathrm{i}\omega\left(\mathbf{C}+\mathbf{C}_D\right) + \mathbf{K}\right]^{-1}\overline{\mathbf{F}}(\omega) \tag{4.38}$$

$$\overline{\mathbf{Y}} = \begin{Bmatrix} \overline{q}_{B1}(\omega) \\ \overline{q}_{B2}(\omega) \\ \overline{q}_{b1}(\omega) \\ \overline{q}_{b2}(\omega) \end{Bmatrix}; \quad \mathbf{M} = \begin{bmatrix} 1 & 0 & 0 & 0 \\ 0 & 1 & 0 & 0 \\ 0 & 0 & 1 & 0 \\ 0 & 0 & 0 & 1 \end{bmatrix}; \quad \mathbf{K} = \begin{bmatrix} \omega_{B1}^2 & 0 & 0 & 0 \\ 0 & \omega_{B2}^2 & 0 & 0 \\ 0 & 0 & \omega_{b1}^2 & 0 \\ 0 & 0 & 0 & \omega_{b2}^2 \end{bmatrix};$$

$$\mathbf{C}_D = \begin{bmatrix} \frac{2C_D}{m_{B1}} & 0 & -\frac{2C_D}{m_{B1}} & 0 \\ 0 & \frac{2C_D}{m_{B2}} & 0 & -\frac{2C_D}{m_{B2}} \\ -\frac{2C_D}{m_{b1}} & 0 & \frac{2C_D}{m_{b1}} & 0 \\ 0 & -\frac{2C_D}{m_{b2}} & 0 & \frac{2C_D}{m_{b2}} \end{bmatrix}; \quad \overline{\mathbf{F}} = \begin{Bmatrix} \frac{p_0\phi_{B1}(3l/2)}{m_{B1}} \\ \frac{p_0\phi_{B2}(3l/2)}{m_{B2}} \\ 0 \\ 0 \end{Bmatrix}$$

$$\mathbf{C} = \begin{bmatrix} 2\zeta_{B1}\omega_{B1} & 0 & 0 & 0 \\ 0 & 2\zeta_{B2}\omega_{B2} & 0 & 0 \\ 0 & 0 & 2\zeta_{b1}\omega_{b1} & 0 \\ 0 & 0 & 0 & 2\zeta_{b2}\omega_{b2} \end{bmatrix}$$

And the dimensionless ratios are defined as

$$\eta_j = \frac{\omega_{bj}}{\omega_{Bj}};\ \Omega_j = \frac{\omega}{\omega_{Bj}};\ \mu_j = \frac{m_{bj}}{m_{Bj}};\ \xi_{Dj} = \frac{C_D}{2m_{Bj}\omega_{Bj}} \quad (j = 1,2)$$

where η_j, Ω_i, μ_j and ξ_{D_j} are the frequency, excitation frequency, mass and supplemental damping ratio of the jth mode, respectively.
In order to determine the normal coordinate vector of the main beam displacement in frequency domain, Eq. (4.16) may be written as

$$\overline{\mathbf{q}}_B(\omega) = \mathbf{L}_B(\omega)\overline{\mathbf{F}}_B(\omega) = \begin{bmatrix} L_{B11} & L_{B12} \\ L_{B21} & L_{B22} \end{bmatrix} \begin{Bmatrix} F_{B1} \\ F_{B2} \end{Bmatrix} \tag{4.39}$$

After some algebraic manipulation, the components of $\mathbf{L}_B$ may be obtained as

$$L_{B12} = L_{B21} = 0 \tag{4.40a}$$

$$L_{Bjj} = \frac{\mu_j(\eta_j^2 - \Omega_j^2) + 2\mathrm{i}\Omega_j(\xi_{Dj} + \mu_j\eta_j\zeta_{bj})}{\omega_{Bj}^2(E_j + 2\mathrm{i}\Omega_j F_j)} \text{ with } \mathrm{i}^2 = -1 \text{ and } j = 1,2 \tag{4.40b}$$

where

$$E_j = \mu_j(1-\Omega_j^2)(\eta_j^2 - \Omega_j^2) + 4\Omega_j^2\left[\xi_{Dj}^2 - (\zeta_{Bj} + \xi_{Di})(\mu_j\eta_j\zeta_{bj} + \xi_{Dj})\right]$$
$$F_j = (1-\Omega_j^2)(\mu_j\eta_j\zeta_{bj} + \xi_{Dj}) + \mu_j(\zeta_{Bj} + \xi_{Dj})(\eta_j^2 - \Omega_j^2)$$

The displacement of the main beam at coordinate $3l/2$ in frequency domain for both of the first two modes is described as

$$\overline{Z}_B(\omega) = \Phi_B^{\mathrm{T}}(x_0)\mathbf{L}_B(\omega)\overline{\mathbf{F}}_B(\omega) = \sum_{j=1}^{2} \frac{p_0\phi_{Bj}^2\left(\frac{3l}{2}\right)}{m_{Bj}} L_{Bjj} \tag{4.41}$$

And the magnitude of the transfer function is

$$|H_B(\omega)| = \sqrt{\left\{\left[\sum_{j=1}^{2} \frac{\phi_{Bj}^2\left(\frac{3l}{2}\right)}{m_{Bj}} \mathrm{Re}\left[L_{Bjj}(\omega)\right]\right]\right\}^2 + \left\{\left[\sum_{j=1}^{2} \frac{\phi_{Bj}^2\left(\frac{3l}{2}\right)}{m_{Bj}} \mathrm{Im}\left[L_{Bjj}(\omega)\right]\right]\right\}^2} \tag{4.42}$$

By substituting $m_{Bj} = \int_0^{2l} \overline{m}_B(x)\phi_{Bj}^2(x)\mathrm{d}x = \overline{m}_B l$ into Eq. (4.42), it may be simplified as

$$|H_B(\omega)| = \frac{1}{\overline{m}_B l}\sqrt{\left\{\sum_{j=1}^{2} \mathrm{Re}\left[L_{Bjj}(\omega)\right]\right\}^2 + \left\{\sum_{j=1}^{2} \mathrm{Im}\left[L_{Bjj}(\omega)\right]\right\}^2} \tag{4.43}$$

Similarly, the magnitude of the acceleration transfer function may be determined as

$$|H_{aB}(\omega)| = \frac{1}{\overline{m}_B l}\sqrt{\left\{\sum_{j=1}^{2}\mathrm{Re}\left[L_{aBjj}(\omega)\right]\right\}^2 + \left\{\sum_{j=1}^{2}\mathrm{Im}\left[L_{aBjj}(\omega)\right]\right\}^2} \tag{4.44}$$

$$L_{aBjj} = \frac{\mu_j(\eta_j^2 - \Omega_j^2)\Omega^2 + 2\mathrm{i}\Omega_j^3(\xi_{Dj} + \mu_j\eta_j\zeta_{bj})}{(E_j + 2\mathrm{i}\Omega_j F_j)}$$

The optimal damping coefficients of the FVDs retrofitted in the double-span beam may be found by substituting Eq. (4.43) into (4.21) and using the the numerical optimization method. The optimization process for the first mode, the second mode and both of the modes is calculated by setting index j in Eq. (4.43).

4.4 Numerical verification and discussion

Based on the theoretical derivations described above, the numerical investigations are performed in this section.

4.4.1 Dynamic response of structure with linear FVD system

4.4.1.1 Analysis of simply supported structures

The Brustjaernsbaecken bridge[9] with the physical properties of the main beam listed in Table 2.2 will be analyzed. One FVD is installed between the mid-span sections of the main beam and the auxiliary beam. The HSLM-A8 high speed train is used as an external load acting on the bridge.

The previous study[12] proved that for a particular main beam, its maximum transverse response monotonically decreases when the height of the auxiliary beam increases. Therefore the size of the auxiliary beam should be the minimum size but it has to guarantee an admissible performance of the superstructure, when connected to the main beam with the optimal dampers. The bridge after the retrofit has to guarantee the requirements and the criteria in standard for bridge design[8] such as the maximum deck vertical acceleration under the rail track at the Serviceability Limit State, not exceeding given stress limits, checking for fatigue failure, maximum deformation criteria, etc. The most important two criteria also related to this study are the vertical acceleration and the maximum deflection of the bridge under the track[15].

FVDs are known for their energy dissipation capabilities, as compared to others. Museros *et al.*[12] estimated that the damping systems including FVDs and auxiliary beams may

be considered as an effective solution for improvement and maintenance of existing railway bridges and could substitute classical strengthening solutions. The reasons for these are FVDs' capacity to dissipate energy in a wide frequency band and not only at particular frequencies as tuned mass dampers. The stable operation, maintenance costs and replacement process without interfering with everyday rail traffic are also advantages of FVDs.

Besides, by varying the current height of the main beam ($h_B = 2.5$ m) as shown in Table 4.2, then the maximum accelerations at midspan of the main beam without FVDs under the high-speed train HSLM-A8 are presented in figure 4.3a. The results show that the stiffness of the main beam without FVDs needs to be increased at least four times to satisfy the limiting acceleration of 3.5 $\mathrm{m/s^2}$ in the high speed range. Thus, the use of FVDs in the design of new bridges also needs to be considered as a matter of preference.

Table 4.2: Physical properties of the main, auxiliary beam and the maximum acceleration versus their height

Beam	h_B (m)	EI ($\mathrm{Nm^2}$)	A ($\mathrm{m^2}$)	m ($\mathrm{kg/m}$)	$a_{\max}$ ($\mathrm{m/s^2}$)
Main beam	2.5	8.38×10^{10}	4.34	2.51×10^4	7.42
	3.0	12.96×10^{10}	5.40	3.12×10^4	6.03
	3.3	18.96×10^{10}	6.53	3.77×10^4	4.92
	3.6	26.87×10^{10}	7.78	4.49×10^4	4.33
	3.9	37.02×10^{10}	9.13	5.27×10^4	3.58
	4.2	49.79×10^{10}	10.58	6.11×10^4	3.08
Aux. beam	1.52	1.75×10^{10}	0.27	0.21×10^4	

Note: $a_{\max}$ is the maximum acceleration of the main beam without FVD under the HSLM-A8 train and A is the area of the beam cross section.

In the next step, the comparison of the proposed analytical method with the numerical method and the previous analytical method is presented. In figures 4.4, the optimal damping ratio of the FVD ξ_D is plotted versus the structural damping ratio ζ_B and the auxiliary beam height h_b. The numerical solution is obtained by minimizing the objective function (4.20) in which the structural damping is included. Therefore, the results obtained by the numerical method are almost exact and used to compare with the analytical solutions obtained by the proposed method and the previous method.

It may be observed that when the structural damping ζ_B increases, the curve of the optimal damping ratio ξ_D obtained by the previous method has a tendency to separate from the exact curve by the numerical method. Especially, this tendency is very clear in the range of large structural damping ratios. This is equivalent to the attenuation

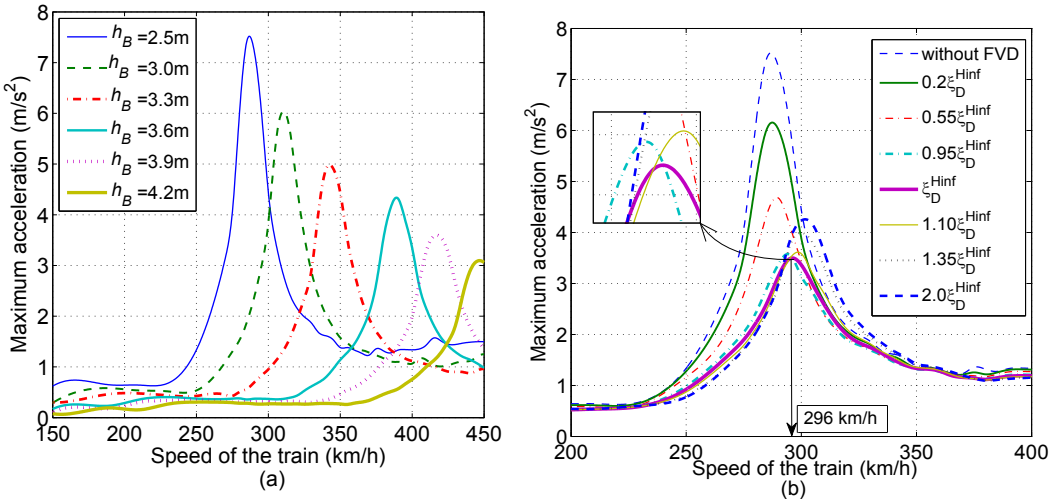

Figure 4.3: (a) Maximum acceleration at midspan of unretrofitted main beams versus speed of the HSLM-A8 train and (b) maximum acceleration at midspan of the main beam with the height of 2.5 m equipped with the FVD system optimized by Eq. (4.30) ($\mu = 0.084$, $\eta = 1.58$)

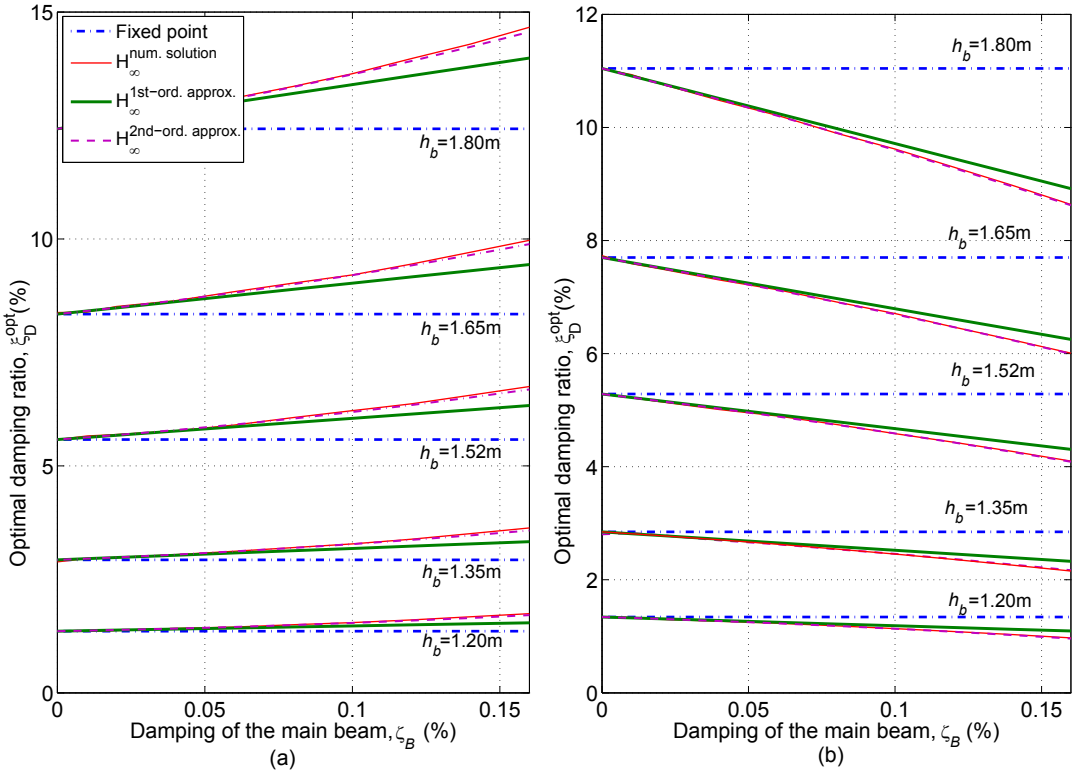

Figure 4.4: Solutions for $H_\infty^{num.\ sol.}$, $H_\infty^{1st\text{-}ord.\ approx.}$, $H_\infty^{2nd\text{-}ord.\ approx.}$ and fixed-point method in the case that (a) transfer function of the main beam displacement is minimized, (b) transfer function of the main beam acceleration is minimized

of the effectiveness of the previous method. Meanwhile, the second-order solution obtained by the proposed method is almost identical to the solution obtained by the numerical optimization. Therefore, the second-order solution may be considered as a quite exact solution for the design of optimal fluid viscous dampers connected to the retrofitted bridges.

Besides, in order to clarify the effectiveness of the proposed analytical formulae, the Brustjaernsbaecken bridge[9] with the structural damping ratio varied in a larger range and the given height of the auxiliary beam $h_b = 1.52$ m is analyzed in detail in Table 4.3. The results show that in the case of the structural damping ratio ζ_B=1%, the different percentages of the results obtained by the methods are small (Δ_{Fix}=1.4% and Δ_{H_∞}=0.3%). However, in larger structural damping ranges, the effectiveness of the H_∞ norm method is quite noticeable when compared to the previous method. It can be seen that the presented method can tune dampers to the vicinity of the exact values in every case of structural damping.

Table 4.3: Evaluate optimal damping ratios of FVDs obtained by the methods ($\mu = 0.084$, $\eta = 1.58$)

FVD's damping ratio	Structural damping ratio, ζ_B					
	0.01	0.04	0.06	0.08	0.12	0.16
ξ_D^0 (exact method)	5.660	5.773	5.899	6.064	6.369	6.750
ξ_D^{Fix} (previous method)	5.581	5.581	5.581	5.581	5.581	5.581
$\xi_D^{\text{H}_\infty}$ (proposed method)	5.675	5.790	5.911	6.044	6.342	6.684
$\Delta_{\text{Fix}} = \left\lvert \frac{\xi_D^{\text{Fix}} - \xi_D^0}{\xi_D^0} \right\rvert 100\%$	1.4	3.4	5.4	8.0	12.4	17.3
$\Delta_{\text{H}_\infty} = \left\lvert \frac{\xi_D^{\text{H}_\infty} - \xi_D^0}{\xi_D^0} \right\rvert 100\%$	0.3	0.3	0.2	0.3	0.4	1.0
$\Delta_{\text{Fix-H}_\infty} = \left\lvert \frac{\xi_D^{\text{Fix}} - \xi_D^{\text{H}_\infty}}{\xi_D^{\text{H}_\infty}} \right\rvert 100\%$	1.7	3.6	5.6	7.7	12.1	16.5

Note: Δ_{Fix} and Δ_{H_∞} show the error percentages of the previous and proposed methods when they are compared to the exact method; $\Delta_{\text{Fix-H}_\infty}$ can be considered as the different percentage between the previous and proposed methods; ξ_D^0, ξ_D^{Fix} and $\xi_D^{\text{H}_\infty}$ are the optimal damping ratios of FVDs obtained by the numerical method, the previous method and the presented method, respectively.

Moreover, in the case that the optimal damping ratio of FVD $\xi_D^{\text{Fix}} = 0.95\xi_D^{\text{Hinf}}$ corresponding to $\Delta_{\text{Fix-H}_\infty} \approx 5\%$ in Table 4.3 presented above, then Fig. 4.3b can show that the acceleration response peak under the HSLM-A8 train increases from 3.45 m/s^2 to 3.59 m/s^2 when ξ_D^{Hinf} is detuned to $0.95\xi_D^{\text{Hinf}}$ ($=\xi_D^{\text{Fix}}$). This shows the attenuation of the effectiveness of the case with ξ_D^{Fix}. In practice, designing high-speed railway bridges to guarantee both the maximum acceleration criterion 3.50 m/s^2 in Annex A2 and eco-

nomic requirements is a challenge[90].

In Figs 4.5a and 4.5b, it may be seen that the damping ratios of the FVDs determined above can lead to the minimum response of the main system in a large frequency range. Besides, the higher modes contribution to the acceleration amplitudes is significant when $\omega > 150$ rad/s. In practice, this can only happen when the speed of the train is extremely high.

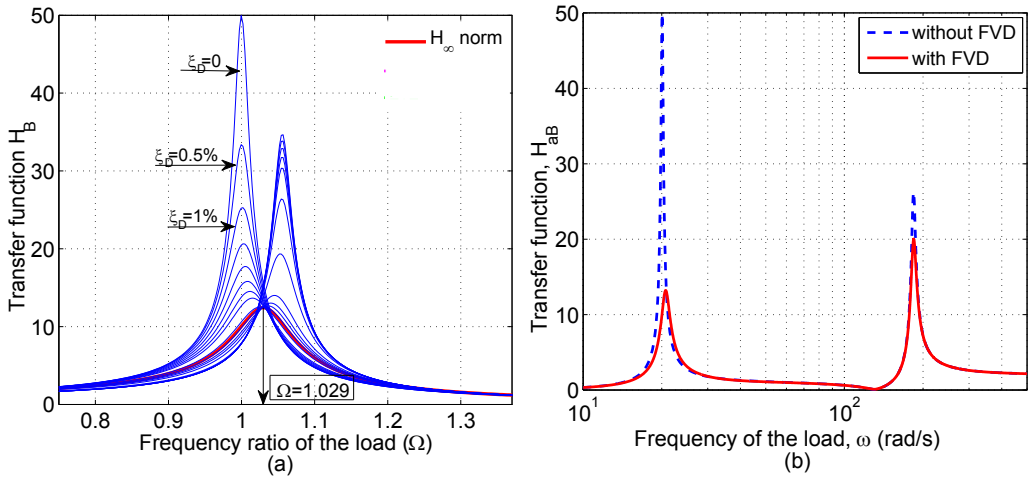

Figure 4.5: (a) Transfer function of displacement (b) transfer function of acceleration at midspan versus frequency of the load

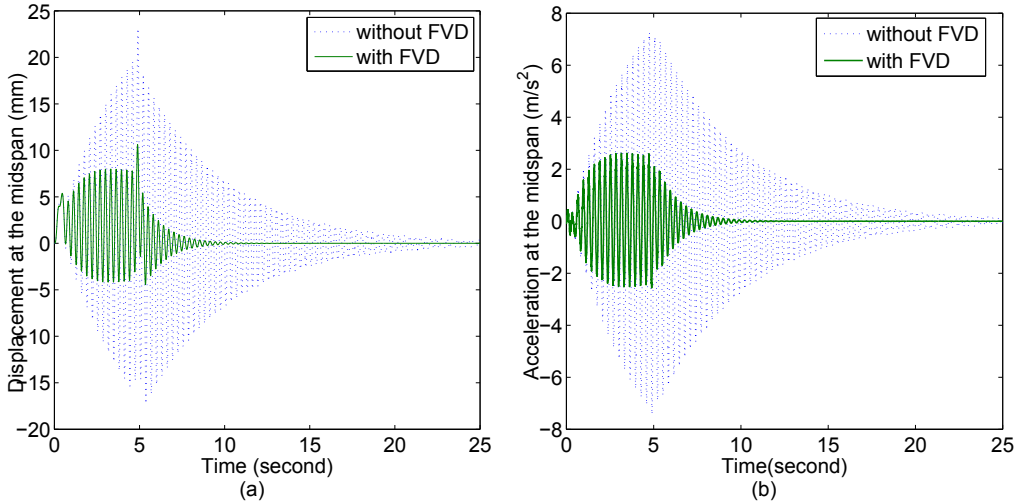

Figure 4.6: (a) Response of the main beam under the train load at the resonant speed v =296 km/h: (a) displacement at midspan and (b) acceleration at midspan

For the height of the auxiliary beam of $h_b = 1.52$ m corresponding to $\xi_D^{\text{opt}} = 5.68\%$, the maximum dynamic displacement and acceleration shown in figure 4.6 are 12.34

mm and 3.458 m/s^2, respectively. The vibrations are reduced by 47.22% for the displacement and 54.54% for the acceleration response and therewith are less than the limiting value in Annex A2 of Eurocode (see table B.1 of appendix B). Besides, the maximum normal stress at midspan of the auxiliary beam is 5.03 MPa. This stress is much smaller than commercial steels maximum admissible stress.

Finally, in order to evaluate the accuracy level of the proposed model, the finite element method (FEM) and the numerical time-stepping method (NTM) for MDOF systems are used to analyze sensitivity of the results obtained by the presented method. The combination of the FEM and NTM can solve directly the general moving load problem in equations 4.5 and give quite exact results. It should be noticed that the FEM does not depend on how many modes need to be included in simulation models. Besides, the HSLM-A8 moving load model instead of the fixed harmonic point load is also used in this analyzing process. Firstly, to evaluate the sensitivity of the optimal damping ratio of FVDs obtained by the proposed method based the H_∞ norm in which the only fundamental mode (for the case of simply supported beams) and a fixed harmonic excitation are considered, a plot of the exact acceleration response at midspan of the main beam under the HSLM-A8 moving load model, versus speed of the train and several detuned FVDs' optimal damping coefficients is performed in figure 4.3b. The plot shows that the structural response peak corresponding to the non-detuned optimal damping coefficient of FVDs, obtained by the proposed model, reaches the minimum value over the frequency range of interest. It can be confirmed that the present model to predict the optimal parameters of FVDs is quite exact.

Besides, another parameter which can be used to evaluate the accuracy level of the proposed model is the resonant frequency of the load. Because when the optimal damping ratio of FVDs is varied, the resonant frequency of the load is also varied correspondingly. Fig. 4.3b also shows that the resonant response of the beam directly excited by the moving-load system HSLM-A8 corresponding to the case of the non-detuned optimal damping ratio of FVD happens at a speed in the vicinity of 296 km/h. Fig. 4.5a shows that the resonant frequency of the fixed harmonic point load model is 20.58 rad/s ($= 1.029 \times 20 = \Omega\omega_B$). This frequency can be converted approximately into the resonant speed of the train about 295 km/h ($= 20.58 \times 25 \times 3.6/(2\pi) = \frac{\omega D}{2\pi}$), where D=25 m is the coach length of HSLM-A8. This formula can be found in previous research [16,23]. This clarifies that the resonant frequencies of the fixed harmonic point load and the moving-load system HSLM-A8 are not significantly different.

4.4.1.2 Analysis of double-span continuous structure

In this section, the double-span continuous beams with the physical properties given in Table 2.2 and the height of the auxiliary beam of $h_b = 1.4$ m, whose properties are

presented in Table. 4.4, are considered as a prototype of a multi-resonant structure. A damping system consists of two FVDs, each of which is installed at each of the midspans of the beams.

Table 4.4: Properties of the auxiliary beam,[12]

Beam	L_b (m)	$\overline{m}_b$ kg/m	ζ_{bi} (%)	ω_1	ω_2	ω_3
Double-span continuous beam	20	1.8×10^3	0.5	65.5	102.3	261.8

Note: L_b is the span length; $\overline{m}_b$ is the mass per unit length; ω_i (rad/s) and ζ_{bi} are the ith natural frequency and the ith structural modal damping of the auxiliary beam, respectively

The FVD system will be employed to reduce the first and second resonant peaks of the main structure. The optimal damping ratios of the FVDs calculated by minimizing the performance index H_∞ norm in (4.21) with the transfer functions in Eqs. (4.43) and (4.44) are shown in Table 4.5.

Table 4.5: FVDs' optimal coefficients

Contribution of modes	Optimization for $H_B(\omega)$		Optimization for $H_{aB}(\omega)$	
	C_{D1} (Ns/m)	C_{D2} (Ns/m)	C_{D1} (Ns/m)	C_{D2} (Ns/m)
First mode	28.532×10^5	28.532×10^5	22.949×10^5	22.949×10^5
Second mode	43.010×10^5	43.010×10^5	33.961×10^5	33.961×10^5
Both modes	28.872×10^5	28.872×10^5	34.932×10^5	34.932×10^5

Fig. 4.7 shows that the peak values of the transfer function are minimized over the frequency range of interest. As it may be seen, the contribution of different modes in the optimization process can lead to the different optimal damping coefficients of the FVDs and the different peak values of the response. The first resonant value of the transfer function with the FVDs optimized for the first mode is smaller than that for the second mode. In contrast, the second resonant value of the transfer function with the FVD systems optimized for the first mode is larger than that for the second mode. In the case that the simultaneous contribution of both of the modes has been considered, the optimal curve of the transfer function lies between the curves with FVDs optimized for the individual modes.

Moreover, Fig. 4.7a also shows that the contribution of the second mode is significant. Thus, the optimization for the damping ratios of the FVDs by using the acceleration transfer function with the second mode or both of the modes can lead to better results as shown in Fig. 4.7b.

In order to validate the use of a fixed harmonic excitation instead of a moving load

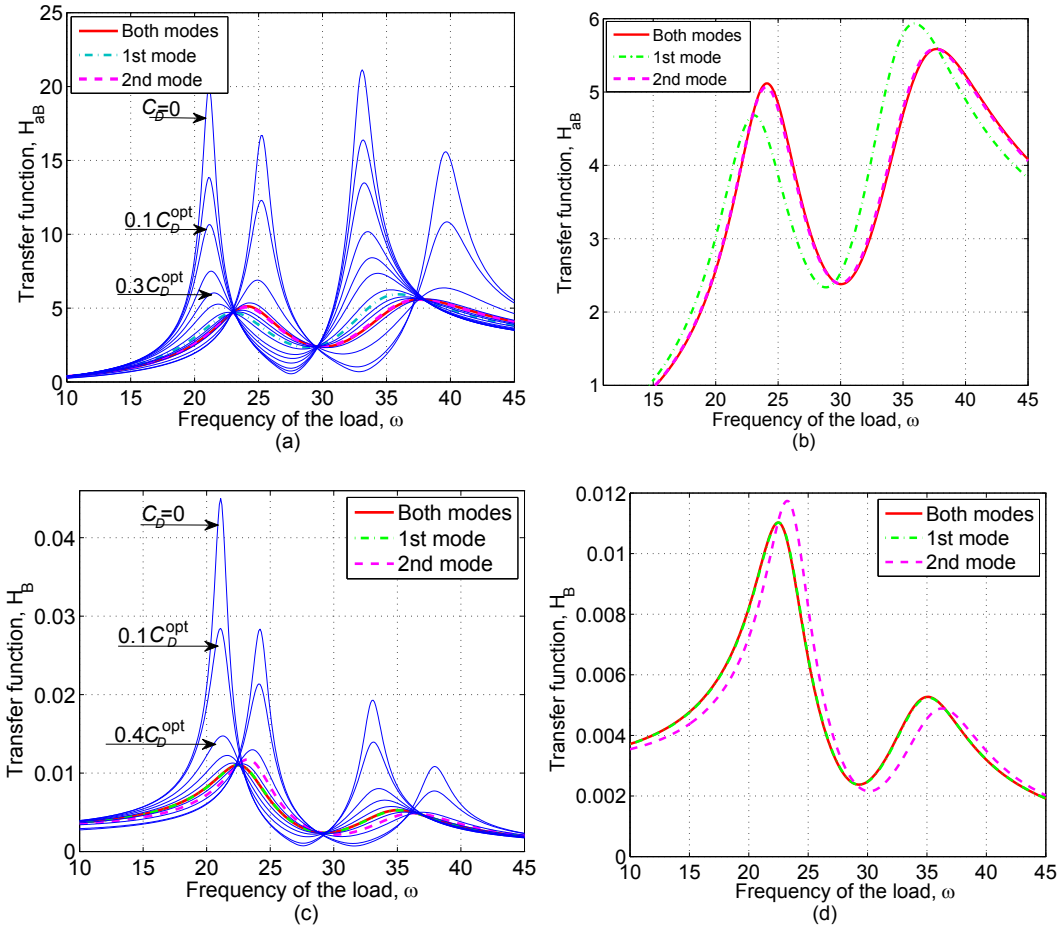

Figure 4.7: Variation of the transfer functions versus damping ratio of FVD and load frequency: (a),(b) transfer function of acceleration at the second midspan; (c),(d) transfer function of displacement at the second midspan

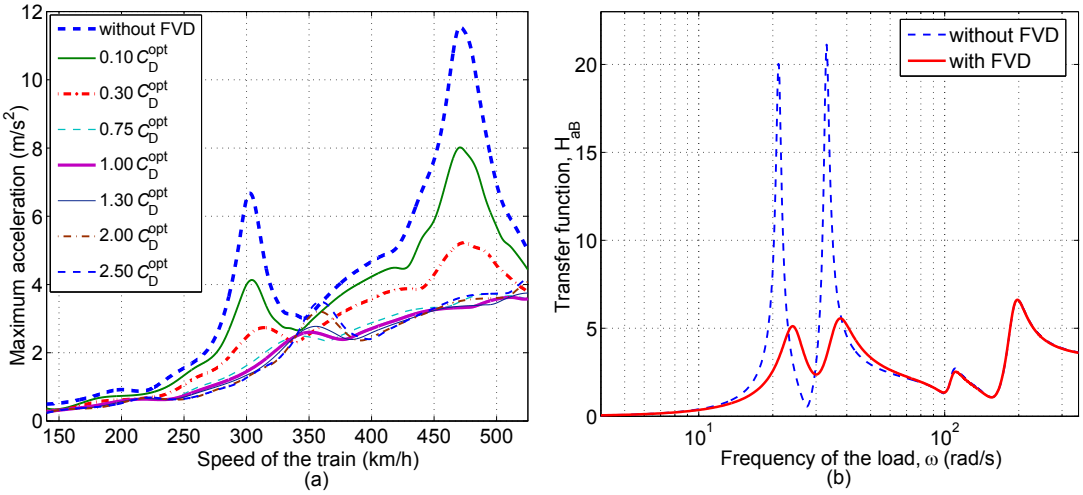

Figure 4.8: (a) Maximum acceleration at the second midspan versus FVDs coefficient and speed of the train; (b)Variation of the structural transfer function of the acceleration at the second midspan with FVD and without FVD versus load frequency.

system in the optimization process, a plot of the acceleration response at the second midspan of the main beam under the HSLM-A8 train load versus several FVD coefficients is performed in Fig. 4.8a. It shows that the response corresponding to the FVDs coefficient optimized by the proposed method is the smallest over the frequency range of interest. Again, it can be confirmed that a train load system can be replaced by a fixed harmonic load in the optimization process for FVDs.

Fig. 4.8b presents the magnitude of the transfer function established by the contribution of the first four modes versus the load frequencies. It can be seen that the contribution of the high modes different from the first two modes is significant in the frequency range $\omega > 160$ rad/s. However, this case cannot happen for the maximum speed of current high-speed trains.

Table 4.6: Maximum acceleration at the second midspan of the main beam with FVDs optimized by the acceleration transfer function, $Z_B(3l/2)$ (m/s^2)

Contribution of modes	H_∞ norm optimization	
	1st peak value	2nd peak value
First mode	2.459	3.852
Second mode	2.586	3.421
Both modes	2.600	3.465

By using the optimal damping coefficients of FVDs in Tables 4.5 to analyze the response of the beams under the high speed train HSLM A8, the results are shown in Table 4.6 and figure 4.9. Table 4.6 shows that the maximum acceleration is significantly different between the optimization cases of the first and second mode contribution or

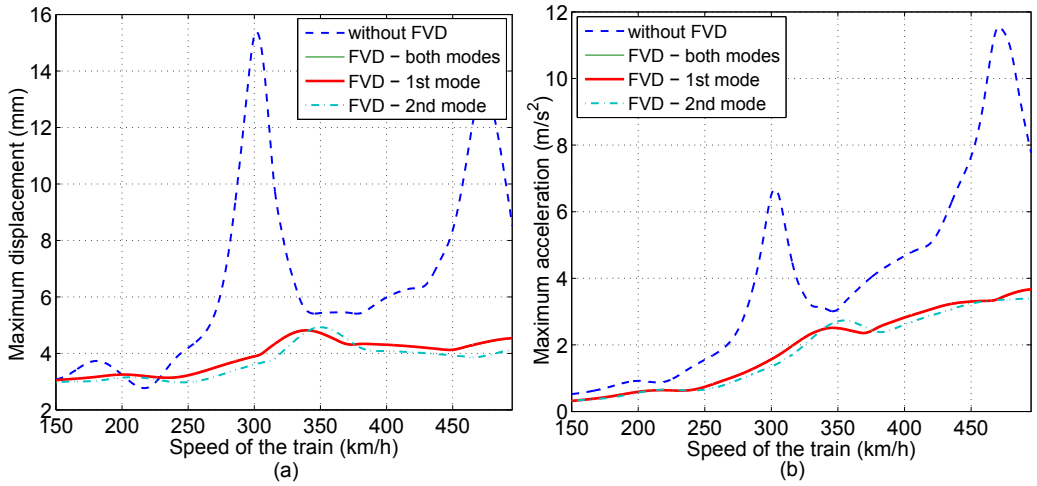

Figure 4.9: Response at the second midspan with FVDs optimized by the displacement transfer function: (a),(b) Optimal FVDs coefficients are calculated by H_∞ norm optimization

both of the modes. However, in the displacement case as shown in Fig. 4.9, the variation of the maximum displacements corresponding to the contribution of the different modes is not noticeable. It may be found that the displacements of the beams with the fluid viscous dampers are not so sensitive to the natural frequency change of the main system. Because of this, FVD systems are not significantly affected by estimation errors in manufacturing of FVDs in practice. This is one of advantages of FVDs in comparison to other passive damping devices such TMD systems.

4.4.2 Dynamic response of structure with nonlinear FVD system

In this section, evaluating the effectiveness of nonlinear FVD systems retrofitted into the Brustjaernsbaecken bridge under the high speed train HSLM-A8 is presented. The physical properties of the main structure in section 5.1.1 are also used in this case.

The optimal damping coefficients of the nonlinear FVDs may be found by solving the optimization problems with the performance index (4.21). However, Eq. (4.4) shows that the equivalent damping coefficients of the nonlinear FVDs depend on the displacement amplitude of the main structure $Y^{(\alpha-1)}$. This can lead to a situation in which the optimization problem with the performance index (4.21) cannot be solved. To overcome this problem, an approximate process to eliminate Y in the equivalent damping ratio (4.4) is conducted in appendix A1. The result may be rewritten as

$$\xi_D = \frac{2\omega_B^{\alpha-1}\overline{\Gamma}(\alpha)}{\pi \overline{m}_B l}\left(|C_n|\,Q\right)^{\alpha-1}\sum_{k=1}^{N_D} C_{\alpha k}\phi^{\alpha+1}(d_k) \tag{4.45}$$

By substituting ξ_D into the transfer function (4.43) and the performance index (4.21), then the optimal damping coefficients of the nonlinear FVDs may be found.

However, some assumptions used in appendix A1 can make the optimal damping coefficients of the nonlinear FVDs deviated. A simple line search technique[91] shown as a flow chart in appendix A2 to improve the damping coefficients may be needed. This process may be considered as the second procedure of the optimization process to find reasonable damping ratios of the nonlinear fluid viscous dampers. In practice, the optimal parameters may be found after a few iterations in the second procedure.

The simply supported beam with the length of 30 m shown in Table 2.2 and the auxiliary beam with the height of 1.52 m are used for verifying the effectiveness of the nonlinear FVD systems. Then, the damping coefficients of the nonlinear FVDs are obtained by minimizing the performance index (4.21) and using the flow graph in appendix A2. The results are presented in Table 4.7. It is observed that the optimal damping coefficients of the nonlinear FVD reduce noticeably as the velocity exponent α decreases.

Table 4.7: Optimal damping coefficients of FVD

Damping coefficient	Damper non-linearity parameter, α			
	1.00	0.75	0.50	0.25
$C_\alpha^{\text{opt}} \times 10^{-4}$ [N(s/m)$^\alpha$]	85.655	51.614	27.453	14.246

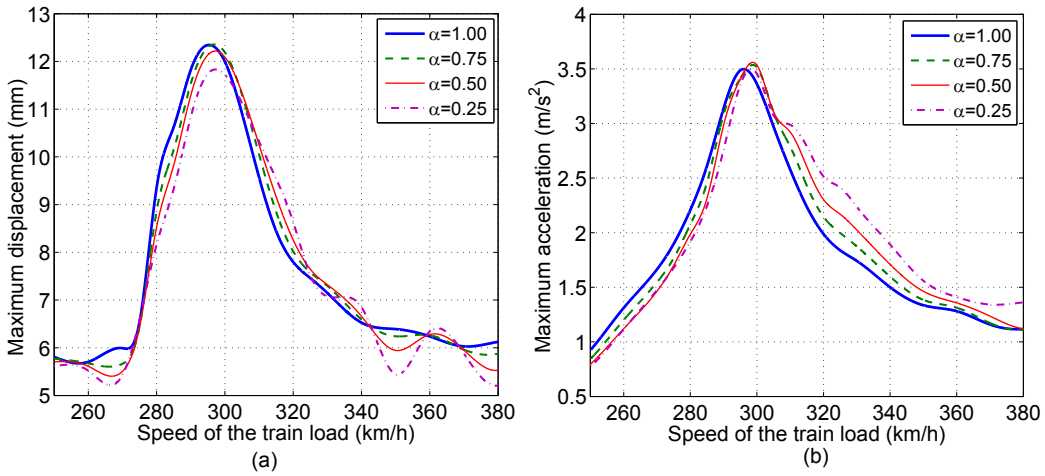

Figure 4.10: Response of the main beam with nonlinear FVD optimized to minimize the displacement of the main beam: (a) displacement at midspan of the main beam; (b) acceleration at midspan of the main beam

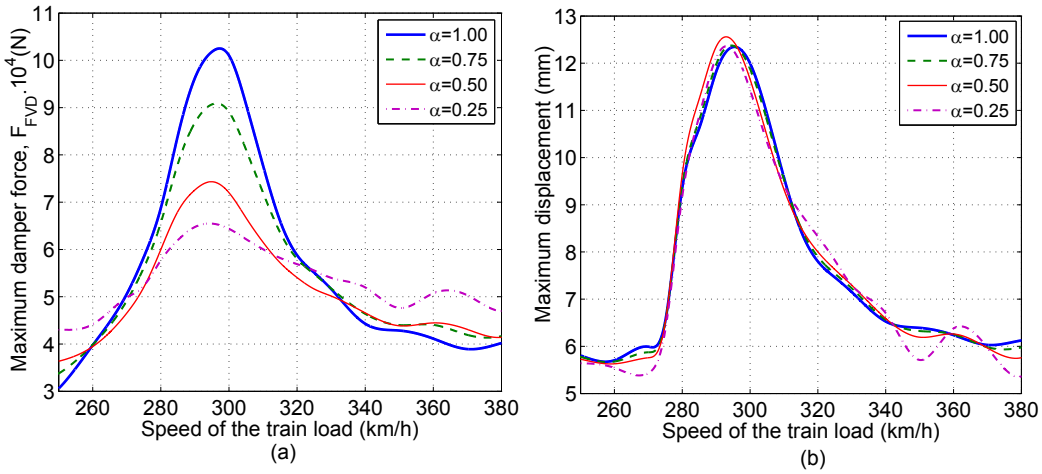

Figure 4.11: Response of the main beam with nonlinear FVD in Table 4.8: (a) displacement at midspan of the main beam; (b) acceleration at midspan of the main beam

Fig. 4.10 shows the response in terms of displacement and acceleration at midspan of the main beam with the nonlinear FVD versus the speed of the high-speed train HSLM A8. The results indicate that the response decreases when the non-linear parameter α decreases but this variation is not remarkable. It is well known that the biggest advantage of nonlinear FVDs is to limit the peak damping forces meanwhile the response of the primary structures are still reduced significantly. Therefore, for comparison between the damping forces in nonlinear FVDs and in linear FVDs, the damping coefficients of the nonlinear FVDs in Table 4.7 are optimized again in order to achieve the same reduction in acceleration as well as displacement of the main beam with linear FVDs. As a result, the percentage reduction in the damper force due to the nonlinear FVD is 10.93, 26.99 and 35.69% for α=0.75, 0.50 and 0.25, respectively. These results are also given in Table 4.8 and figure 4.11.

Table 4.8: Response of the system when damping coefficients of nonlinear FVDs are modified

Parameter	Damper non-linearity parameter, α			
	1.00	0.75	0.50	0.25
$C_\alpha \times 10^{-4}$ [N(s/m)$^\alpha$]	85.655	41.688	19.217	10.291
a_B(m/s^2)	3.49	3.48	3.47	3.47
$F_{\text{FVD}} \times 10^{-4}$ (N)	10.180	9.067	7.433	6.547
Δ_{FVD} (%)	0.00	10.93	26.99	35.69

Note: a_B is the maximum acceleration of the main beam;
$\Delta_{\text{FVD}}\% = \frac{F_{\text{FVD}}^{\text{linear}} - F_{\text{FVD}}^{\text{nolinear}}}{F_{\text{FVD}}^{\text{linear}}} 100\%$

It may be indicated that the nonlinear fluid viscous damper is advantageous because it achieves essentially the same reduction in displacement and acceleration but with a significantly reduced damper force. For high velocity applications in order not to exceed the devices force capacity or the forces transmitted to the superstructure, nonlinear FVDs may be used.

4.5 Conclusions

This study devoted to the investigation of H_∞ optimization for fluid viscous damper systems to reduce the excessive vibrations that high-speed railway bridges may experience under resonant conditions leads to following conclusions:

- In order to tune FVDs parameters to the vicinity of the exact values, analytical formulae which can include structural damping are derived based on the perturbation method. The proposed formulae can be considered as an improvement of the previous analytical formulae, especially for beams with large structural damping.

- Besides, a new procedure to determine the optimal damping ratios of nonlinear FVDs is also suggested based on H_∞ norm and Symans' linearization formula. The simulation results show that the reduction in the damper forces can reach by 35%, meanwhile, they still ensures that the structural response is minimized. Therefore, for high velocity applications in order not to exceed the devices force capacity or the forces transmitted to the superstructures, this procedure may be used.

- Finally, it can be seen that that the proposed objective function based on H_∞ norm is convenient. This function can be used to optimize the parameters of FVDs over a chosen frequency range, include individual and simultaneous contribution of modes for analyzing multi-span beams in which the effect of high modes on optimal FVDs coefficients is significant, and also be extended to solve nonlinear FVDs problems.

Chapter 5

Semi-active magnetorheological damper in double-beam system

5.1 Introduction

In this chapter, a new combination of MR dampers and a double-beam system will be investigated to reduce the resonant response of high-speed railway bridges. An H_∞ control algorithm to drive magnetorheological damping forces of MR dampers is derived. Feasible solutions for an uncertain time-delay model are obtained by using standard linear matrix inequality techniques. Weight functions as a loop shaping procedure are also introduced in the feedback controllers to improve the tracking ability of magnetorheological damping forces. Finally, the effectiveness of magnetorheological dampers controlled by the proposed scheme, along with the effects of the uncertain and the time-delay parameters on the models, are evaluated and compared to the performance of fluid viscous dampers in similar applications reported in previous research through numerical simulations.

5.2 Problem formulation

5.2.1 Dynamic modeling of structural system

The system configuration considered consists of a main beam, an auxiliary beam with MR dampers installed to connect both of the beams and a series of vehicles as shown in Fig. 5.1. The structural parameters and the modal properties of the systems are given in Table 2.2.

The auxiliary beams, which are connected to the main beams through the MR dampers, are considered as steel box girders with constant cross section inside which the dampers

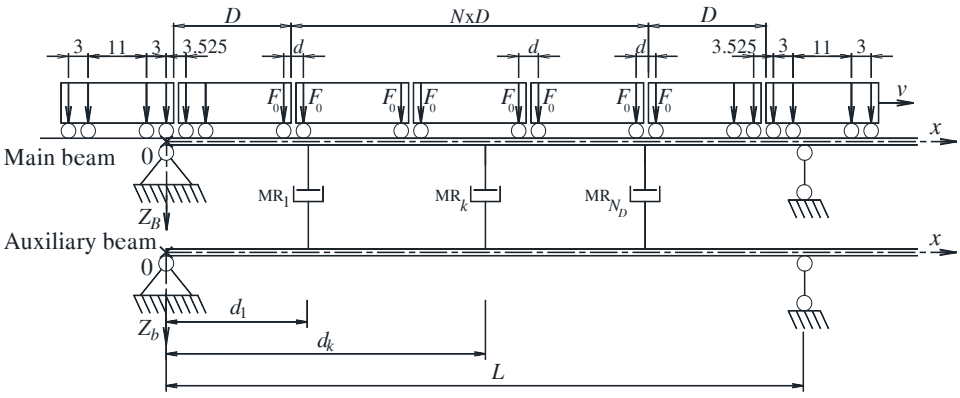

Figure 5.1: Train-bridge system with MR dampers

are to be installed. The dimensions of the auxiliary beams are determined based on guaranteeing the accomplishment of the Serviceability Limit State of vertical acceleration of the main beams (bridges)[8]. Defining the auxiliary beam geometry properties is presented in section 4.3.1.

The equations of motion may be derived by using standard techniques[64]:

$$\begin{cases} \frac{\partial^2}{\partial x^2}\left[EI_B\frac{\partial^2 Z_B(x,t)}{\partial x^2}\right]+\overline{m}_B\frac{\partial^2 Z_B(x,t)}{\partial t^2}+c_B\frac{\partial Z_B(x,t)}{\partial t}=F_v(x,t)-F_{MR}(x,t) \\ \frac{\partial^2}{\partial x^2}\left[EI_b\frac{\partial^2 Z_b(x,t)}{\partial x^2}\right]+\overline{m}_b\frac{\partial^2 Z_b(x,t)}{\partial t^2}+c_b\frac{\partial Z_b(x,t)}{\partial t}=F_{MR}(x,t) \end{cases} \tag{5.1}$$

where the origin of the $Z_{B/b}$ coordinates is assumed to be at the left support of each beam; $Z_{B/b}$, $EI_{B/b}$, $\overline{m}_{B/b}$ and $c_{B/b}$ are the vertical displacement, bending stiffness, mass per unit length and viscous damping of the main / auxiliary beam, respectively; $F_v(x,t)$ is the vertical force of the train acting on the main beam as shown in Eq. (2.2).

$F_{MR}(x,t)$ is the total force generated by the MR dampers determined as follows

$$F_{MR}(x,t)=\sum_{j=1}^{N_D}\delta(x-d_j)f_{MRj};\quad f_{MRj}=f(Z_{Bbj},\dot{Z}_{Bbj},u_j) \tag{5.2}$$

where N_D is the total number of MR dampers; d_j is the distance from the left end of the beams ($x=0$) to the jth MR damper. The jth MR damper force, f_{MRj}, depends on the relative displacement Z_{Bbj} and the relative velocity $\dot{Z}_{Bbj}$ between the beams at the jth MR damper location and on the input voltage u_j.

5.2.2 Equation of motion in modal state space

In the equations of motion (5.1), the deflection of the main beam, $Z_B(x,t)$ and of the auxiliary beam, $Z_b(x,t)$ can be expressed in a series as

$$Z_B(x,t) = \sum_{i=1}^{N_B} \phi_{Bi}(x) q_{Bi}(t) = \Phi_B^{\mathrm{T}}(x)\mathbf{q}_B(t) \tag{5.3}$$

$$Z_b(x,t) = \sum_{j=1}^{N_b} \phi_{bj}(x) q_{bj}(t) = \Phi_b^{\mathrm{T}}(x)\mathbf{q}_b(t) \tag{5.4}$$

and

$$\Phi_{B/b}^{\mathrm{T}} = \left\{ \begin{array}{cccc} \phi_{B1/b1} & \phi_{B2/b2} & \cdots & \phi_{BN_B/bN_b} \end{array} \right\}; \quad \mathbf{q}_{B(b)}^{\mathrm{T}} = \left\{ \begin{array}{cccc} q_{B1/b1} & q_{B2/b2} & \cdots & q_{BN_B/bN_b} \end{array} \right\} \tag{5.5}$$

where N_B and N_b are the number of modes to be considered for the main and auxiliary beam, respectively; $q_{Bi/bj}$ is the generalized coordinate or modal amplitude of the main beam (the auxiliary beam) corresponding to the ith/jth mode, $\phi_{Bi/bj}$.

If Eqs. (5.3) and (5.4) are introduced into equation (5.1) and multiplied by the ith/jth normal mode of the main/ auxiliary beam, the ith/ jth modal equation of motion is obtained by virtue of the normal modes orthogonality condition. Equation (5.1) can then be written as

$$\left\{ \begin{array}{l} \ddot{q}_{Bi}(t) + 2\zeta_{Bi}\omega_{Bi}\dot{q}_{Bi}(t) + \omega_{Bi}^2 q_{Bi}(t) = F_{vi}(t) - F_{cBi}(t); \quad i = 1...N_B \\ \ddot{q}_{bj}(t) + 2\zeta_{bj}\omega_{bj}\dot{q}_{bj}(t) + \omega_{bj}^2 q_{bj}(t) = F_{cbj}(t); \quad j = 1...N_b \end{array} \right. \tag{5.6}$$

where $\omega_{Bi/bj}$, $\zeta_{Bi/bj}$ and $m_{Bi(bj)}$ are the ith/jth circular natural frequency, modal damping ratio and modal mass of the main beam (the auxiliary beam), respectively. The MR force F_{MR} has been replaced by the active control force $\mathbf{f}_c$ in physical space or $F_{cBi/cbj}$ in modal space.

The relation between the ith modal control force F_{cBi} and the control forces $\mathbf{f}_c$ can be described as

$$F_{cBi}(t) = \frac{1}{m_{Bi}} \int_0^L \sum_{k=1}^{N_D} \delta(x - d_k) f_{ck} \phi_{Bi}(x) \mathrm{d}x = \frac{1}{m_{Bi}} \sum_{k=1}^{N_D} \phi_{Bi}(d_k) f_{ck} = \Phi_{mBi}\mathbf{f}_c \tag{5.7}$$

with

$$\Phi_{mBi} = \left\{ \begin{array}{cccc} \frac{\phi_{Bi}(d_1)}{m_{Bi}} & \frac{\phi_{Bi}(d_2)}{m_{Bi}} & \cdots & \frac{\phi_{Bi}(d_{N_D})}{m_{Bi}} \end{array} \right\}; \quad \mathbf{f}_c = \left\{ \begin{array}{cccc} f_{c1} & f_{c2} & \cdots & f_{cN_D} \end{array} \right\}^{\mathrm{T}}$$

Then, the jth modal control force F_{cbj} can be approximately determined as

$$F_{cbj} = \frac{1}{m_{bj}} \int_0^L \sum_{k=1}^{N_D} \delta(x-d_k) f_{ck}\, \phi_{bj}(x) \mathrm{d}x = \Phi_{mbj} \mathbf{f}_c \approx \Phi_{mbj} \Phi_{mBj}^{+} F_{cBj} \tag{5.8}$$

where

$$\Phi_{mbj} = \left\{ \begin{array}{cccc} \frac{\phi_{bj}(d_1)}{m_{bj}} & \frac{\phi_{bj}(d_2)}{m_{bj}} & \cdots & \frac{\phi_{bj}(d_{N_D})}{m_{bj}} \end{array} \right\}$$

and Φ_{mBj}^{+} denotes the pseudo-inverse of Φ_{mBj}[82].

In general, the modal active control forces $F_{cBi}(t)$ and $F_{cbi}(t)$ lead to a coupled system of differential Eqs. (5.6). However, if each modal active control force is designed to depend on q_{Bi}, q_{bj}, $\dot{q}_{Bi}$ and $\dot{q}_{bj}$ alone[81], and it is assumed that $i = j$ in which the main and auxiliary beams respond mainly with the same mode, then

$$F_{cBi} = -(G_{1i} q_{Bi} + G_{2i} q_{bi} + G_{3i} \dot{q}_{Bi} + G_{4i} \dot{q}_{bi}) = -\mathbf{G}_i \mathbf{v}_i \tag{5.9}$$

where $\mathbf{G}_i = \{G_{1i}\ \ G_{2i}\ \ G_{3i}\ \ G_{4i}\}$ are the ith modal control gains and the ith modal state vector is denoted by $\mathbf{v}_i = \{q_{Bi}\ \ q_{bi}\ \ \dot{q}_{Bi}\ \ \dot{q}_{bi}\}^{\mathrm{T}}$. These assumptions are justified as (i) in the case of the simply-supported and continuous beams analyzed in section 5, the contribution of coupling terms is negligible in the optimization process, based on the previous study of the authors[92]; (ii) the assumptions are only considered to predict the optimal control forces of the dampers and not the dynamic response of the retrofitted structure. Then, Eqs. (5.6) become mutually independent. More commonly, this design procedure is called independent modal space control (IMSC)[81].

Besides, the ith modal external force $F_{vi}(x,t)$ may be determined as

$$F_{vi}(t) = \frac{1}{m_{Bi}} \int_0^L \sum_{k=1}^{N_v} F_k \delta\left[x - (vt - a_k)\right] H(t-t_k) \phi_{Bi}(x) \mathrm{d}t \tag{5.10a}$$

$$= \frac{1}{m_{Bi}} \sum_{k=1}^{N_v} F_k H(t-t_k) \phi_{Bi}(vt - a_k) \tag{5.10b}$$

It is convenient to rearrange modal equations, given in Eq. (5.6), in the modal state-space form as

$$\dot{\mathbf{v}}_i = \mathbf{A}_{0i} \mathbf{v}_i + \mathbf{B}_{0i} F_{cBi} + \mathbf{C}_{0i} F_{vi} \tag{5.11}$$

where

$$\mathbf{v}_i = \left\{ \begin{array}{c} q_{Bi} \\ q_{bi} \\ \dot{q}_{Bi} \\ \dot{q}_{bi} \end{array} \right\};\ \mathbf{A}_{0i} = \left[\begin{array}{cccc} 0 & 0 & 1 & 0 \\ 0 & 0 & 0 & 1 \\ -\omega_{Bi}^2 & 0 & -2\omega_{Bi}\zeta_{Bi} & 0 \\ 0 & -\omega_{bi}^2 & 0 & -2\omega_{bi}\zeta_{bi} \end{array} \right];$$

$$\mathbf{B}_{0i} = \begin{Bmatrix} 0 \\ 0 \\ -1 \\ \Phi_{mbi}\Phi^{+}_{mBi} \end{Bmatrix}; \; \mathbf{C}_{0i} = \begin{Bmatrix} 0 \\ 0 \\ 1 \\ 0 \end{Bmatrix}$$

Physical control force and modal coordinate

Converting modal control forces into physical control forces and discrete measurements into modal coordinates is a part of the independent modal space control procedure. Eq. (5.7) which transforms the physical control forces into modal space through the modal participation matrix can be rewritten as

$$\mathbf{F}_{cB} = \mathbf{L}_B \mathbf{f}_c \tag{5.12}$$

where $\mathbf{L}_B$ is the $N_B \times N_D$ modal matrix

$$\mathbf{L}_B = \{ \; \Phi_{mB1} \quad \Phi_{mB2} \quad \ldots \quad \Phi_{mBN_B} \; \}^{\mathrm{T}}; \quad \mathbf{F}_{cB} = \{ \; F_{cB1} \quad F_{cB2} \quad \ldots \quad F_{cBN_B} \; \}^{\mathrm{T}}$$

Note that if the number of controlled modes N_B is equal to the number of MR dampers N_D, the matrix $\mathbf{L}_B$ becomes square. In that case, the physical control vector $\mathbf{f}_c$ is found from Eq. (5.12) as

$$\mathbf{f}_c = \mathbf{L}_B^{-1} \mathbf{F}_{cB} \tag{5.13}$$

If $N_B \neq N_D$, the inverse of $\mathbf{L}_B$ does not exist. However, $\mathbf{f}_c$ can be approximated by means of the pseudo-inverse of $\mathbf{L}_B$ [82] as follows

$$\mathbf{f}_c \approx \mathbf{L}_B^{+} \mathbf{F}_{cB} \tag{5.14}$$

where

$$\mathbf{L}_B^{+} = \begin{cases} \mathbf{L}_B^{\mathrm{T}} (\mathbf{L}_B \mathbf{L}_B^{\mathrm{T}})^{-1} & \text{if } N_D > N_B \\ (\mathbf{L}_B \mathbf{L}_B)^{-1} \mathbf{L}_B^{\mathrm{T}} & \text{if } N_D < N_B \end{cases} \tag{5.15}$$

Additionally, in order to improve the effectiveness of the retrofit, the MR damper locations d_k should be chosen points near the antinodes of the controlled modes. Mathematically, this choice avoids singularity of $\mathbf{L}_B^{-1}$ or $\mathbf{L}_B^{+}$.

Moreover, to determine the control forces in modal space, the modal displacements and velocities need to be extracted from measurements of actual displacements and velocities as they cannot be measured directly. After some algebraic manipulations from Eqs. (5.3) and (5.4), the modal response of the main and auxiliary beam can be reformulated as

$$\mathbf{q}_B = \mathbf{D}_B^{-1} \mathbf{Z}_{Bs} \text{ and } \mathbf{q}_b = \mathbf{D}_b^{-1} \mathbf{Z}_{bs} \tag{5.16}$$

where $\mathbf{D}_{B/b}$ is the $N_s \times N_{B/b}$ modal matrix

$$\mathbf{D}_{B/b} = \{ \ \Phi^{\mathrm{T}}_{B(b)}(x_1) \quad \Phi^{\mathrm{T}}_{B/b}(x_2) \quad \ldots \quad \Phi^{\mathrm{T}}_{B/b}(x_{N_s}) \ \}^{\mathrm{T}}$$

and $\mathbf{Z}_{Bs/bs}$ is the $N_s \times 1$ actual response vector corresponding to the number of sensors N_s at the positions $x_1, x_2, \ldots x_{N_s}$ on the beams

$$\mathbf{Z}_{Bs/bs} = \{ \ Z_{B/b}(x_1) \quad Z_{B(b)}(x_2) \quad \ldots \quad Z_{B(b)}(x_{N_s}) \ \}^{\mathrm{T}}$$

If $N_s \neq N_{B(b)}$, the inverse matrix $\mathbf{D}^{-1}_{B/b}$ can be replaced by the pseudo-inverse matrix $\mathbf{D}^{+}_{B/b}$ as per Eq. (5.15).

In this work, it should be noticed that the above feedback control design is also based on the assumption that the full state vector is available for measurement. As mentioned in Section 3.3.2, it is not practical to measure the full state vector, but only some certain structural responses because using so many sensors can lead to a higher implementation cost as well as difficulty in measuring all the needed variables. Thus, the design of observers, such as the Kalman observer, the H_∞ observer and other nonlinear observer approaches[83] that introduce an algorithm permitting an estimate of a full state vector from some measured data with high accuracy and noise reduction is necessary. This topic has been discussed in many previous papers and lectures about control engineering[82,83] and thus, it is not presented here.

5.2.3 H_∞ controller design

Every mode of vibration is individually controlled in the independent modal space control. The selection of the modal control gains $\mathbf{G}_i$ must ensure a suitable disturbance attenuation ability for the controlled mode. Therefore, the H_∞ controller design is adopted here.

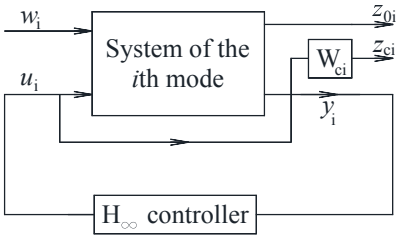

Figure 5.2: Framework of the static state feedback control system in modal state space

In the H_∞ based control system design, a controller is selected to internally stabilize the system in such a way that the H_∞ norm of a transfer matrix, which describes

certain design objectives, is minimized or becomes smaller than a specified value γ.

A controlled output considered as a design objective in the H_∞ control is formulated here. To satisfy the limit acceleration and displacement requirements of the main beam in[8], the controlled output is defined as $\mathbf{z}_{0i} = [\ddot{q}_{Bi} \quad \alpha(q_{Bi} - q_{bi})]$, then $\mathbf{z}_{0i}$ can be written

$$\mathbf{z}_{0i} = \mathbf{E}_{1i}\mathbf{v}_i + \mathbf{D}_i F_{vi} + \mathbf{E}_{2r} F_{cBi} \tag{5.17}$$

where

$$\mathbf{E}_{1i} = \begin{bmatrix} -\omega_{Bi}^2 & 0 & -2\omega_{Bi}\zeta_{Bi} & 0 \\ \alpha & -\alpha & 0 & 0 \end{bmatrix}; \ \mathbf{D}_i = \begin{Bmatrix} 1 \\ 0 \end{Bmatrix}; \ \mathbf{E}_{2i} = \begin{Bmatrix} -1 \\ 0 \end{Bmatrix}$$

and the scalar weighting α is used to control the trade-off between the control objectives.

From Eqs. (5.11) and (5.17), the mathematical model of the control system can be rewritten as

$$\begin{Bmatrix} \dot{\mathbf{v}}_i \\ \mathbf{z}_{0i} \end{Bmatrix} = \begin{bmatrix} \mathbf{A}_{0i} & \mathbf{C}_{0i} & \mathbf{B}_{0i} \\ \mathbf{E}_{1i} & \mathbf{D}_i & \mathbf{E}_{2i} \end{bmatrix} \begin{Bmatrix} \mathbf{v}_i \\ F_{cBi} \\ F_{vi} \end{Bmatrix} \tag{5.18}$$

Fig. 5.2 represents the control system with the model expressed by Eqs. (5.18) and the weighting function $W_{ci}(s)$. It is a low-pass filter in order to improve the tracking ability of the magnetorheological dampers. This function concentrates the control force on a defined frequency range.

The state space of the weighting function in modal state space[93] is

$$\begin{cases} \dot{\mathbf{x}}_{ci} = \mathbf{A}_{ci}\mathbf{x}_{ci} + \mathbf{B}_{ci}F_{cBi} \\ \mathbf{z}_{ci} = \mathbf{C}_{ci}\mathbf{x}_{ci} + \mathbf{D}_{ci}F_{cBi} \end{cases} \tag{5.19}$$

where

$$\mathbf{A}_{ci} = \begin{bmatrix} 0 & 1 \\ -\omega_c^2 & -\sqrt{2}\omega_c \end{bmatrix}; \ \mathbf{B}_{ci} = \begin{bmatrix} 0 \\ 1 \end{bmatrix}; \ \mathbf{C}_{ci} = \begin{bmatrix} \omega_c^2 & 0 \end{bmatrix}; \ \mathbf{D}_{ci} = 0;$$

and ω_c is the cutoff frequency of the filter.

Now, gathering the state-space representations of (5.18) and (5.19), the generalized plant is rewritten as

$$\begin{cases} \dot{\mathbf{x}}_i = \mathbf{A}_i\mathbf{x}_i + \mathbf{B}_{di}u_i + \mathbf{B}_{wi}w_i \\ \mathbf{z}_i = \mathbf{C}_i\mathbf{x}_i + \mathbf{H}_{di}u_i + \mathbf{D}_{wi}w_i \end{cases} \tag{5.20}$$

with the notations $w_i = F_{vi};\ u_i = \mathbf{K}_i\mathbf{x}_i;\ \mathbf{K}_i = \begin{bmatrix} \mathbf{G}_i & \mathbf{G}_{ci} \end{bmatrix}$;

$$\mathbf{x}_i = \begin{bmatrix} \mathbf{v}_i \\ \mathbf{x}_{ci} \end{bmatrix};\ \mathbf{A}_i = \begin{bmatrix} \mathbf{A}_{0i} & \mathbf{0} \\ \mathbf{0} & \mathbf{A}_{ci} \end{bmatrix};\ \mathbf{B}_{di} = \begin{bmatrix} \mathbf{B}_{0i} \\ \mathbf{B}_{ci} \end{bmatrix};\ \mathbf{B}_{wi} = \begin{bmatrix} \mathbf{C}_{0i} \\ \mathbf{0} \end{bmatrix};\ \mathbf{z}_i = \begin{bmatrix} \mathbf{z}_{0i} \\ z_{ci} \end{bmatrix};$$

$$\mathbf{C}_i = \begin{bmatrix} \mathbf{E}_{1i} & \mathbf{0} \\ \mathbf{0} & \mathbf{C}_{ci} \end{bmatrix};\ \mathbf{H}_{di} = \begin{bmatrix} \mathbf{E}_{2i} \\ \mathbf{D}_{ci} \end{bmatrix};\ \mathbf{D}_{wi} = \begin{bmatrix} \mathbf{D}_{0i} \\ \mathbf{0} \end{bmatrix}$$

where $\mathbf{G}_{ci}$ is the control gain vector corresponding to $\mathbf{x}_{ci}$.

Then, by taking Laplace transform of Eqs. (5.20) the ith modal system transfer function $\mathbf{T}_i(s)$ from the disturbance w_i to $\mathbf{z}_i$ as pointed out in Fig. 5.2 is given by

$$\mathscr{L}\{\mathbf{z}_i\} = \mathbf{T}_i(s)\mathscr{L}\{w_i\} \tag{5.21}$$

$$\mathbf{T}_i(s) = (\mathbf{C}_i + \mathbf{H}_{di}\mathbf{K}_i)[s\mathbf{I} - (\mathbf{A}_i + \mathbf{B}_{di}\mathbf{K}_i)]^{-1}\mathbf{B}_{wi} + \mathbf{D}_{wi};\ s = \mathrm{j}\omega \tag{5.22}$$

If modeling uncertainty and actuator time delays are considered, Eq. (5.20) can be expressed as

$$\begin{cases} \dot{\mathbf{x}}_i(t) = [\mathbf{A}_i + \Delta\mathbf{A}_i(t)]\,\mathbf{x}_i(t) + [\mathbf{B}_{di} + \Delta\mathbf{B}_{di}(t)]\,u_i(t-\tau) + \mathbf{B}_{wi}w_i(t) \\ \mathbf{z}_i(t) = \mathbf{C}_i\mathbf{x}_i(t) + \mathbf{H}_{di}u_i(t) + \mathbf{D}_{wi}w_i(t) \end{cases} \tag{5.23}$$

where τ is the time-delay of the system; and ΔA_i and ΔB_{di} are real matrix functions representing time-varying parameter uncertainties[94]. The admissible uncertainties are assumed to be of the form

$$\Delta\mathbf{A}_i(t) = \mathbf{L}_1\mathbf{F}_1(t)\mathbf{E}_1;\ \Delta\mathbf{B}_{di}(t) = \mathbf{L}_d\mathbf{F}_d(t)\mathbf{E}_d$$

where $\mathbf{F}_1(t)$ and $\mathbf{F}_d(t)$ are unknown real time-varying matrices with Lebesgue measurable elements satisfying $\|\mathbf{F}_1(t)\| \le 1$ and $\|\mathbf{F}_d(t)\| \le 1,\ \forall t$; $\mathbf{L}_1$, $\mathbf{L}_d$, $\mathbf{E}_1$ and $\mathbf{L}_d$ are known real constant matrices which represent the structure of uncertainties.

Theorem: The system (5.23) with $|u_i| \le u_{\max}$ is robustly closed-loop stable with disturbance attenuation $\gamma > 0$ for any time-delay τ satisfying $0 \le \tau \le \bar{\tau}$, if there exist symmetric positive definite matrices $\mathbf{X}, \mathbf{P}_1, \mathbf{P}_2, \mathbf{P}_3, \mathbf{Q}$, a matrix $\mathbf{Y}$, a scalar $\varepsilon_i > 0$, $i = 1, \ldots, 5$ and $\rho_0 > 0$, satisfying the following LMIs:

$$\begin{bmatrix} \mathbf{M}_c & \mathbf{G}_c & \mathbf{U}_c & \bar{\tau}\mathbf{N}_c & \mathbf{U}_w \\ \mathbf{G}_c^{\mathrm{T}} & -\mathbf{J}_1 & \mathbf{0} & \mathbf{0} & \mathbf{0} \\ \mathbf{U}_c^{\mathrm{T}} & 0 & -\bar{\tau}\mathbf{J}_2 & \mathbf{0} & \mathbf{0} \\ \bar{\tau}\mathbf{N}_c^{\mathrm{T}} & 0 & 0 & -\bar{\tau}\mathbf{J}_3 & \mathbf{0} \\ \mathbf{U}_w^{\mathrm{T}} & 0 & 0 & 0 & \mathbf{J}_w \end{bmatrix} \prec 0;\ \begin{bmatrix} \mathbf{Q} & \mathbf{Y} \\ \mathbf{Y}^{\mathrm{T}} & \mathbf{X} \end{bmatrix} \succeq 0;\ \mathbf{X} - \mathbf{P}_1 - \mathbf{P}_2 - \mathbf{P}_3 \succeq 0 \tag{5.24}$$

$$\begin{bmatrix} -\mathbf{X}\rho_0 & \mathbf{Y}^{\mathrm{T}} \\ \mathbf{Y} & -\mathbf{I} \end{bmatrix} \preceq 0 \tag{5.25}$$

where $u_{\max}$ is the maximum controlled damping force;

$$\mathbf{M}_c = \mathbf{X}\mathbf{A}_i^{\mathrm{T}} + \mathbf{A}_i X + \mathbf{Y}^{\mathrm{T}}\mathbf{B}_{di}^{\mathrm{T}} + \mathbf{B}_{di}\mathbf{Y} + \bar{\tau}\mathbf{B}_{di}\mathbf{Q}\mathbf{B}_{di}^{\mathrm{T}} + \varepsilon_1\mathbf{L}_1\mathbf{L}_1^{\mathrm{T}} + \varepsilon_2\mathbf{L}_d\mathbf{L}_d^{\mathrm{T}} + \bar{\tau}\varepsilon_3\mathbf{L}_d\mathbf{L}_d^{\mathrm{T}};$$

$$\mathbf{G}_c = [\mathbf{X}\mathbf{E}_1^{\mathrm{T}}\ \mathbf{Y}^{\mathrm{T}}\mathbf{E}_d^{\mathrm{T}}];\ \mathbf{J}_1 = \mathrm{diag}\{\varepsilon_1\mathbf{I},\ \varepsilon_1\mathbf{I}\};\ \mathbf{U}_c = \tau\mathbf{B}_{di}\mathbf{Q}\mathbf{E}_d^{\mathrm{T}};\ \mathbf{J}_2 = \varepsilon_3\mathbf{I} - \mathbf{E}_d\mathbf{Q}\mathbf{E}_d^{\mathrm{T}};$$

$$\mathbf{N}_c = [\mathbf{X}\mathbf{A}_i^{\mathrm{T}}\ \mathbf{X}\mathbf{E}_1^{\mathrm{T}}\ \mathbf{Y}^{\mathrm{T}}\mathbf{B}_{di}^{\mathrm{T}}\ \mathbf{Y}^{\mathrm{T}}\mathbf{E}_d^{\mathrm{T}}];\ \mathbf{J}_3 = \mathrm{diag}\{(\mathbf{P}_1 - \varepsilon_4\mathbf{L}_1\mathbf{L}_1^{\mathrm{T}}),\ \varepsilon_4\mathbf{I},\ (\mathbf{P}_2 - \varepsilon_5\mathbf{L}_d\mathbf{L}_d^{\mathrm{T}}),\ \varepsilon_5\mathbf{I}\};$$

$$\mathbf{U}_{c2} = \tau\mathbf{B}_{di}\mathbf{Q}\mathbf{E}_d^{\mathrm{T}};\ \mathbf{U}_w = [\mathbf{B}_{wi}\ (\mathbf{X}\mathbf{C}^{\mathrm{T}} + \mathbf{Y}^{\mathrm{T}}\mathbf{H}_d^{\mathrm{T}})\ \mathbf{0}];$$

and $\mathbf{J}_w = \begin{bmatrix} -\gamma^2\mathbf{I} & \mathbf{D}_{wi}^{\mathrm{T}} & \tau\mathbf{B}_{wi}^{\mathrm{T}} \\ \mathbf{D}_{wi} & -\mathbf{I} & \mathbf{0} \\ \tau\mathbf{B}_{wi} & \mathbf{0} & -\tau\mathbf{P}_3 \end{bmatrix}$

Proof. See appendix B1.

Remark: It is noted that inequalities (5.24) and (5.25) are LMIs. In order to obtain the lower of H_∞ performance index, the variable γ^2 should be minimized. Therefore, if $\bar{\tau}$ is assumed to be given, the controller design problem to determine $\mathbf{K}_i$ can be transformed into a problem of finding a solution to

$$\min_{\mathbf{K}_i}\ \gamma^2 \text{ subject to LMIs (5.24) and (5.25).} \tag{5.26}$$

Moreover, the problem of finding the largest $\bar{\tau}$ for a given γ , using the method as presented in the above theorem can be solved as

$$\min_{\mathbf{K}_i}\ \bar{\tau} \text{ subject to inequalities (5.24), (5.25) and } \bar{\tau} > 0. \tag{5.27}$$

This minimization problem can be solved by using the LMI Toolbox in MATLAB®.

To this end, the semi-active H_∞ control system can be depicted in Fig. 5.3.

5.3 Simulation result and discussion

In this section, the performance of the semi-active static output feedback H_∞ controller applied to the simply supported beam and the continuous beam under the circulation of the HSLM-A8 high-speed train is evaluated. The physical properties of the beams and the train HSLM-A8 are listed in section2.2.1.

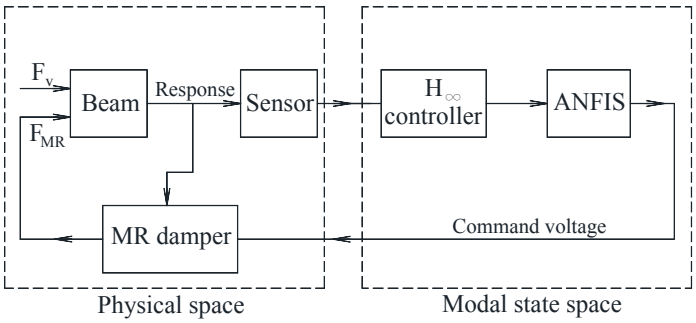

Figure 5.3: Structure of the semi-active controller for reducing the vibration of beams with MR dampers

5.3.1 Simply supported beam with semi-active MR dampers

In the previous study[12], the influence of the auxiliary beam natural frequency was analyzed in detail in the reduction of the main beam response when the retrofit was performed with fluid viscous dampers in the similar double-beam configuration. It showed that the higher the natural frequency of the auxiliary beams is, the higher the attenuation of the main beam resonant response is. This is one of the important parameters in the designing of FVD systems to guarantee the serviceability limit states in bridge design as per Eurocodes EN 1990 Annex A2[8]. From the physical parameters of the main beam listed in Table 2.1, the auxiliary beam height of $h_b = 1.52$ m is chosen in this study. The width and thickness of the auxiliary beam box section for this height are 0.912 m and 0.058 m, respectively. Then, its geometric properties are presented in Table 5.1.

Table 5.1: Properties of the auxiliary beam,[12]

Beam	L_b (m)	$\overline{m}_b$ (kg/m)	ζ_{bi} (%)	ω_1	ω_2	ω_3
Simply supported beam	30	2.1×10^3	0.5	31.6	126.8	289.5

Note: L_b is the span length; $\overline{m}_b$ is the mass per unit length; ω_i (rad/s) and ζ_{bi} are the ith natural frequency and the ith structural modal damping of the auxiliary beam, respectively.

In the first approach, only the contribution of the fundamental modes of the main and auxiliary beams are considered. To satisfy the desired control force obtained in the optimization process, the controller requires a maximum force almost twice the maximum force of the MR damper with the data presented in Table 3.1. Therefore, two MR dampers connecting the same mid-span sections of both beams are suggested in this case. The two processes shown in Fig. 5.3 are carried out to analyze the structure

retrofitted with the MR dampers. First, the response of the complete system including the beams, the MR dampers and the disturbance load is simulated in the modal state space to determine the optimal control force. Then, in order to calculate the response of the beams and the MR forces more accurately, the dynamic responses of the double beam system are obtained by using finite element model of the retrofitted structure, therefore not assuming the simplifications from the first process.

$\mathbf{H}_\infty$ *controller design*

The design objective of the H_∞ controller is to find the control gain $\mathbf{K}_1$. By setting the cutoff frequency of the filter ω_c =5 Hz, $\alpha = 20$ and the factor $\rho_0 = 0.015$, then the matrix gain may be obtained $\mathbf{K}_1 = [-29.508 \ -2.629 \ 3.656 \ -0.049 \ 4.896 \ 0.617]$ and the upper bound $\gamma_1 = 5.024$. This result is presented in Fig. 5.4. It shows the gain plots of the closed-loop transfer function T_1 from the disturbance w_1 to $\mathbf{z}_1$ shaped by the weighting function W_{c1}. It can be seen that the magnitude of T_1 is reduced significantly in the vicinity of the resonance frequency.

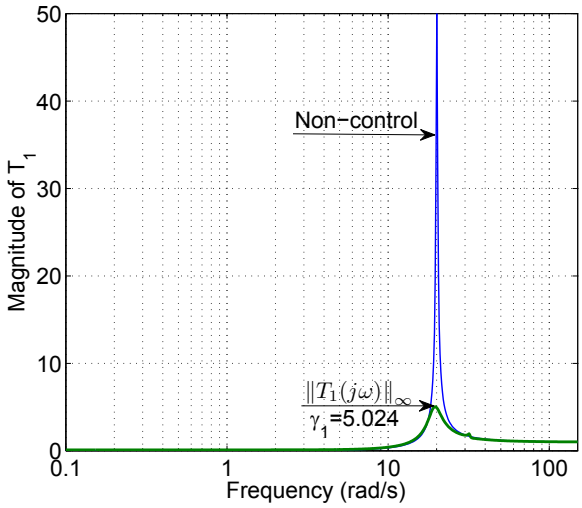

Figure 5.4: Magnitude of closed-loop transfer functions $T_1(j\omega)$ from w_i to $\mathbf{z}_i$

The acceleration response at mid-span of the main beam with the semi-active MR dampers under the high-speed train HSLM-A8 at the resonant speed of 305 km/h is presented in Fig. 5.5. In the case of $\gamma_1 = 5.024$, the results show that the maximum acceleration of the main beam is reduced about 66.64 % when compared to the acceleration of the bare structure subjected to the train passage at the resonant speed of $v = 287.33$ km/h. From Fig. 5.5b, it can be found that the actual damping force generated by the MR dampers can track the desired control force very well and the ANFIS model provides a very smooth command voltage diagram in Fig. 5.5c. Besides, it can be seen that when the MR damper force and the desired control force are not in phase,

the input voltage is set to zero and the MR damper is operated as a passive-off MR damper. This shows that the operation of the control algorithm is reasonable. Fig. 5.5 also shows that the phenomenon of the control spillover is not evident in this case. This confirms that the response of the structure with the static H_∞ state feed-back control is absolutely stable. From this discussion, it may be concluded that the system is effective in controlling the MR damping force to reduce the vibration of the main beam under the high-speed train circulation.

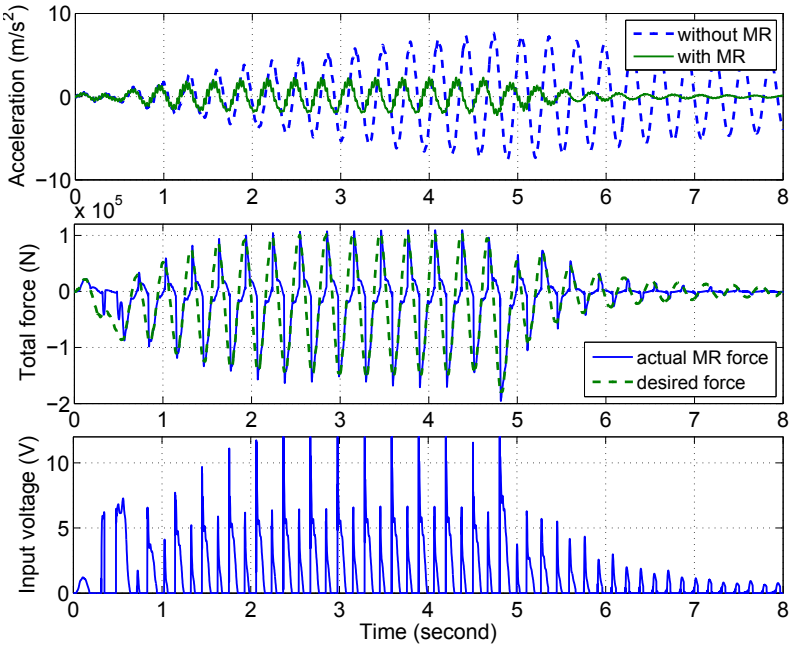

Figure 5.5: Response in the time domain: (a) main beam acceleration without MR damper and with MR damper versus time; (b) comparison of the actual MR damper force and the desired control force; (c) input voltage to MR damper

In order to evaluate the performance of the semi-active controller with MR dampers, three situations are considered in which the MR damper is employed in a passive-off, passive-on and semi-active mode. In the case of the passive-off mode, the command voltage to the MR dampers is set at 0 V and in the passive-on mode, it is set at the maximum voltage level (12 V). Besides, the effectiveness of MR dampers is also clarified through the comparison with a hypothetical retrofit using one equivalent fluid viscous damper in the same configuration and using the same auxiliary beam. FVDs are pure damping devices [12] connected between the same sections of the main and auxiliary beam. The FVD force may be expressed in the linear case in the simple form $F_{FVD} = C_D\dot{z}$ where $\dot{z}$ is the relative velocity between the FVD ends and C_D is assumed to be the optimal equivalent damping coefficient determined analytically in [12] as fol-

lows:

$$C_D^{\text{optimal}} = \frac{2m_B\omega_B\mu\left(\eta^2-1\right)}{\sqrt{4+2\mu+6\mu\eta^2+3\mu^2\eta^2+2\mu^2\eta^4+\mu^3\eta^4}} \tag{5.28}$$

where m_B and ω_B are the modal mass and circular frequency of the main beam in its fundamental mode, respectively; μ and η are the frequency ratio and the mass ratio between the auxiliary and main beam. By substituting $\mu = 0.084$ and $\eta = 1.575$, which are calculated based on the parameters in Table 5.1, into Eq. (5.28), then the optimal equivalent damping coefficient C_D^{optimal} is 7.971×10^5 Ns/m.

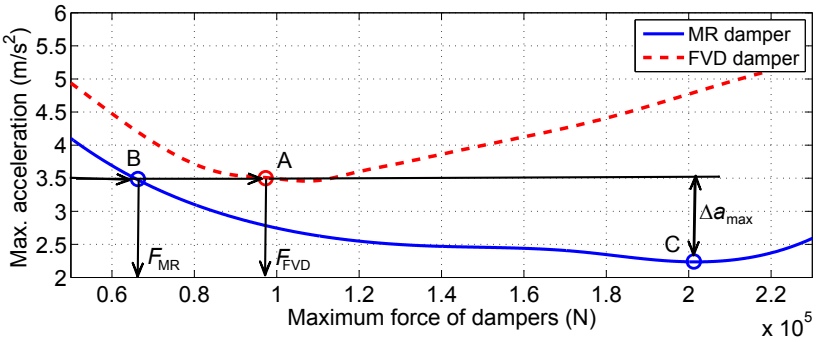

Figure 5.6: Maximum acceleration at the the main beam midspan ($a_{\max}$) versus maximum total damping force ($F_{\max}$)

The maximum response of the main beam with semi-active MR dampers and FVD under the high-speed train HSLM-A8 versus the maximum force of the dampers is shown in Fig. 5.6. For the case of FVD, each point of $(F_{\max}, a_{\max})$ corresponds to a different damper constant C_D and the point "A" is the case of C_D^{optimal}. Each point on the curve for the case of the MR dampers corresponds to a different upper bound force $u_{\max}$ of the total controlled force in Eq. (B.7). It can be observed that the required maximum MR force (F_{MR}) at point "B" in Fig. 5.6 is much smaller than the required FVD force (F_{FVD}) at point "A" to guarantee that the maximum acceleration of the main beam is smaller than the allowable acceleration $a_{max} = 3.5$ m/s^2 considered (limit for ballasted tracks). This is one of the greatest advantages of the retrofit with MR dampers when compared to FVDs in high-speed applications in order not to exceed the devices force capacity and the forces transmitted to the superstructure. Furthermore, it should be noted that the maximum acceleration response can be reduced to a higher degree by application of MR dampers. Compared to the response obtained with FVD the minimal value provided in the case of MR dampers is 2.306 m/s^2 corresponding to point "C" and $\Delta a_{max} = 1.264$ m/s^2, or (36.11%) lower in this example. This permits to reduce the natural frequency of the auxiliary beam, and therefore its height which is essential in order to minimize the occupied space under bridge deck associated with the retrofit installation.

Considering frequency or speed domain, the maximum accelerations and displacements at midspan of the main beam are presented in Fig. 5.7 and Table 5.2. The reduction of the maximum response with passive-off, passive-on, semi-active MR, active damper and the FVDs are 31.40, 12.20, 68.91, 83.50 and 53.36 % for the acceleration and 29.60, 19.82, 59.36, 69.70 and 46.58 % for the displacement, respectively. These results show again the effectiveness of the active and semi-active damper. Besides, it can be seen that the reduction of acceleration is higher than that of displacements in the semi-active and active control cases. This is caused by the selection of the weight factor $\beta = 20$ in the controlled output vector z_{11}. It minimizes the acceleration response rather that the displacement response. Another interesting issue withdrawn from these results is that the forces applied by the MR damper operating in semi-active mode are always smaller than those corresponding to the damper operating in the passive-on mode with a maximum input voltage 12 V. In contrast, the reduction of the beam response in semi-active mode is larger than that in passive-on one. It is indicated that higher damping forces are not always associated with better results. It should be mentioned that the maximum normal stress at midspan of the auxiliary beam is 14.587 MPa. This stress is much smaller than the yield stress of steel.

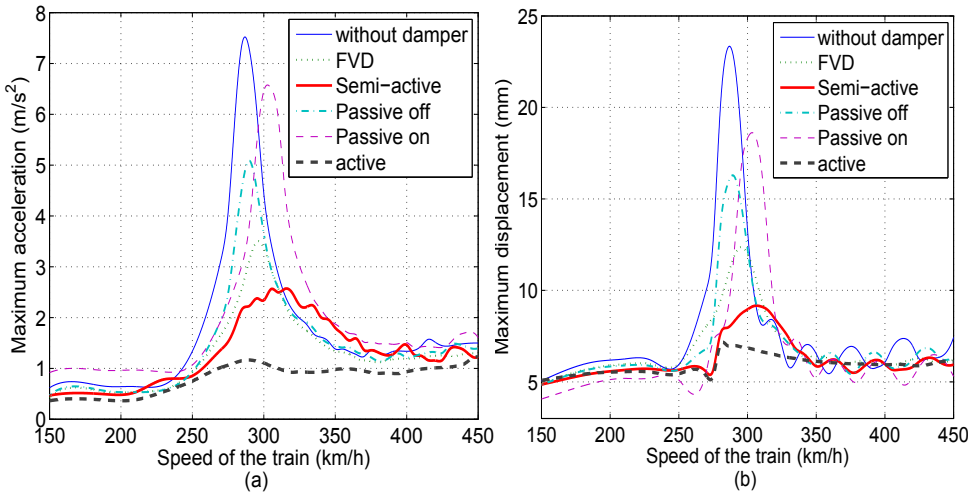

Figure 5.7: Response of the main beam versus speed of the train: (a) maximum acceleration at midspan of the main beam; (b) maximum displacement at midspan of the main beam

$\mathbf{H}_\infty$ *controller design on uncertain model*

It is well-known that the optimal gain matrices used to generate the desired control forces are significantly affected by the controlled structure frequencies. Therefore, knowledge of the controlled primary structure is required in order to accurately calcu-

Table 5.2: Maximum acceleration and displacement at midspan of the main beam under the train load

Response	Peak-to-peak value					
	w/o damper	FVD	semi-active	passive-off	passive-on	active
a (m/s^2)	7.417	3.459	2.306	5.085	6.513	1.221
d (mm)	23.111	12.330	9.393	16.262	18.529	6.999

late control forces. Even if the modal parameters of the bridge are available from tests, its natural frequencies may vary considerably and lead to detuning effects[23]. Thus, an uncertain model to optimize the control forces is desirable to provide a solution to these detuning effects and is more reliable and applicable for vibration control. To clarify the effectiveness of the proposed uncertain model, a numerical simulation for the former beam system is presented here. First, uncertain parameters in Eq. (5.23) are set as follows: $\mathbf{L}_1$, $\mathbf{E}_1$ and $\mathbf{L}_d$ are 6×1, 1×6 and 6×1 matrices, respectively and their elements are defined as

$$(L_1)_{i1}=\begin{cases}0\,,\ i\neq3\\ 1\,,\ i=3\end{cases};\ (E_1)_{1i}=\begin{cases}0\,,\ i\neq1\\ -\lambda\,\omega_{B1}^2\,,\ i=1\end{cases};\ (L_d)_{i1}=0;\ E_d=1 \tag{5.29}$$

where ω_{B1} is the fundamental circular natural frequency of the main beam and λ is a factor considering the detuning effect of ω_{B1}. The inequalities (5.29) show that the frequency change of the main beam through the uncertain factor λ transform the model into an uncertain model. Then, the control gain matrices on the uncertain models are obtained by solving Eq. (5.26) without the constrain (5.25) and are presented in Table 5.3.

Table 5.3: Gain matrices of the control system for the fundamental mode

λ	γ	Control gain, $\mathbf{K}_1$
0.00	1.68	$10^6\times[-3.963\ \ -1.483\ \ 0.367\ \ 0.016\ \ 1.635\ \ 0.036]$
0.20	1.80	$10^6\times[-5.570\ \ -2.830\ \ 0.956\ \ 0.034\ \ 4.633\ \ 0.117]$
0.40	1.97	$10^6\times[-3.508\ \ -2.937\ \ 1.264\ \ 0.040\ \ 6.221\ \ 0.166]$
0.60	2.23	$10^7\times[-0.413\ \ -1.084\ \ 0.558\ \ 0.017\ \ 2.626\ \ 0.071]$
0.80	2.64	$10^7\times[+0.201\ \ -0.467\ \ 0.273\ \ 0.008\ \ 1.170\ \ 0.031]$

To illustrate the efficiency of this model, the transfer function of the acceleration at the main beam's midspan versus the variation of the uncertain factor λ and detuning effect of the main beam frequency $\Delta\omega_{B1}$ are shown in Fig. 5.8. It is evident that for the case of no-detuned frequency $\Delta\omega_{B1}=0$, the larger the uncertain factor λ is, the higher

the transfer function peak. This means that optimal control forces obtained from the uncertain models are less effective in reducing the peak value of the transfer function than those from the certain model. However, if the detuned frequency $\Delta\omega_{B1} = +20$ %, the transfer function peak value with $\lambda = 0$ increases to 10.11 % of the peak value with $\lambda = 0.4$. This is equivalent to the attenuation of the effectiveness of the optimal control force obtained from the certain model ($\lambda = 0$) in the case of detuning. Fig. 5.8c also shows that the control force obtained from the certain model may almost destabilize the system in the case of a detuned frequency $\Delta\omega_{B1} = -10$ %. Thus, it can be concluded that the optimal control forces obtained from the uncertain models are more effective in reducing the bridge response under the existence of detuned frequencies as shown in Figs. 5.8b and c, and improve the reliability and applicability of MR dampers in practical implementations.

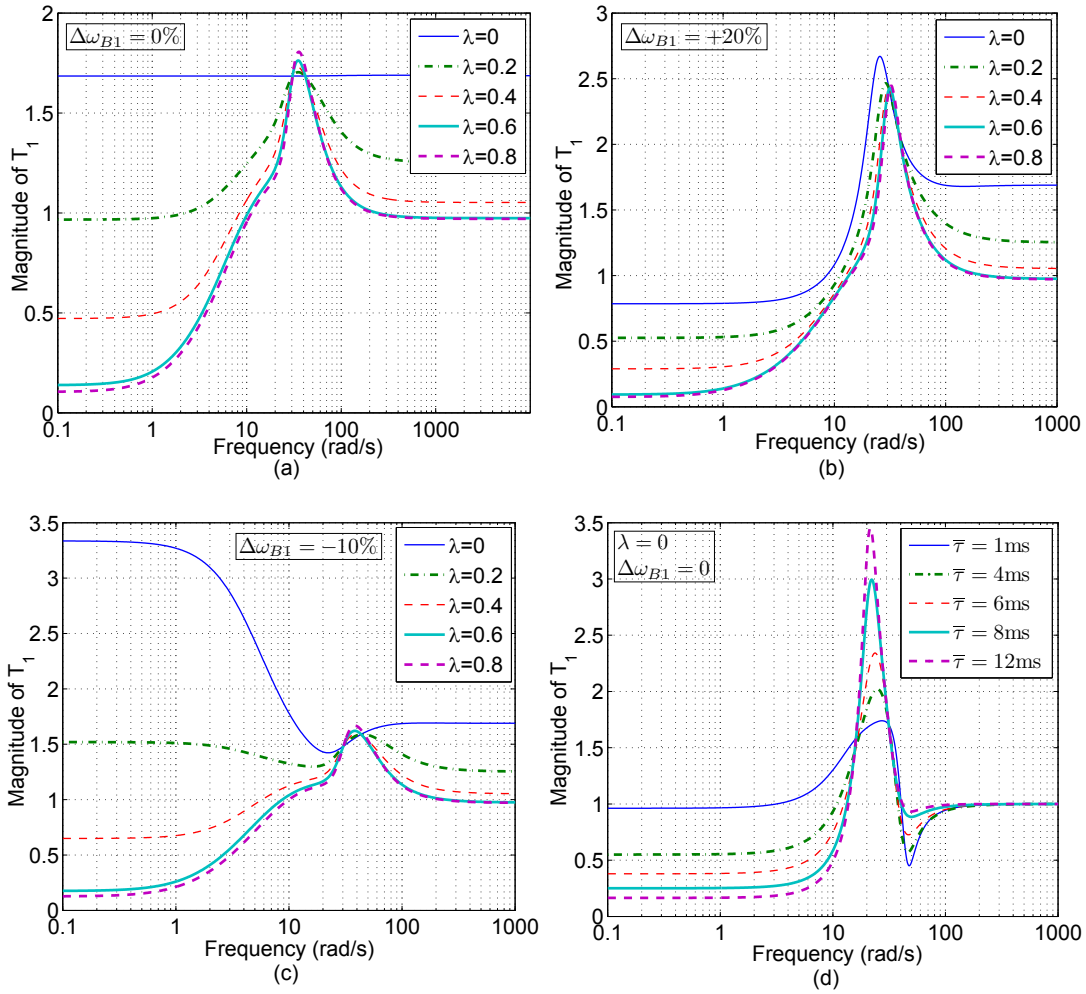

Figure 5.8: Effect of uncertain parameters on the transfer function: (a) no-detuned frequency; (b) detuned frequency +20%; (c) detuned frequency -10%; (d) time-delay

Concerning the time-delay $\bar{\tau}$ introduced at the control input, the maximum time-delay $\bar{\tau}_{max}$ can be obtained by solving Eq. (5.27). The meaning of this quantity is that the system is still stable if the time-delay of MR dampers can be increased by $\bar{\tau}_{max}$. However, the controller is less effective if the time-delay increases as shown in Fig. 5.8d.

5.3.2 Multi-mode control of double-span beam with multi-semi-active MR dampers

The dynamic performance of the double-span bridge, which properties are included in Table 2.2, after the retrofit is now evaluated. The contribution of the first two modes of vibration of each beam is now taken into account in the optimization process to predict the desired control force. Then, the finite element method and the numerical time-stepping method for MDOF systems are used to analyze the structural response.

The first two modes of the double-span beam in Table 2.2 are controlled. The chosen height of the auxiliary beam h_b is now 1.4 m and its mechanical properties are included in Table 4.4. The optimal locations for the placement of MR dampers, when the number of devices is intended to be minimum, are at the sections of maximum modal amplitude. For the two-span continuous beam, due to dominance of the first and second modes, optimal locations are the mid section of each span. Two MR dampers are assumed to be placed at the locations $L/4$ and $3L/4$ where $L/2$ is the length of each span. The MR dampers are employed to reduce simultaneously responses of the first two modes of the main structure under the circulation of the HSLM-A8 train in the range of velocities $[150;500]$ km/h.

Similarly, the gain vectors of the control system without the weighting function can be determined as shown in Table 5.4.

In Fig. 5.9, the results show that the response of the main beam at the second midspan using the MR dampers is reduced significantly at both resonances. The vibrations are reduced by 70.01 % for the maximum displacement response and by 72.21 % for the acceleration. It is seen that the static H_∞ state feedback control with the ANFIS inverse model may significantly reduce the resonant response of the beams.

Table 5.4: Gain vectors in the control system

Mode no.	$\mathbf{G}_i$
1	$[-0.0305 \quad -0.0013 \quad -5.4388 \quad 0.0000]$
2	$[-0.0096 \quad -0.0004 \quad -7.2034 \quad 0.0000]$

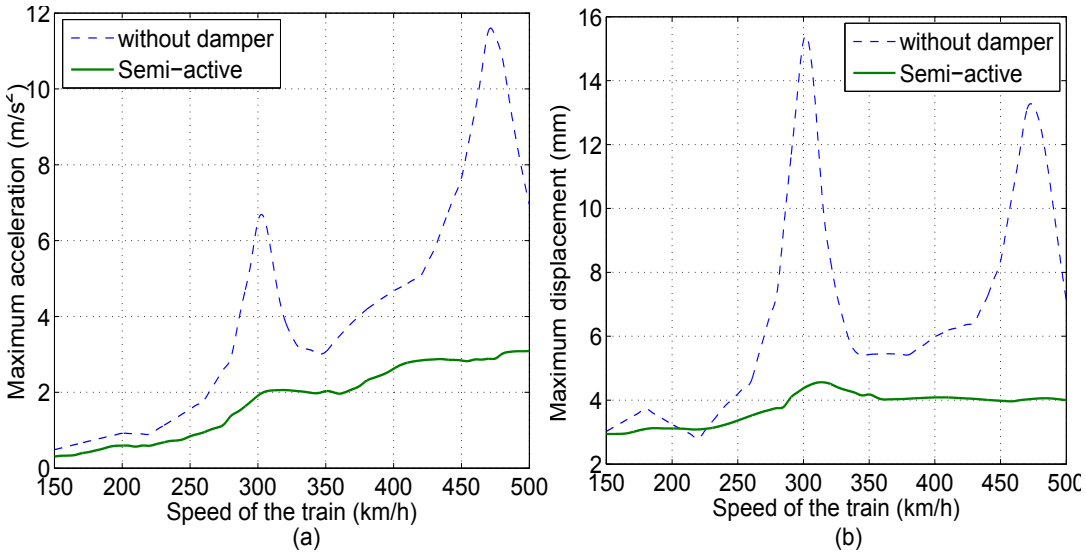

Figure 5.9: Response of the main beam versus speed of the train: (a)maximum acceleration at midspan of the main beam; (b)maximum displacement at midspan of the main beam

5.4 Conclusions

The possibility of controlling the transverse vibrations of railway bridges under high-speed traffic by means of semi-active magnetorheological dampers has been investigated. From the analysis performed, the following conclusions are derived:

- A control algorithm for MR dampers implemented into double-beam systems is proposed here. It can generate optimal control forces to suppress the structural resonant responses by combining versatilely the response components of both of the main and auxiliary beams with the control gains. Thus, MR dampers become much more effective than other control elements in recent research.

- Structural property estimation, modeling errors and time-variant material properties, which lead to detuning, may affect the control effectiveness of MR dampers. Thus, an uncertain model in this study has been considered leading to a control system less affected by the detuning effects and more reliable.

- Proper selection of the input data for the ANFIS model in this work can lead to fairly exact command voltage prediction. This makes the control voltage evolution with time become smoother and avoid sudden changes in the MR damper force in order to increase the effectiveness of MR dampers.

- Finally, the proposed control scheme, validated with numerical simulations, indicates that the static output feedback H_∞ controller combined with the ANFIS inverse model of the MR dampers model as proposed in this work may lead to a successful performance.

Chapter 6

Comparison of dampers

In this chapter, tuned mass dampers, semiactive tuned mass dampers, fluid viscous dampers and MR dampers will be compared based on their performance, in which the abilities of the dampers to reduce the resonant vibrations of the primary structure are considered.

For tuned mass dampers and semi-active tuned mass dampers, in principle, the response of primary structures retrofitted by these dampers decreases monotonically with increasing the mass ratio, μ_s. Therefore, a TMD is effective if a sufficiently large TMD mass can be accommodated. The mass ratios are often restricted by the load bearing capacity of primary structures. Referring to previous research[23,95], this ratio should be chosen to be smaller than 2%.

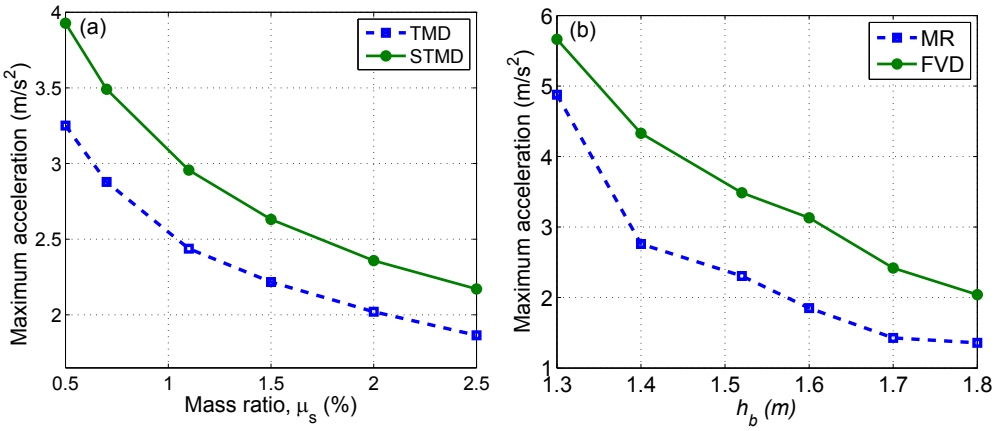

Figure 6.1: Response of the main beam versus speed of the train

In the case that the beam bridge with the properties as shown in Table. 2.2 retrofitted by a single TMD is considered, the variation of the maximum acceleration at midspan of the beam versus mass ratio μ_s is shown in Fig. 6.1a. It can be found that the choice

of μ_s =0.7% can reduce the maximum acceleration of the beam to 3.5 m/s^2, which satisfies the limiting vertical acceleration in Annex A2[8]. Thus, a single TMD with μ_s =0.7% can be used to retrofit this primary structure. Meanwhile, Fig. 6.1a also shows that if the mass ratio of a single STMD is equal to 0.4%, it can ensure that the maximum acceleration of the beam is also less than the limiting value 3.5 m/s^2. More generally, by comparing the performance of TMD and STMD with the same mass ratios shown in Fig. 6.1a, it can be seen that the maximum acceleration of the main beam with STMD is always smaller than that with TMD, at least 17%. This is one of STMD's advantages.

For fluid viscous dampers and magnetorheological dampers in double-beam systems, their abilities to reduce resonant structural vibrations mainly depend on the natural frequency of the auxiliary beams, here represented by their height, h_b. Fig. 6.1b shows that for the considered main beam, its maximum response monotonically decreases if the height of the auxiliary beam increases. Especially, in the case of FVD, if the auxiliary beam height h_b is equal to 1.52 m, the maximum acceleration is about 3.5 m/s^2 satisfying the limiting acceleration. Fig. 6.1b also shows that for the same auxiliary beam heights, the magnetorheological damper produces a larger improvement in performance (about 32%) compared to the FVD. Therefore, the combination of MR dampers and double-beam systems proposed in this dissertation is very promising to improve the performance of passive FVDs. This also permits to reduce the natural frequency of the auxiliary beam, and thus its height which is essential in order to minimize the occupied space under the bridge deck associated with the retrofit installation.

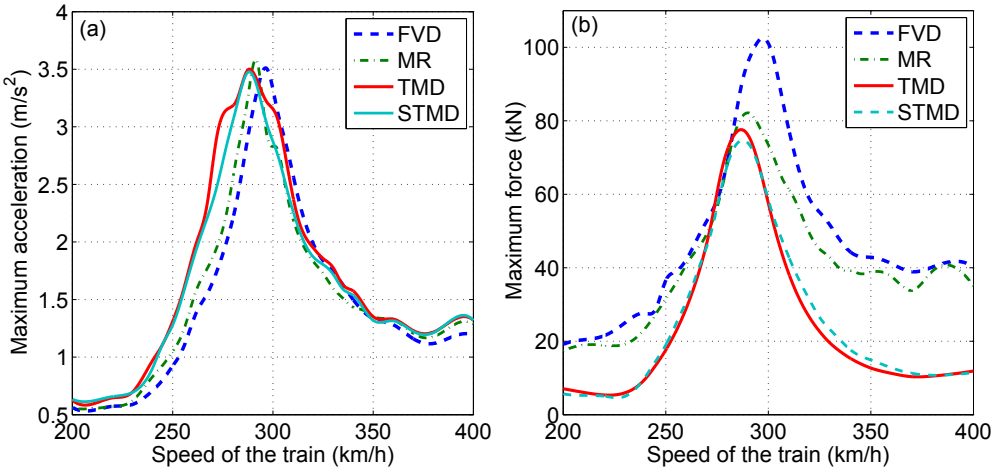

Figure 6.2: Response of the main beam and damper force versus speed of the train

For comparison between the damping forces in the dampers, their parameters are chosen and optimized again in order to achieve the same reduction in acceleration of the

main beam. For the TMD and STMDs, their mass ratio μ_s of 0.7% is chosen, and for the FVD and MR damper, the auxiliary beam height h_b is 1.52 m. Then, the maximum accelerations of the main beam with the different cases of the dampers are shown in Fig. 6.2a and the maximum damper forces transmitted to the superstructure are also shown in Fig. 6.2b. The total damper forces for the FVD, MR damper, TMD and STMD are 102.5, 81.6, 77.6 and 74.7 kN, respectively. It may be indicated that the use of MR damper in the STMD and the double-beam system can reduce significantly the damper forces applied to the primary structure. Therefore, for high velocity applications in order not to exceed the device force capacity or the forces transmitted to the superstructures, MR dampers may be used.

Additionally, it is well-known that the optimal parameters of the dampers much depend on the natural frequencies of the primary structure. Under the effect of live loads or environmental parameters, these frequencies may change. This problem is often called detuning effect[23], and it will also be considered here.

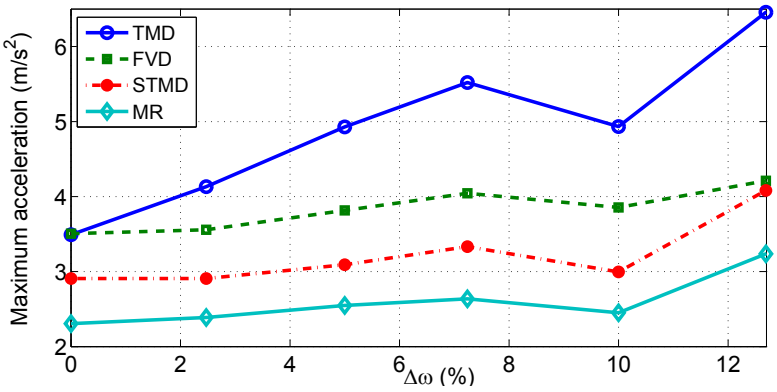

Figure 6.3: Maximum acceleration at the main beam midspan versus incorrectly tuned frequency

Fig. 6.3 shows that if the original frequency of the main beam is incorrectly tuned by $\Delta\omega$, the maximum acceleration of the main beam with TMD increases significantly, meanwhile the others are still very stable. It can be seen that the efficiency of TMD is very sensitive to changes of the frequency of the primary structure. This is the most serious drawback of TMD systems in practical design.

Besides, the decay rates of the beam responses after the train leaves is also shown in Figs. 6.4. It can be seen that the decay rates corresponding to the different dampers are almost the same.

Actually, choosing a kind of damper to retrofit an existing bridge is not only based

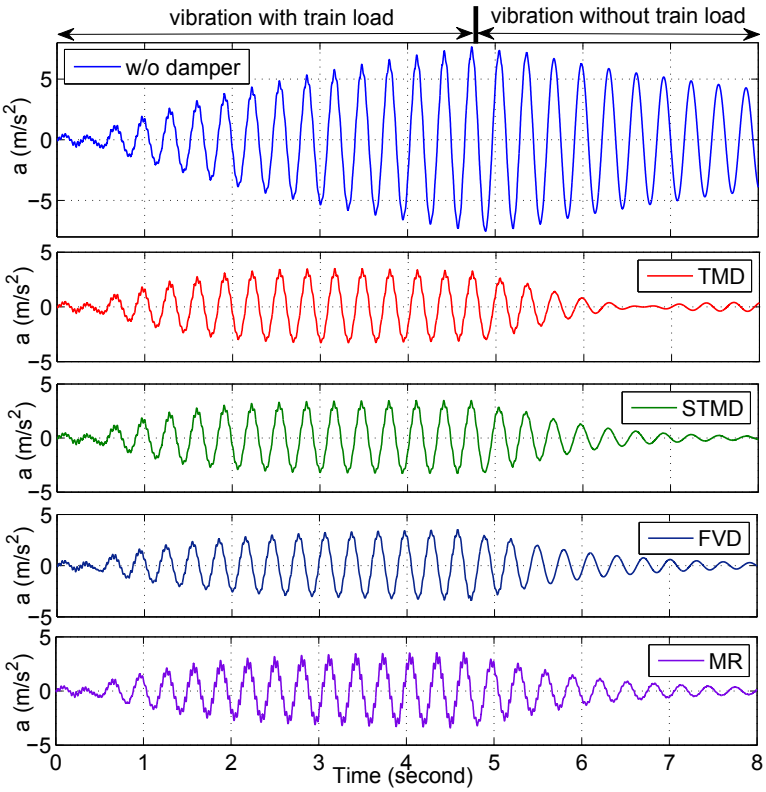

Figure 6.4: Acceleration at midspan of the main beam with the different dampers versus time

on its ability to reduce structural vibrations but also its investment and maintenance cost, durability and ageing characteristics in practical design. For instance, TMDs and FVDs are passive control systems which do not require an external power source for operation but only utilize the motion of the structure to develop their control forces. Therefore, their mechanics structures are often simple, reliable, and especially their cost is much lower than that of the semi-active dampers. This is one of the greatest advantages of the retrofit with TMD and FVD systems. However, as mentioned, TMDs are very sensitive to an incorrect frequency tuning and changes of the natural frequencies of primary structures which is their major drawback. To overcome this problem, FVD might be one of better choices because of its reliability and the stability of the mechanical properties of the fluid in FVDs over a wide temperature range (-40^0C to $+70^0$C)[11] but actually this device also has some other weaknesses such as the occupied space under bridges to install auxiliary beams, and it can clamp the primary structure at small vibration velocities due to the relatively large damper force. If the structure is clamped at damper position, the damper relative displacement and therefore energy dissipation become zero. Consequently, the entire excitation energy excites the rest of the structure.

For STMD-MR dampers and MR dampers, they are classified as semi-active damping devices which typically require a small external power source such as battery (on the order of tens of watts)[96] and utilize the motion of the structure to develop the control forces, the magnitude of which can be adjusted by the external power source. The control forces are developed also based on feedback from sensors that measure the responses of structures. Because of this, semi-active dampers are often more effective than passive dampers. However, they also have some disadvantages such as their cost and the need for frequent maintenance.

Chapter 7

Conclusions

7.1 Summary of achievements

This dissertation was devoted to the investigation of H_∞ optimization for tuned mass dampers, semi-active tuned mass dampers, fluid viscous dampers and magnetorheological dampers in double-beam systems to reduce the excessive vibrations that high-speed railway bridges may experience under resonant conditions. Although the structural vibration control has been extensively studied for decades, its application to large scale structures, especially railway bridge structures is still a task full of challenge. As reviewed in the first chapter, the methods developed in the previous works have more or less limitations. Therefore, in this dissertation, the new methods and the improved methods are derived to enable efficient and reliable applications of the structural vibration control technology to high-speed railway bridges. From the work that has been done, the achievements are summarized as follows:

1. Tuned mass damper

    - It can be concluded that the parameters of TMDs systems optimized by the proposed method is more effective than the previous method. The response of the multi-resonant beam structures can be reduced by 14% compared to the previous method. The reason for this effectiveness is that the parameters of TMDs can be optimized directly and simultaneously on different modes contributing significantly to the multi-resonant peaks. This approach can explore the different possible combinations of parameters and make the TMDs more effective and robust. Meanwhile, for the previous method its theoretical foundation was developed based on Den Hartog's classical method only applied for a single TMD and a fundamental mode. Thus, an iteration procedure was derived to improve multi-TMDs systems

implemented in multi-resonant structures. This might cause a drawback to the previous method in optimization process.

- The simulation results also show that the H_∞ optimization method can reduce in the number of TMDs in multi-mode cases meanwhile it still ensures that the structural response is acceptable compared to the previous method.
- Finally, the optimization of multiple tuned mass dampers on an uncertain model is also another advantage in this work. It can reduce detuning effect in a narrow frequency band around the natural frequency of the main system.

2. Semi-active tuned mass damper

   - An optimization methodology for semi-active tuned mass damper systems was derived based on H_∞ norm optimization criteria with *DK-iteration* procedure with norm-bounded uncertainties in frequency domain. The use of this algorithm can achieve compatible performance. Through the numerical simulations, it can be seen that the band of suppression frequency is extended. The detuning effect is reduced significantly, and the main drawback of the traditional TMD systems is overcome.
   - Moreover, the approach of the MR damper inverse model by using the ANFIS model in this work can provide the quite exact predictions about command voltage to control MR dampers effectively.

3. Fluid viscous damper

   - In order to tune FVDs parameters to the vicinity of the exact values, analytical formulae which can include structural damping are derived based on the perturbation method. The proposed formulae can be considered as an improvement of the previous analytical formulae, especially, for beams with large structural damping.
   - Besides, a new procedure to determine the optimal damping ratios of nonlinear FVDs is also suggested based on H_∞ norm and Symans' linearization formula. The simulation results show that the reduction in the damper forces can reach 35%, meanwhile, they still ensure that the structural response is minimized. Therefore, this procedure may be used for high speed applications in order not to exceed the devices force capacity or the forces transmitted to the superstructures.
   - Finally, it can be seen that the proposed objective function based on H_∞ norm is convenient. This function can be used to optimize the parameters of FVDs over a chosen frequency range, include individual and simultaneous

contribution of modes for analyzing multi-span beams in which the effect of high modes on optimal FVDs coefficients is significant, and also be extended to solve nonlinear FVDs problems.

4. Magnetorheological damper in double-beam system

   - A control algorithm for MR dampers implemented into double-beam systems is proposed here. It can generate optimal control forces to suppress the structural resonant responses by combining versatilely the response components of both of the main and auxiliary beams with the control gains. Thus, MR dampers become much more effective than other control elements in recent research.
   - The use of the actuator saturation nonlinearity condition and the weighting function to shape the controlled output can improve the tracking ability of MR forces to the desired control forces.
   - Structural property estimation, modeling errors and time-variant material properties, which lead to detuning , may affect the control effectiveness of MR dampers. Thus, an uncertain model in this study has been considered leading to a control system less affected by the detuning effects and more reliable.
   - Through the comparison of the passive-off, passive-on, semiactive and active cases, it is concluded that larger damping forces do not always correlate with better performance of the retrofitted structure.
   - Finally, the proposed control scheme, validated with numerical simulations, indicates that the static output feedback H_∞ controller combined with the ANFIS inverse model of the MR dampers model as proposed in this work may lead to a successful performance.

7.2 Outlook

The presented work established the frameworks for design and application of tuned mass dampers, semi-active tuned mass dampers, fluid viscous dampers and magnetorheological dampers for reducing the resonant structural responses in high-speed railway bridges. A few possible extensions to the current work can be suggested as follows:

- In order to achieve the higher level of confidence and reliability, the validity of the developed design methodologies for resonant vibration reduction of high-speed railway bridges using tuned mass dampers, semi-active tuned mass

dampers, fluid viscous dampers and magnetorheological dampers should be tested through experimental studies.

- In the cases of semi-active tuned mass dampers and MR dampers, using so many sensors can lead to a higher implementation cost as well as difficulty in measuring all the needed responses. Thus, the design of observers to estimate a full state vector from some measured data with high accuracy and noise reduction is very necessary for large-scale structures. Besides, the optimal locations of dampers and sensors should also be studied further to improve the effectiveness of dampers retrofitted into complicated bridge structures.
- Concerning optimization control algorithms, the objective functions should be established based on the mathematical modeling of dynamic structures such as orthotropic plates and more complicated bridge structures such as truss bridges and cable stayed bridges under high-speed moving loads.

Appendix A

A.1 Equivalent Damping of Nonlinear FVD

The equivalent damping coefficient of the kth fluid viscous damper for the fundamental mode of the simply supported beams in equation (4.4) may be rewritten as following

$$C_{eqk} = \frac{2}{\pi} C_{\alpha k} |Y_k|^{(\alpha-1)} \omega_B^{(\alpha-1)} \frac{\Gamma(1+\frac{\alpha}{2})\Gamma(\frac{1}{2})}{\Gamma(\frac{3}{2}+\frac{\alpha}{2})} = \frac{2}{\pi} C_{\alpha k} |Y_{ki}|^{(\alpha-1)} \omega_{Bi}^{(\alpha-1)} \overline{\Gamma}(\alpha) \quad \text{(A.1)}$$

$$\overline{\Gamma}(\alpha) = \frac{\Gamma(1+\frac{\alpha}{2})\Gamma(\frac{1}{2})}{\Gamma(\frac{3}{2}+\frac{\alpha}{2})}$$

where $C_{\alpha k}$ is the damping coefficient of the kth fluid viscous damper; $|Y_k|$ is the displacement amplitude of the kth FVD. By substituting C_{eqk} into equation (4.22), then

$$C_D = \sum_{k=1}^{N_D} \frac{2}{\pi} C_{\alpha k} |Y_k|^{(\alpha-1)} \omega_B^{(\alpha-1)} \overline{\Gamma}(\alpha) \phi^2(d_k) = \frac{2}{\pi} \omega_B^{(\alpha-1)} \overline{\Gamma}(\alpha) \sum_{k=1}^{N_D} C_{\alpha k} |Y_k|^{(\alpha-1)} \phi^2(d_k) \quad \text{(A.2)}$$

The displacement of the kth FVD for the fundamental mode may be determined as

$$y_k(t) = [q_B(t) - q_b(t)]\, \phi(d_k) \quad \text{(A.3)}$$

In frequency domain, equation (A.3) is rewritten

$$Y_k(\omega) = [\overline{q}_B(\omega) - \overline{q}_b(\omega)]\, \phi(d_k) \quad \text{(A.4)}$$

By considering the fundamental mode, substituting $\overline{q}_{Bi}(\omega)$ and $\overline{q}_{bi}(\omega)$ in equations (4.16) into equation (A.4), the result is as

$$Y_k(\omega) = [L_B(\omega) - L_b(\omega)]\, F_v(\omega) \phi(d_k) \quad \text{(A.5)}$$

The excitation load in frequency domain $F_v(\omega)$ may be found by decomposing the train load into a Fourier series proposed by Barbero[97] as follows.
The train load for the fundamental mode may be given as

$$F_v(t) = \frac{1}{m_B}\int_0^l \sum_{k=1}^{N_v} \delta\left(x-(vt-a_k)\right) F_k \mathrm{H}\left(t-t_k\right)\phi(x)\mathrm{d}x \tag{A.6}$$

where $\phi(x) = \sin(\pi x/l)$; N_v is the total number of axles; F_k is the gravity force of the kth wheel-axle set; v is the speed of the train; a_k is the longitudinal distance from the kth wheel-axle set to the first wheel-axle set; t_k is the time when the kth wheel-axle reaches the bridge; l is the span of the bridge; $\delta(x-a)$ and $\mathrm{H}(t-t_k) = \mathrm{H}_0(t-t_k) - \mathrm{H}_0(t-t_k-v/l)$ are the Dirac delta and Heaviside function.
It is assumed that the load of F_v is a periodic function of T corresponding to the total time that the train crosses the bridge. Then,

$$F_v(t) = \sum_{n=-\infty}^{+\infty} C_n \mathrm{e}^{\mathrm{i}n\omega t}; C_n = \frac{F_0 l}{\pi \overline{m}_B (x_N + l)} \frac{1}{1-\left(\frac{n\omega l}{\pi v}\right)^2}\left(1+\mathrm{e}^{-\frac{\mathrm{i}n\omega l}{v}}\right)\sum_{k=1}^{N_v}\mathrm{e}^{-\mathrm{i}n\omega t_k} \tag{A.7}$$

where $F_0 = F_1 = \ldots = F_k$; $\omega = 2\pi v/(x_N + l)$; x_N and v are the length and speed of the train, respectively.
By setting $n = 1$ and finding the Fourier transform of equation (A.7), using the assumption $\zeta_B = \zeta_b = 0$ and substituting equations (4.24) into equation (A.5) , then equation (A.5) may be rewritten as

$$Y_k(\omega) = C_1 \phi(d_k) \frac{\mu(\eta^2-\Omega^2)}{\omega_B^2\left[\mu(1-\Omega^2)(\eta^2-\Omega)+2\mathrm{i}\Omega\xi_D((1-\Omega^2)+\mu(\eta^2-\Omega^2))\right]} \tag{A.8}$$

By substituting equation (A.8) into equation (A.2) and using $\xi_D = C_D/(l\overline{m}_B\omega_B)$, then the equivalent damping ratio of nonlinear FVDs can be determine as

$$\xi_D = \frac{2\omega_B^{\alpha-2}\overline{\Gamma}(\alpha)}{\pi\overline{m}_B l}\left(|C_1|Q\right)^{\alpha-1}\sum_{k=1}^{N_D} C_{\alpha k}\phi^{\alpha+1}(d_k) \tag{A.9}$$

where

$$Q = \sqrt{\frac{\mu^2(\eta^2-\Omega^2)^2}{\omega_B^4[\mu(1-\Omega^2)(\eta^2-\Omega)]^2+[2\Omega\xi_D\omega_B^2((1-\Omega^2)+\mu(\eta^2-\Omega^2))]^2}}$$

$$|C_1| = \frac{F_0 l}{\pi\overline{m}_B(x_N+l)}\frac{2\left|\cos\left(\frac{\pi l}{x_N+l}\right)\right|}{1-\left(\frac{\omega l}{\pi v}\right)^2}\sqrt{\left(\sum_{k=1}^{N_D}\cos\omega t_k\right)^2+\left(\sum_{k=1}^{N_D}\sin\omega t_k\right)^2}$$

For $\alpha = 1$, (A.9) becomes an equivalent damping ratio of linear FVDs mentioned in section 4

$$\xi_D = \frac{1}{\overline{m}_B l \omega_B} \sum_{k=1}^{N_D} C_k \phi^2(d_k) \; ; \; C_D = \sum_{k=1}^{N_D} C_k \phi^2(d_k) \tag{A.10}$$

A.2 Flow graph of simple line search technique

Flow graph to improve the fluid damping coefficients is given in Fig. A.1.

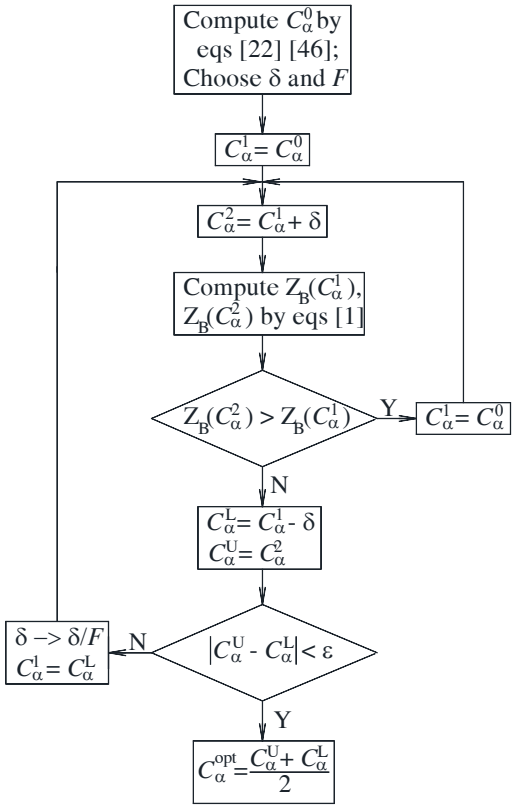

Figure A.1: Flow graph to improve the optimal damping coefficient of nonlinear FVD (the second procedure).

Note: δ, F, and ε are the interval step parameter, refinement factor and specified tolerance, respectively.

Appendix B

B.1 Details in deriving LMIs in inequalities (5.24) and (5.25)

Some basic lemmas are used without proof:

Lemma 1[98]. *Schur complement*

For a given symmetric matrix $\mathbf{S} = \mathbf{S}^{\mathrm{T}} = \begin{bmatrix} \mathbf{S}_{11} & \mathbf{S}_{12} \\ * & \mathbf{S}_{22} \end{bmatrix}$, where $\mathbf{S}_{11} \in R^{r \times r}$, the following conditions are equivalent:

(a) $\mathbf{S} < 0$;

(b) $\mathbf{S}_{11} < 0$, $\mathbf{S}_{22} - \mathbf{S}_{12}^{\mathrm{T}} \mathbf{S}_{11}^{-1} \mathbf{S}_{12} < 0$; and

(c) $\mathbf{S}_{22} < 0$, $\mathbf{S}_{11} - \mathbf{S}_{12} \mathbf{S}_{22}^{-1} \mathbf{S}_{12}^{\mathrm{T}} < 0$.

Lemma 2[94].
Let $\mathbf{A}$, $\mathbf{L}$, $\mathbf{E}$ and $\mathbf{F}$ be real matrices of appropriate dimensions with $\|\mathbf{F}\| \leq 1$. Then,
(a) For any scalar $\mu > 0$,

$$\mathbf{LFE} + \mathbf{E}^{\mathrm{T}} \mathbf{F}^{\mathrm{T}} \mathbf{L}^{\mathrm{T}} \leq \mu^{-1} \mathbf{L}\mathbf{L}^{\mathrm{T}} + \mu \mathbf{E}^{\mathrm{T}} \mathbf{E};$$

(b) For any real matrix $\mathbf{P} = \mathbf{P}^{\mathrm{T}} > 0$ and a scalar $\mu > 0$ such that $\mu \mathbf{I} - \mathbf{E}\mathbf{P}\mathbf{E}^{\mathrm{T}} > 0$,

$$(\mathbf{A} + \mathbf{LFE})\mathbf{P}(\mathbf{A} + \mathbf{LFE})^{\mathrm{T}} \leq \mathbf{A}\mathbf{P}\mathbf{A}^{\mathrm{T}} + \mathbf{A}\mathbf{P}\mathbf{E}^{\mathrm{T}}(\mu \mathbf{I} - \mathbf{E}\mathbf{P}\mathbf{E}^{\mathrm{T}})^{-1} \mathbf{E}\mathbf{P}\mathbf{A}^{\mathrm{T}} + \mu \mathbf{L}\mathbf{L}^{\mathrm{T}};$$

(c) For any real matrix $\mathbf{P} = \mathbf{P}^{\mathrm{T}} > 0$ and a scalar $\mu > 0$ such that $\mathbf{P} - \mu \mathbf{L}\mathbf{L}^{\mathrm{T}} > 0$,

$$(\mathbf{A} + \mathbf{LFE})^{\mathrm{T}} \mathbf{P}^{-1} (\mathbf{A} + \mathbf{LFE}) \leq \mathbf{A}^{\mathrm{T}} (\mathbf{P} - \mu \mathbf{L}\mathbf{L}^{\mathrm{T}})^{-1} \mathbf{A} + \mu^{-1} \mathbf{E}^{\mathrm{T}} \mathbf{E}.$$

Lemma 3[94].

For any vectors $\mathbf{u},\mathbf{v}$ and any matrix $\mathbf{S}=\mathbf{S}^{\mathrm{T}}>0$ of appropriate dimensions, then

$$-2\mathbf{u}^{\mathrm{T}}\mathbf{v}\leq\mathbf{u}^{\mathrm{T}}\mathbf{S}\mathbf{u}+\mathbf{v}^{\mathrm{T}}\mathbf{S}^{-1}\mathbf{v}$$

Proof of inequality (5.24):
Leading to a set of LMIs (5.24) for the system (5.23) is based on Xili's idea[99], in which the controlled output is described by $\mathbf{z}_i(t)=\mathbf{C}_i\mathbf{x}_i(t)$ whereas here $\mathbf{z}_i(t)=\mathbf{C}_i\mathbf{x}_i(t)+\mathbf{H}_{di}u_{ci}+D_{wi}w_i$. Firstly, the Lyapunov function is defined as follows:

$$V_i(x,t)=V_{1i}(x,t)+W_i(x,t) \tag{B.1}$$

where $V_{1i}(x,t)=\mathbf{x}_i^{\mathrm{T}}(t)\mathbf{P}\mathbf{x}_i(t)$; $\mathbf{P}$ is a symmetric positive definite matrix;

$$\begin{aligned}W_i(x,t)=&\int_{-\tau}^{0}\int_{t+\theta}^{t}x_i^{\mathrm{T}}(s)\bar{\mathbf{A}}_i^{\mathrm{T}}(s)\mathbf{P}_1^{-1}\bar{\mathbf{A}}_i(s)x_i(s)\mathrm{d}s\mathrm{d}\theta+\\&+\int_{-\tau}^{0}\int_{t+\theta-\tau}^{t}\mathbf{x}_i^{\mathrm{T}}(s)\mathbf{K}_i^{\mathrm{T}}\bar{\mathbf{B}}_{di}^{\mathrm{T}}(s+\tau)\mathbf{P}_2^{-1}\bar{\mathbf{B}}_{di}(s+\tau)\mathbf{K}_i\mathbf{x}_i(s)\mathrm{d}s\mathrm{d}\theta+\\&+\int_{-\tau}^{0}\int_{t+\theta}^{t}w_i^{\mathrm{T}}(s)\mathbf{B}_{wi}^{\mathrm{T}}(s)\mathbf{P}_3^{-1}\mathbf{B}_{wi}(s)w_i(s)\mathrm{d}s\mathrm{d}\theta;\end{aligned} \tag{B.2}$$

and $\mathbf{P}_1$, $\mathbf{P}_2$ and $\mathbf{P}_3$ are symmetric positive definite matrices; $\bar{\mathbf{A}}_i=\mathbf{A}_i+\Delta\mathbf{A}_i(t)$; $\bar{\mathbf{B}}_{di}=\mathbf{B}_{di}+\Delta\mathbf{B}_{di}(t)$.

Besides, for any function $f(s)$ and

$$W_i(x,t)=\int_{-\tau}^{0}\int_{t+\theta}^{t}f(s)\mathrm{d}s\mathrm{d}\theta,$$

the time derivative of $W_i(x,t)$ is

$$\frac{\partial W_i(x,t)}{\partial t}=\tau f(t)-\int_{-\tau}^{0}f(t+\theta)\mathrm{d}\theta \tag{B.3}$$

Then, by differentiating equation (B.1) and using lemmas 2, 3, and equation (B.3)

$$\dot{V}_i \leq \mathbf{x}_i^{\mathrm{T}}(t)\mathbf{S}\mathbf{x}_i(t) + +w_i^{\mathrm{T}}(t)\mathbf{B}_{wi}^{\mathrm{T}}\mathbf{P}\mathbf{x}_i(t) + \mathbf{x}_i^{\mathrm{T}}(t)\mathbf{P}\mathbf{B}_{wi}w_i(t) + \tau w_i^{\mathrm{T}}(t)\mathbf{B}_{wi}^{\mathrm{T}}\mathbf{P}_3^{-1}\mathbf{B}_w w_i(t); \tag{B.4a}$$

$$\mathbf{P}_1 - \varepsilon_4\mathbf{L}_1\mathbf{L}_1^{\mathrm{T}} > 0;\ \mathbf{P}_2 - \varepsilon_5\mathbf{L}_d\mathbf{L}_d^{\mathrm{T}} > 0 \tag{B.4b}$$

where

$$\begin{aligned}\mathbf{S}_i =& \mathbf{A}_i^{\mathrm{T}}\mathbf{P} + \mathbf{P}\mathbf{A}_i + \mathbf{K}_i^{\mathrm{T}}\mathbf{B}_{di}^{\mathrm{T}}\mathbf{P} + \mathbf{P}\mathbf{B}_{di}\mathbf{K}_i + \varepsilon_1^{-1}\mathbf{E}_1^{\mathrm{T}}\mathbf{E}_1 + \varepsilon_2^{-1}\mathbf{K}_i^{\mathrm{T}}\mathbf{E}_d^{\mathrm{T}}\mathbf{E}_d\mathbf{K} + \varepsilon_1\mathbf{P}\mathbf{L}_1L_1^{\mathrm{T}}\mathbf{P} + \ldots \\ &+ \varepsilon_2\mathbf{P}\mathbf{L}_d\mathbf{L}_d^{\mathrm{T}}\mathbf{P} + \tau\mathbf{P}[\mathbf{B}_d\mathbf{Q}\mathbf{B}_d^{\mathrm{T}} + \varepsilon_3\mathbf{L}_d\mathbf{L}_d^{\mathrm{T}} + \mathbf{B}_{di}\mathbf{Q}\mathbf{E}_d^{\mathrm{T}}(\varepsilon_3\mathbf{I} - \mathbf{E}_d\mathbf{Q}\mathbf{E}_d^{\mathrm{T}})^{-1}\mathbf{E}_d\mathbf{Q}\mathbf{B}_{di}^{\mathrm{T}}]\mathbf{P} + \ldots \\ &+ \tau[\mathbf{A}_i^{\mathrm{T}}(\mathbf{P}_1 - \varepsilon_4\mathbf{L}_1\mathbf{L}_1^{\mathrm{T}})^{-1}\mathbf{A}_i + \varepsilon_4^{-1}\mathbf{E}_1\mathbf{E}_1^{\mathrm{T}} + \mathbf{K}_i^{\mathrm{T}}\mathbf{B}_{di}^{\mathrm{T}}(\mathbf{P}_2 - \varepsilon_5\mathbf{L}_d\mathbf{L}_d^{\mathrm{T}})^{-1}\mathbf{B}_{di}\mathbf{K}_i + \ldots \\ &+ \varepsilon_5^{-1}\mathbf{K}_i^{\mathrm{T}}\mathbf{E}_d^{\mathrm{T}}\mathbf{E}_d\mathbf{K}_i]\end{aligned}$$

and the rest of the parameters are defined in inequality (5.24).

Next, the H_∞ performance of the system under zero initial condition is established as

$$\dot{V}_{\gamma i} = \dot{V}_i + \mathbf{z}_i^{\mathrm{T}}(t)\mathbf{z}_i(t) - \gamma^2 w_i^{\mathrm{T}}(t)w_i(t) \tag{B.5}$$

where

$$\begin{aligned}\mathbf{z}_i^{\mathrm{T}}(t)\mathbf{z}_i(t) =& \mathbf{x}_i^{\mathrm{T}}(t)(\mathbf{C}_i^{\mathrm{T}}\mathbf{C}_i + \mathbf{K}_i^{\mathrm{T}}\mathbf{H}_{di}^{\mathrm{T}}\mathbf{H}_{di}\mathbf{K}_i + \mathbf{C}_i^{\mathrm{T}}\mathbf{H}_{di}\mathbf{K}_i + \mathbf{K}_i^{\mathrm{T}}\mathbf{H}_{di}^{\mathrm{T}}\mathbf{C}_i)\mathbf{x}_i(t) + \ldots \\ &+ w_i^{\mathrm{T}}(t)\mathbf{D}_{wi}^{\mathrm{T}}\mathbf{D}_{wi}w_i(t) + \mathbf{x}_i^{\mathrm{T}}(t)(\mathbf{C}_i^{\mathrm{T}}\mathbf{D}_{wi} + \mathbf{K}_i^{\mathrm{T}}\mathbf{H}_d^{\mathrm{T}}\mathbf{D}_{wi})w_i(t) + \ldots \\ &+ w_i^{\mathrm{T}}(t)(\mathbf{D}_{wi}^{\mathrm{T}}\mathbf{C}_i + \mathbf{D}_{wi}^{\mathrm{T}}\mathbf{H}_d\mathbf{K}_i)\mathbf{x}_i(t)\end{aligned}$$

Defining the new variable $\mathbf{X} = \mathbf{P}^{-1}$, substituting inequality (B.4) into inequality (B.5), multiplying its both sides by $\mathbf{X}$, setting $\mathbf{Y} = \mathbf{K}_i\mathbf{X}$ and using Schur complement in lemma 1, it can be seen that if the constraints in inequalities (5.24) are guaranteed, then

$$\dot{V}_i + \mathbf{z}_i^{\mathrm{T}}(t)\mathbf{z}_i(t) - \gamma^2 w_i^{\mathrm{T}}(t)w_i(t) < 0 \tag{B.6}$$

By integrating both sides of inequality (B.6) from zero to infinity and using $V_i(0) = 0,\ V_i(\infty) \geq 0$, it is obtained

$$\frac{\|\mathbf{z}_i(t)\|_2}{\|w_i(t)\|_2} < \gamma$$

Therefore, the system satisfies the H_∞ performance for all nonzero $w_i(t) \in L_2[0,\infty)$.

Proof of inequality (5.25):
The actuator saturation nonlinearity is described by

$$|u(t)| \leq u_{max} \tag{B.7}$$

where u_{max} is the maximum controlled damping force.
It can be seen that $\mathbf{z}_i^{\mathrm{T}}(t)\mathbf{z}_i(t) > 0$, thus inequality (B.6) can be written as

$$\dot{V}_i(x,t) < \gamma^2 w_i^{\mathrm{T}}(t) w_i(t) \tag{B.8}$$

By integrating both sides of inequality (B.8) and substituting $V_i(x,t) = \mathbf{x}_i^{\mathrm{T}}(t)\mathbf{P}\mathbf{x}_i(t)$ into (B.8), then

$$\mathbf{x}_i^{\mathrm{T}}(t)\mathbf{P}\mathbf{x}_i(t) < \int_0^t \gamma^2 w_i^{\mathrm{T}}(t) w_i(t)\mathrm{d}t \le \gamma^2 \left\| w_i(t) \right\|_2^2 = \gamma^2 w_{i,max} = \rho \tag{B.9}$$

Define $\bar{\mathbf{x}}_i(t) = \mathbf{P}^{1/2}\mathbf{x}_i(t)$, from (B.9), it follows that $\bar{\mathbf{x}}_i(t)^{\mathrm{T}}\mathbf{x}_i(t) < \rho$. Hence,

$$\max_{t\ge 0} |u_i(t)|^2 = \max_{t\ge 0} \left\| \mathbf{K}_i \mathbf{x}_i(t) \right\|_2^2 = \max_{t\ge 0} \left\| \bar{\mathbf{x}}_i^{\mathrm{T}}(t)\mathbf{P}^{-1/2}\mathbf{K}_i^{\mathrm{T}}\mathbf{K}_i\mathbf{P}^{-1/2}\bar{\mathbf{x}}_i(t) \right\|_2 < \ldots$$

$$< \rho \lambda_{\max}[\mathbf{P}^{-1/2}\mathbf{K}_i^{\mathrm{T}}\mathbf{K}_i\mathbf{P}^{-1/2}] \le u_{\max}$$

$$\Rightarrow \mathbf{P}^{-1/2}\mathbf{K}_i^{\mathrm{T}}\mathbf{K}_i\mathbf{P}^{-1/2} < \frac{u_{\max}^2}{\rho}\mathbf{I} = \rho_0\mathbf{I} \Leftrightarrow \mathbf{P}^{-1}\mathbf{K}_i^{\mathrm{T}}\mathbf{K}_i\mathbf{P} - \rho_0\mathbf{P}^{-1} < 0 \tag{B.10}$$

where ρ, $\rho_0 (= u_{max}^2/\rho)$ are positive upper bounds; λ_{max} represents the maximum eigenvalue and $\mathbf{I}$ is an appropriate identity matrix. By using $\mathbf{X} = \mathbf{P}^{-1}$ and $\mathbf{Y} = \mathbf{K}_i\mathbf{P}^{-1}$ and Schur complement, then inequality (5.25) may be found.

References

[1] S. Nagarajaiah, E. Sonmez. Structures with semiactive variable stiffness single/multiple tuned mass dampers. *Journal of Structural Engineering*, 2007. viii, 6, 7

[2] J. D. Yau and Y. B. Yang. Vibration reduction for cable-stayed bridges traveled by high-speed trains. *Journal of Finite Elements in Analysis and Design*, 40:341–359, 2004. viii, 3, 17, 26, 30, 32, 73

[3] J.D Yau and Y.B Yang. A wideband MTMD system for reducing the dynamic response of continuous truss bridges to moving train loads. *Journal of Structural Engineering*, 26:1795–1807, 2004. viii, 3, 11, 26, 30, 32

[4] D. Q. Truong and K. K. Ahn. MR fluid damper and its application to force sensorless damping control system. *Smart Actuation and Sensing Systems - Recent Advances and Future Challenges,*, pages 383–425, 2012. viii, 36, 37, 38

[5] R. Stanway, J. L. Sproston, and A. K. El-Wahed. Applications of electro-rheological fluids in vibration control: a survey. *Smart Mater. Struct.*, 5:464–482, 1996. viii, 38, 39

[6] D. H. Wang and W. H. Liao. Magnetorheological fluid dampers: a review of parametric modelling. *Smart materials and structures,*, pages 1–35, 2011. viii, 39

[7] B. F. Spencer, S. J. Dyke, M. K. Sain and J. D. Carlson. Phenomenological model for magnetorheological dampers. *Journal of Engineering Mechanics*, 123, 1997. viii, 35, 37, 40, 41

[8] European Committee. *European Committee for Standardisation: Basis of Structural Design. Annex A2: Application for bridges, Final PT Draft EN 1990prAnnex A2*. 2002. xii, 19, 24, 34, 76, 90, 95, 98, 109

[9] R. Karoumi and J. Wiberg. *Kontrol av Dynamiska Effekter av Passerande Tag Pa Botniabanans Broar Sammanfattning*. Stockholm: Royal Institute of Technology (KTH), Structural Design and Bridges, 2006. xii, 26, 76, 79

[10] Y. Wang, Q. C. Wei, J. Shi and X. Long. Resonance characteristics of two-span continuous beam under moving high speed trains. *Latin American Journal of Solid and Structures*, 7:185–199, 2010. xii, 26

[11] M. D. Symans and M. C. Constantinou. Passive fluid viscous damping systems for seimic energy dissipation. *ISET Journal of Earthquake Technology*, 35, 1998. xii, 11, 12, 60, 61, 112

[12] P. Museros and M. D. Martinez-Rodrigo. Vibration control of simply supported beams under moving loads using fluid viscous dampers. *Journal of Sound and Vibration*, 2007. xii, 11, 18, 73, 76, 82, 98, 100

[13] L. Fryba. A rough assessment of railway bridges for high speed trains. *Journal of Engineering Structures*, 23:548–556, 2001. 1

[14] S. I. Kim, J. Lee, and S. Kim. Dynamic behavior comparison of steel-composite and concrete high speed railway bridges. *International Journal of Steel Structures*, 11:445–455, 2011. 1

[15] R. Calcada, R. Delgado, and A. C. Matos. *Bridges for high-speed railways*. CRC Press, Balkema, 2009. 1, 76

[16] Y. B. Yang. *Vehicle-Bridge Interaction Dynamics with Applications to High-Speed Railways*. World Scientific Publishing Co. Pte. Ltd, 2004. 1, 81

[17] J. E. Brock. A note on the damped vibratin absorber. *American Society of Mechanical Engineers*, A:284, 1946. 2

[18] J. P. Den Hartog. *Mechanical Vibrations*. McGraw-Hill, 1947. 2

[19] T. Asami, O. Nishihara. Closed-form exact solution to H-infinity optimization of dynamic vibration absorbers (appication to different transfer functions and damping systems. *Journal of Vibration and Acoustics*, 125:398–405, 2003. 3

[20] B. W. Jo, G. H. Tae, and D. W. Lee. Structural vibration of tuned mass damper-installed three-span steel box bridge. *International Journal of Pressure Vessels and Piping*, 78:667–675, 2001. 3

[21] A. S. Joshi and R. S. Jangid. Optimum parameters of multiple tuned mass dampers for base-excited damped systems. *Journal of Sound and Vibration*, 202, 1997. 3

[22] L. Kitis, B. P. Wang and W. D. Pilkey. Vibration reduction over a frequency range. *Journal of Sound and Vibration*, 89, 1982. 3

[23] C. C. Lin, J. F. Wang, and B. L Chen. Train-induced vibration control of high-speed railway bridges equipped with multiple tuned mass dampers. *Journal of Bridge Engineering ASCE*, 10, 2005. 4, 18, 27, 81, 103, 108, 110

[24] B. F. Spencer, T. T. Song. New applications and development of active, semi-active and hybrid control techniques for seismic and non-seismic vibration in the usa. *Proceedings of the International Post-SMiRT Seminar on Seismic Isolation, Passive Energy Dissipation and Active Control of Vibration of Structures, Cheju, Korea*, 1999. 5

[25] H. N. Li, Q. Jin. Amd active control for irregular buildings using ga-bp neural network. *Earthquake Engineering and Engineering Vibration*, 23:134–142, 2003. 5

[26] I. Nishimura, T. Kobori, M. Sakamoto, N. Koshika, K. Sasaki, S. Ohrui. Active tuned mass damper. *Smart Materials and Structures*, 14:306–311, 1992. 5

[27] S. J Dyke. *Acceleration feedback control strategies for active and semi-active control systems: modeling, algorithm development, and experimental verification*. Doctoral thesis, University of Notre Dame, Notre Dame, Indiana, USA, 1996. 5

[28] J. D. Carlson. Multi-degree of freedom magnetorheological devices and system for using same US. *Patent Specification,*, page 312492, 1996. 5, 36

[29] T. Kobori, M. Takahashi, T. Nasu and N. Niva. Seismic response controlled structure with active variable stiffness system. *Earthquake Engineering and Structural Dynamics*, 1993. 5

[30] M. Q. Feng and M. Shinozuka. Use of a variable damper for hybrid control of bridge response under earthquake. *Proc., U.S. National Workshop on Structural Control Research*, 1990. 6

[31] K. Kawashima and S. Unjoh. Seismic response control of bridges by variable dampers. *Journal of Structural Engineering*, 120, 1994. 6

[32] R. L. Sack and W. Patten. Semiactive hydraulic structural control. *Proc., Int. Workshop on Structural Control*, USC Publication Number CE-9311:417–431, 1993. 6

[33] M. D. Symans and M. C. Constantinou. Seismic testing of a building structure with a semiactive fluid damper control system. *Earthquake Eng. Struct. Dyn*, 26, 1999. 6

[34] F. Jabbari and J. E. Bobrow. Vibration suppression with resettable device. *Journal of Engineering Mechanics*, 128, 2002. 6

[35] Z. Xu, X. Gong and X. Chen. Development of a mechanical semi-active vibration absorber. *Advances in Vibration Engineering*, 10, 2011. 6

[36] J. Liu and K. Liu. A tunable electromagnetic vibration absorber: characterization and application. *Journal of Sound and Vibration*, 295:708724, 2006. 7

[37] G. Jiang and L. M. Hanagan. Semi-active tmd with piezoelectric friction dampers in floor vibration control. *Proc. SPIEInt. Soc. Opt. Eng.*, 6169, 2006. 8

[38] S. Hidaka, Y. K. Ahn, and S. Morishita. Adaptive vibration control by a variable-damping dynamic absorber using ER fluid. *Journal of Vibration and Acoustics*, 121:373–378, 1999. 8

[39] P. Y. Lin and L. L. Chung. Semiactive control of building structures with semiactive tuned mass damper. *Computer-Aided Civil and Infrastructure Engineering*, 20:35–51, 2005. 8

[40] J. Kang, H. S. Kim, and D. G. Lee. Mitigation of wind response of a tall building using semi-active tuned mass dampers. *The Structural Design Of Tall And Special Buildings*, 20:552–565, 2011. 8

[41] J. H. Koo, M. Ahmadian, and M. Setareh. Experimental evaluation of magneto-rheological dampers for semi-active tuned vibration absorbers. *Smart Structures and Materials*, 5052:83–91, 2003. 8

[42] F. Yang. *Optimal vibration suppression of beamtype structures using passive and semiactive tuned mass dampers*. Doctoral thesis, Concordia University, Canada, 2008. 8

[43] R. Stanway, J. L. Sproston, and N. G. Strvens. Non-linear modeling of an electro-rheological vibration damper. *Journal of Electrostatics*, 20:167–184, 1987. 8

[44] T. T. Soong. *Active structural control: Theory and Practice*. Longman Scientific and Technical, 1990. 9

[45] W. K. Gawronski. *Advanced Structural Dynamics and Active Control of Structures*. Springer, 2004. 9, 10, 21, 25, 68

[46] L. Meirovitch. *Dynamics and control of structures*. John Wiley & Sons, Inc, 1990. 9

[47] C. C. Lee. Fuzzy logic in control systems: Fuzzy logic controller. *IEEE Transactions on Systems, Man, and Cybernetics*, 20:404–418, 1990. 10

[48] M. Battaini, F. Casciati, and L. Faravelli. Fuzzy control of structural vibration, an active mass system driven by a fuzzy controller. *Earthquake Engineering and Structural Dynamics,*, 27:1267–1276, 1998. 10

[49] K. C. Schurter and P. N. Roschke. Neuro-fuzzy control of structures using acceleration feedback. *Smart Materials and Structures*, 10:770–779, 2001. 10

[50] C. Christopoulos and A. Filiatrault. *Principles of Passive Supplemental Damping and Seismic Isolation*. IUSS Press, 2006. 11

[51] I. D. Aiken. Dampers for seismic protection: 1. Friction and viscous damper; 2. Viscoelastic and metallic dampers. *Technical Seminar on Seismic Isolation and Energy Dissipation Technology*, 1997. 11

[52] M. D. Martinez-Rodrigo and P. Museros. Optimal design of passive viscous dampers for controlling the resonant response of orthotropic plates under high-speed moving loads. *Journal of Sound and Vibration*, 2011. 11

[53] M. D. Martinez-Rodrigo, J. Lavado, and P. Museros. Dynamic performance of existing high-speed railway bridges under resonant conditions retrofitted with fluid viscous dampers. *Journal of Structural Engineering*, 32, 2010. 11, 63

[54] J. Li, M. Su, L. Fan. Vibration control of railway bridges under high-speed trains using multiple tuned mass dampers. *Journal of Bridge Engineering*, 10:312–320, 2005. 11

[55] J.F. Wang, C.C. Lin, B.L. Chen. Vibration suppression for high-speed railway bridges using tuned mass dampers. *International Journal of Solids and Structures*, 40:465–491, 2003. 11

[56] H.C. Kwon, M.C. Kim, and I.W. Lee. Vibration control of bridges under moving loads. *Computers & Structures*, 66:473–480, 1998. 11

[57] W. H. Lin and A. K. Chopra. Earthquake response of elastic single-degree-of-freedom systems with non-linear fluid viscous dampers. *Journal of Earthquake Engineering and Structural Dynamics*, 31, 2002. 12, 60

[58] P. P. Diotallevi, L. Landi and A. Dellavalle. Simplified design methodology for systems equipped with non-linear viscous dampers. *The 14th World Conference on Earthquake Engineering*, 2008. 12

[59] M. Kargahi and C. G. Ekwueme. Structural optimization of viscous dampers using genetic algorithms for improving seismic performance of existing buildings. *Journal of American Society of Civil Engineers*, 2010. 12

[60] O. Lavan and R. Levy. Gradient based optimization of added viscous damping in seismic applications. *Journal of Advances in Engineering Structures, Mechanics and Construction*, 2006. 12

[61] Z. Jiang and R. Christenson. Experimental verivication of an MR damper controlled highway bridge. *19th Analysis and Computation Specialty Conference*, 2010. 13

[62] S. Skogestag and I. Postlechtwaite. *Multivariable feedback control, analysis and design*. John Willey and Sons, Chichester, 1996. 17, 22, 25, 48

[63] Eurocode. *Eurocode 1: Actions on Structures - Part 2: Traffic loads on bridge.* 2003. 18

[64] R. W. Clough and J. Penzien. *Dynamics of Structures*. McGraw-Hill, 1993. 18, 45, 64, 90

[65] K. D. Weiss, J. D. Carlson, D. A. Nixon. Viscoelastic properties of magneto- and electro-rheological fluids. *Journal of Intelligent Material Systems and Structures*, 5:772–775, 1994. 36

[66] W. Kordonsky. Magnetorheological effect as a base of new devices and technologies. *Journal of Magnetism and Magnetic Materials,*, 122:395398, 1993. 36

[67] K. D. Weiss and T. G. Duclos. Controllable fluids: the temperature dependence of post-yield properties. *Proc. 4th Int. Conf. on ER Fluids - Singapore: World Scientific,*, page 4359, 1994. 36

[68] I.H. Shames and F.A. Cozzarelli. *Elastic and inelastic stress analysis*. Prentice Hall, Englewood Cliffs, New Jersey, 1992. 37

[69] C. C. Chang and P. Roschke. Neural network modeling of a magnetorheological damper. *Journal of Intelligent Material Systems and Structures,*, pages 755–764, 1998. 40

[70] K.C. Schurter and P. Roschke. Fuzzy modeling of a magneto-rheological damper using Anfis. *The Ninth IEEE International Conference,*, pages 122–127, 2000. 40

[71] R. Bouc. Mathematical model for hysteresis. *Acustica,*, pages 16–25, 1971. 40

[72] G. Yang, B. F. Spencer Jr., J. D. Carlson and M. K. Sain. Large-scale mr fluid dampers: modeling and dynamic performance considerations. *Journal of Engineering Structures*, 24:309–323, 2002. 41

[73] Z. LI L. XU. Semi-active predictive control strategy for seismically excited structures using MRF-04K dampers. *Journal of Central South University*, 19:2496–2501, 2012. 41

[74] S. B. Choi, S. K. Lee, and Y. P. Park. A hysteresis model for the field-dependent damping force of a magnetorheological damper. *Journal of Sound and Vibration*, 245, 2001. 41

[75] E.R.Wang, X.Q. Ma, S. Rakhela, , and C.Y. Su. Modelling the hysteretic characteristics of a magnetorheological fluid damper. *Proc. Inst. Mech. Eng. D, J. Automob*, 217:537550, 2003. 41

[76] C. Sakai, H. Ohmori, and A. Sano. Modeling of mr damper with hysteresis for adaptive vibration control. *42nd IEEE Conference on Decision and Control,*, 2003. 41

[77] R.K.L. Su H.H. Tsang and A.M. Chandler. Simplified inverse dynamics models for mr fluid dampers. *Journal of Engineering Structures*, 28, 2006. 41

[78] D.H.Wang andW.H. Liao. Modeling and control of magnetorheological fluid dampers using neural networks. *Smart Mater. Struct*, 14, 2005. 41

[79] J. R. Jang. ANFIS: Adaptive-network-based fuzzy inference systems. *IEEE Transactions on Systems, Man, and Cybernetics*, 23, 1993. 41, 42

[80] The MathWorks. *Fuzzy Logic Toolbox 2 - User's Guide*. Matlab, 3 Apple Hill Drive - Natick, MA 01760-2098, 2010. 41

[81] T.T Soong. *Active Structural Control: Theory and Practice*. Longman Scientific and Technical, 1990. 46, 92

[82] L. Meirovitch. *Dynamics and Control of Structures*. John Wiley and Sons, 1990. 50, 92, 93, 94

[83] D. Simon. *Optimal state estimation: Kalman, H-infinity and nonlinear approaches*. John Wiley & Sons, Inc., Hoboken, New Jersey, 2006. 50, 94

[84] P. Museros, E. Moliner , M.D. Martinez-Rodrigo. Free vibrations of simply-supported beam bridges under moving loads: Maximumresonance, cancellation and resonant vertical acceleration. *Journal of Sound and Vibration*, 332:326–345, 2013. 51, 69

[85] L. Meirovitch. *Elements of Vibration Analysis*. McGraw-Hill, New York, 1986. 60, 70

[86] K. Worden and G. R. Tomlinson. *Nonlinearity in Structural Dynamics*. Institute of Physics Publishing, Bristol and Philadelphia, 2001. 61

[87] I. S. Gradshteyn and I. M. Ryzhik. *Table of Integrals, Series, and Products*. Elsevier Academic Press publications, 2007. 62

[88] J. D. Yau. Resonance of continuous bridges due to high speed trains. *Journal of Marine Science and Technology*, 9, 2001. 73

[89] L. Fryba. *Vibration Solids Structures Moving Loads*. Thomas Telford, 1999. 74

[90] C. Mellier. *Optimal Design of Bridges for High-Speed Trains*. Stockholm: Royal Institute of Technology (KTH), Structural Design and Bridges, 2010. 80

[91] M. A. Bhatti. *Practical Optimization Methods with Mathematica Applications*. Springer. 86

[92] M. Luu, M.D. Martinez-Rodrigo, V. Zabel, C. Koenke. H-infinity optimization of fluid viscous dampers for reducing vibrations of high-speed railway bridges. *Journal of Sound and Vibration*, 2014. 92

[93] W. Liu. *Vibration Control of Large Scale Flexible Structures Using Magnetorheological Dampers*. Doctoral thesis, Worcester Polytechnic Institute, Massachusetts, 2005. 95

[94] M. Wu, Y. He, J.H She. *Stability Analysis and Robust Control of Time-Delay Systems*. Springer, 2010. 96, 121, 122

[95] K. Xu and T. Igusa. Vibration control using multiple tuned mass dampers. *Journal of Sound and Vibration*, 175, 1994. 108

[96] M. D. Symans and C. C. Constantinou. Semi-active control systems for seismic protection of structures: a state-of-the-art review. *Journal of Engineering Structures*, 21:469–487, 1997. 112

[97] J. D. Barbero. *Dinmica de puentes de ferrocarril para alta velocidad: mtodos de clculo y estudio de la ressonancia*. Tesis Doctoral, Escuela Tcnica Superior de Ingenieros de Caminos, Canales y Puertos, Universidad Politcnica de Madrid, Madrid, 2001. 118

[98] S. Boyd, L.E Ghaoui, E. Feron, V. Balakrishnan. *Linear Matrix Inequalities in Systems and Control Theory*. SIAM, Philadelphia, 1994. 121

[99] X. Li, M. Guay, B. Huang and D. G. Fisher. Delay-Dependent robust H infinity control of uncertain linear systems with input delay. *Proceedings of the American Control Conference*, 2:800–804, 1999. 122